Aus dem Walther-Straub-Institut für Pharmakologie und Toxikologie der
Ludwing-Maximilians- Universität München

Vorstand: Prof. Dr. Thomas Gudermann

TRPM7 in T-cell signaling

Kinase-Coupled Ion Channel in Immune System Homeostasis

Dissertation zum Erwerb des Doktorgrades der Naturwissenschaften an der
Medizinischen Fakultät der Ludwig-Maximilians-Universität München

vorgelegt von

Valentina Vettore

aus Padua, Italien

2017

Mit Genehmigung der Medizinischen Fakultät der Universität München

Betreuer: Prof. Dr. Alexander Dietrich

Zweitgutachter: Priv. Doz. Dr. Reinhard Obst

Dekan: Prof. Dr. med. dent. Reinhard Hickel

Tag der mündlichen Prüfung: 11.09.2018

Abstract **6**

Zusammenfassung **7**

1. Introduction **9**

1.1. *Transient Receptor Potential* family *9*

1.2. TRPM7 channel-kinase *12*

1.3. Immune system regulation *26*

2. Aim of the thesis **38**

3. Material and methods **39**

3.1. Material *39*

3.2. Methods *39*

4. Results **51**

4.1. Analysis of the gross phenotype of the $TRPM7^{KR/KR}$ mouse model *51*

4.2. TRPM7 kinase activity is not required for channel activity or maintenance of cation homeostasis *54*

4.3. TRPM7 kinase does not affect Ca^{2+} signaling and activation of T lymphocytes *60*

4.4. TRPM7 kinase affects basal cytokine levels in serum *62*

4.5. $TRPM7^{KR/KR}$ mice display normal structure of the gut tissue *66*

4.6. TRPM7 kinase activity is pivotal for immune system regulation *68*

4.7. Cytokine levels in the small intestine *72*

4.8. Potential targets for the TRPM7 kinase *76*

4.9. TRPM7 kinase interaction with SMAD2 is important for immune regulation *80*

5. Discussion **82**

6. Appendix 1 **96**

7. Appendix 2 **105**

Abstract

The *transient receptor potential-melastatin-like 7* (Trpm7) gene encodes a protein that is formed by an ion channel pore and a serine/threonine α-kinase. TRPM7 has been shown to be pivotal for thymopoiesis. A tissue specific abrogation in the thymus elicited a blockade of T cell development at the double negative stage ($CD4^-CD8^-$). Thus, conditional TRPM7 knock-out mice developed a lack of active T cells and an impaired immune system. This study further indicated that the TRPM7 channel and/or the kinase are important for T cell development. They also showed defects in the expression of cytokines and T cell growth factors. To further identify and understand the contribution of the kinase *versus* the channel activity, we performed investigations on a new mouse model carrying an inactive kinase domain due to a single mutation at the active site of the kinase (K1646R). When analyzing channel functionality and expression, we found that the TRPM7 channel without kinase activity is fully functional. We further analyzed serum Mg^{2+} and Ca^{2+} concentrations to confirm that there were no significant differences at the systemic level. Regular Ca^{2+} signaling following T cell activation is maintained to ensure normal T cell proliferation. However, we found a significant decrease in the basal levels of different cytokines, specifically, IL-2, G-CSF, and IL-17. The generalized reduction of cytokines prompted us to deeper investigate the immune system organization at the core site of its activity: the gut. Here we found a dramatic reduction of intraepithelial T cells, which displayed a reduction in the expression of the CD103 protein. CD103 is a gut homing integrin and its expression seems to be influenced by the TRPM7 kinase activity. Recently, SMAD2 was identified as key molecule in the cascade of events up-regulating CD103. In our studies we confirmed that TGFβ-1/SMAD2 pathways are involved in CD103 expression and in turn TRPM7 kinase activity is playing a pivotal role in SMAD2 phosphorylation and activation. In line with an impaired TGFβ-1 signaling cascade also Th17 differentiation was anomalous in the kinase-dead mutant T cells, also explaining the reduced IL-17 levels in the serum. We assume that this is due to impaired SMAD2 phosphorylation, which is either directly or indirectly regulated by TRPM7 kinase activity. The Th17 cell subset is mainly implicated in

the persistency of autoimmune diseases. With our studies we identified an important role for TRPM7 in T cell development and offer new therapeutic insight for possible treatments against pro-inflammatory gut associated diseases, where the TRPM7 kinase is important for T cell colonization of the gut epithelium and Th17 differentiation and thus immune system homeostasis.

Zusammenfassung

Das *Melastatin*-ähnliche *Transiente-Rezeptor-Potential 7* (Trpm7) Gen kodiert für ein Protein das durch einen Poren-formenden Ionenkanal und eine Serin/Threonin α-Kinase gebildet wird. TRPM7 ist wichtig für die Thymopoese und ein gewebsspezifischer Knock-out im Thymus führt zur Blockade der T-Zell-Entwicklung während des Doppelt-Negativen-Stadiums ($CD4^-CD8^-$). Daher entwickeln konditionelle TRPM7 Knock-out Mäuse keine aktiven T-Zellen und haben ein eingeschränktes Immunsystem. Diese Studie zeigt weiter, dass der TRPM7-Kanal und/oder die -Kinase eine wichtige Rolle in der T-Zell-Entwicklung spielen. Außerdem wurden Defekte in der Expression von Zytokinen und T-Zell-Wachstumsfaktoren festgestellt. Um die Rolle der TRPM7-Kinase *versus* -Kanal-Aktivität hierbei genauer zu untersuchen, haben wir uns ein neues Mausmodell zunutze gemacht, das eine einzelne Punktmutation an der aktiven Stelle der Kinase aufweist (K1646R). Eine Analyse der TRPM7-Kanal-Funktion und -Expression ergab, dass der Kanal ohne Kinase-Aktivität voll funktionsfähig ist. Wir haben weiter Mg^{2+} und Ca^{2+} Konzentrationen im Serum analysiert, um zu bestätigen, dass es keine signifikanten Unterschiede auf systemischer Ebene gibt. Charakteristische Ca^{2+} Signale, als Reaktion auf T-Zell-Aktivierung, stellen sicher, dass die T-Zell-Proliferation normal abläuft. Jedoch haben wir signifikante Unterschiede in der basalen Konzentration verschiedener Zytokine, insbesondere IL-2, G-CSF und IL-17 gefunden. Diese allgemeine Reduktion an Zytokinen hat uns dazu geführt, die Organisation des Immunsystems am Kern seiner Aktivität - dem Darm - genauer zu untersuchen. Hier fanden wir in unserer Mausmutante eine dramatische Reduktion der intra-epithelialen T-Zellen, welche das Protein CD103 kaum noch exprimieren. CD103 ist ein ‚Homing'-Integrin des Darms und seine Expression scheint durch die TRPM7-Kinase-Aktivität beeinflusst zu

werden. Kürzlich konnte SMAD2 als Schlüsselmolekül in der Signalkaskade identifizieren werden, die zur Hochregulation von CD103 führt. Unsere Untersuchungen bestätigen, dass TGFβ-1/SMAD2 Signalwege bei der Expression von CD103 involviert sind und somit die TRPM7-Kinase-Aktivität eine wichtige Rolle bei der Phosphorylierung und Aktivierung von SMAD2 spielt. In Übereinstimmung mit den Defekten in der TGFβ-1 Signalkaskade war außerdem die Differenzierung von Kinase-defizienten T-Zellen in Th17 Zellen stark beeinträchtigt, wodurch auch die reduzierten IL-17-Konzentrationen im Serum erklärt werden können. Wir nehmen an, dass für diese beobachteten Unterscheide ein direkter oder indirekter Defekt in der SMAD2-Phosphorylierung durch die TRPM7-Kinase verantwortlich ist. Eine Vermehrung des Th17 Zell-Subtyps wird unter anderem für einen schlechteren Verlauf von Autoimmunkrankheiten verantwortlich gemacht. In unseren Studien haben wir die wichtige Rolle von TRPM7 in der T-Zell-Entwicklung dargelegt und zeigen neue therapeutische Einsichten für mögliche Behandlungen gegen pro-entzündliche Darm-assoziierte Erkrankungen auf. Hier ist die TRPM7 Kinase wichtig für die Kolonisation des Darmepithels mit T-Zellen, sowie die Th17 Differenzierung und somit für die Homöostase des Immunsystems.

1. Introduction

1.1. *Transient Receptor Potential* family

In early 1969 a group of scientists at the University of Edinburgh identified an abnormal electroretinography response in a *Drosophila melanogaster* mutant. The mutation caused only a transient receptor potential in response to light in the eye of these flies (Cosens and Manning, 1969). Therefore, the gene harboring the mutation was called *transient receptor potential* (*trp*) gene (Cosens and Manning, 1969). Further studies confined the TRP protein as predominantly expressed in photoreceptor cells (Montell and Rubin, 1989). Montell and Rubin successfully isolated the entire protein-coding region for the TRP protein and found that it was specifically localized at the rhabdomers, which form a photoreactive area on the cell membrane of the eye. Further they hypothesized a putative protein structure for TRP protein and its activity as "Ca^{2+} pump" involved in ion homeostasis was proposed (Montell and Rubin, 1989).

Via homology screening the first members of the mammalian TRP superfamily were identified and soon subdivided into six families: TRPC (canonical), TRPV (vanilloid), TRPP (polycystin), TRPML (mucolipin), TRPA (ankyrin), and TRPM (melastatin) (Fig. 1) (Nilius and Owsianik, 2011). The subfamilies, share a six-transmembrane structure forming a pore region (within segment 5 and 6) and most of them (TRPC, TRPV, TRPM, TRPA) carry 25 conserved amino acids at the C-terminus, shortly after the sixth transmembrane domain, named the "TRP-like domain" (Fig. 2). The TRPN (No Mechano Receptor Potential Channel-like) family instead, is more distantly related to the others and was not yet detected in mammals (Lazzeri et al., 2009). All TRP channels are expressed mainly in the plasma membrane of almost every cell type, where they regulate out- and in-flux of Ca^{2+}, Na^{+} and other cations. Thus, TRP channels can mediate sensory function such as nociception, taste transduction, pheromone signaling or temperature sensation. Furthermore, this ion channel family regulates homeostatic and motile functions (Nilius and Owsianik, 2011). Some subfamilies were thought to be thermo sensors, such as TRPV, TRPM and TRPA

(Venkatachalam and Montell, 2007). However, further studies demonstrated that only some ion channels within each family are actual functional thermic sensors: TRPV1 (>43°C), TRPV2 (>52°C), TRPV3 (>30°-39°C), TRPV4 (>25°-35°C), TRPM8 (<20°-28°C) and TRPA1 (<17°C) (Belmonte and Viana, 2008). Although it is common to define TRPM as a family of channels sharing structural features, it has been recently shown that they differ in domain structure, as well as, their cation selectivity and activation mechanisms (Schlingmann and Gudermann, 2005)

Despite the above-mentioned observations, TRPM channels exhibit some common features: a unique long conserved N-terminus of unknown function as well as an extended C-terminus. Furthermore, three members of the TRPM family TRPM2, TRPM6 and TRPM7 are characterized by a C-terminal enzymatic domain, which is why they are often referred to as ‘chanzymes’ (Montell, 2003). Specifically, TRPM6 and TRPM7 differ from other TRPM channels, as they are the only known ion channels containing a kinase domain (Schlingmann and Gudermann, 2005). The kinase is a serine/threonine kinase, capable of autophosphorylation and it is known as a homologue to the α-kinase family in its N-terminal lobe secondary and tertiary structure (Yamaguchi et al., 2001).

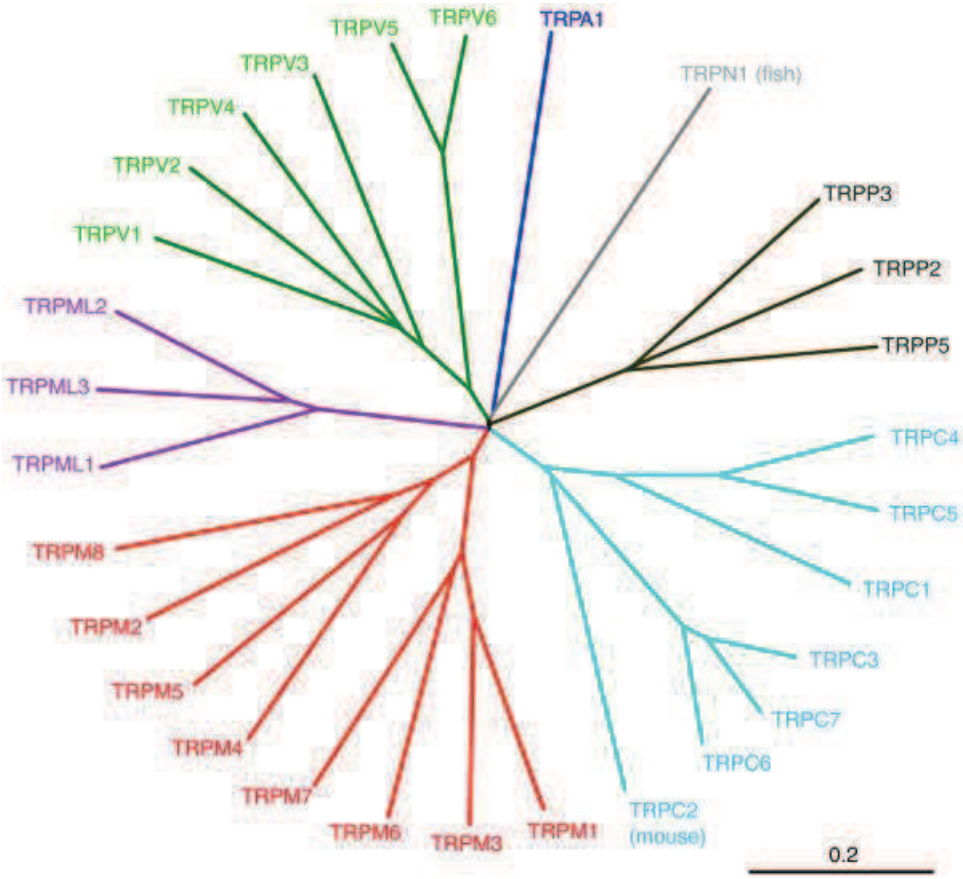

Figure 1: The TRP channel family in vertebrates. The transient receptor potential (TRP) family are integral membrane proteins, which act as ion channels. The TRP family is divided into seven subfamilies:

TRPC (canonical), TRPV (vanilloid), TRPM (melastatin), TRPP (polycystin), TRPML (mucolipin), TRPA (ankyrin) and TRPN (NOMPC-like). The latter TRP is found only in invertebrates and fish, while TRPC2 is a pseudogene in humans but functional in mice. TRP ion channels are expressed in many different tissues and cell types, where they are involved in diverse physiological processes, such as sensation of different stimuli or ion homeostasis. Most TRPs are non-selective cation channels, only a few are highly Ca^{2+} permeable and only two (TRPM6 and TRPM7) are permeable for Mg^{2+}. Figure from Nilius and Owsianik (2011).

1.2. TRPM7 channel-kinase

1.2.1. Identification of TRPM7

The Transient Receptor Potential Melastatin-like 7 channel-kinase, TRPM7, was identified in 2001 (Runnels et al., 2001), initially, it was named TRP-PLIK. The authors identified membrane depolarization due to activation of transient receptor potential channels by phospholipase C. Runnels and colleagues proceeded with a yeast two-hybrid screen on a rat brain library for putative new kinase domains, using PLC-β as bait and identified a kinase with strong similarities to two already known kinases: the myosin heavy chain kinase and the eukaryotic elongation factor-2 kinase. It was named PLIK for ”phospholipase C interacting kinase”. Accordingly, the complete protein consisting of channel and kinase domain was named “TRP-PLIK”. Whole-cell and single-channel recordings on transfected cells, helped to characterize the TRP-PLIK current activity. Runnels et al described an outwardly rectifying current and suggested a putative role of the kinase for channel activation (Runnels et al., 2001).

Shortly thereafter, Nadler et al. named a Mg·ATP regulated channel as LTRPC7, referring to the nomenclature already proposed by Harteneck et al. in 2000 (Harteneck et al., 2000). They demonstrated a fundamental role of the channel for cell survival and transport of Ca^{2+} and Mg^{2+}. If Mg^{2+} was also a regulator for LTRPC7, they questioned the role of the kinase as a possible channel activator. The authors explained that Runnels and colleagues showed an increased current amplitude due to the drop in $[Mg^{2+}]_i$, caused by the addition of 5 mM Na·ATP to a standard intracellular solution. Nadler et al. proposed a different mechanism based on Mg·ATP and Mg^{2+} channel inhibition and a pivotal but still questionable role of the kinase. Nadler and colleagues further concluded that the kinase was not essential for channel activation (Nadler et al., 2001).

In 2001 Yamaguchi et al. also identified a new protein composed of a channel and a kinase domain, which revealed similarities to eukaryotic protein kinases in the catalytic site and to metabolic enzymes characterized by an ATP binding site (Yamaguchi et al., 2001). Until 2002 this “chanzyme” was named differently in

each scientific report: ChaK (Yamaguchi et al., 2001), TRP-PLIK (Runnels et al., 2001) and LTRPC7 (Nadler et al., 2001). Finally a committee in 2002 reunited in order to establish a commonly accepted nomenclature for all TRP channels naming this channel TRPM7 (Montell et al., 2002).

All three research groups simultaneously discovered a protein with the unique feature of an α-kinase domain, belonging to the atypical family of α-kinases, fused to an ion channel domain from the TRP family.

Since then, many further studies on TRPM7 have been performed and their conclusions on the role of the kinase activity, the permeability of the channel and its activation mechanism are not always the same. First, Nadler et al., but also more recent studies, underlined the importance of TRPM7 for cell and mammalian survival (Nadler et al., 2001; Ryazanova et al., 2010). Nonetheless, it remains questionable whether the α-kinase plays a role in channel activation or how it is regulated and activated itself. These open questions are still under investigation.

1.2.2. Structure and properties of TRPM7

TRPM7 is an 1863 amino acid protein and its corresponding gene is located at chromosome 15 in mice. Its structure is quite unique: an ion channel pore and a functional enzyme form the protein. More specifically, TRPM7 is composed of: an N-terminal region, a channel transmembrane region followed by a coiled-coiled region and a C-terminal domain. Exactly at the distal C-terminus the α-kinase is located.

Four TRPM7 proteins form the ion channel. These in turn, are composed of six transmembrane segments (S1-6) (Fig. 2). This tetrameric complex forms the channel pore between the S5 and S6 segments. Within these areas, at amino acids E1047 and Y1049, the locus for divalent cation selectivity was identified in murine TRPM7 (Park et al., 2014). Very early studies defined the channel function as a divalent cation selective transporter for Ca^{2+} and Mg^{2+}. Later

insights outlined a more detailed permeation profile of TRPM7 with $Zn^{2+} \approx Ni^{2+} >> Ba^{2+} > Co^{2+} > Mg^{2+} \geq Mn^{2+} \geq Sr^{2+}$ $Cd^{2+} \geq Ca^{2+}$ (Monteilh-Zoller et al., 2003).

Specific residues (1551-1577) of the kinase domain characterize its structure forming a “domain-swapped bilobate dimer” thanks to the interplay between the residues 1551 and 1577 (Yamaguchi et al., 2001). The kinase domain has specific sites responsible for the kinase activity: amino acids 1553 to 1562 (Fig. 2) (Crawley and Cote, 2009). Similarly, mutation of residues implicated in catalysis, Lys1646 (aa 1648 in human, Schmitz et al. 2003), which is equivalent to the conserved lysine residue of classical kinases that is often mutated to produce a kinase-dead protein. Both Lys1646 and Asp1765 mutations resulted in disrupted kinase activity (Matsushita et al. 2005). In contrast to classical kinase super-families, the C-terminal lobe of the TRPM7 kinase domain seems to contain a zinc domain, and Zn^{2+} appears to play a structural role for TRPM7 (Yamaguchi et al., 2001).

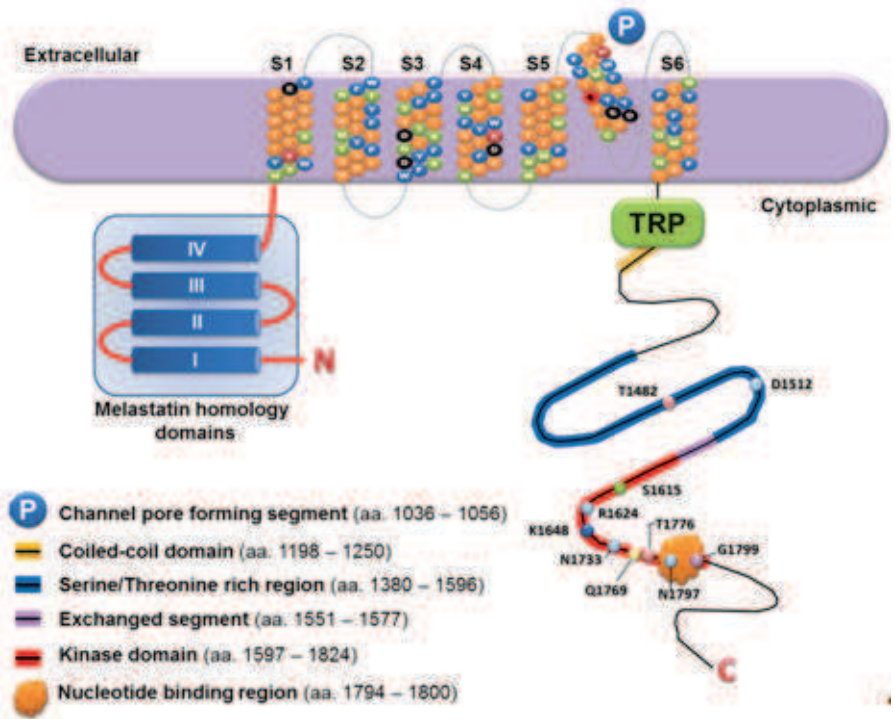

Figure 2: TRPM7 structure. The picture obtained from N. S, Yee et al. published in 2014 is a schematic diagram showing the modular structure of TRPM7. More detailed, a single subunit of TRPM7 contains six transmembrane domains. The intracellular N-terminus harbors a region referred to as melastatin homology domain. The C-terminus includes a TRP box of ~25 highly conserved residues (TRP), the coiled-coil domain (yellow), serine/threonine-rich region (blue) the kinase domain (red). The most studied point mutations within the C-terminus are highlighted.

Figure from Yee et al. (2014). Reprinted by permission: Creative Commons Attribution License 4.0.

While the functional role of the kinase remains elusive, the function of the channel is better characterized. Channel conductance studies using single channel recordings reported a TRPM7 conductance of ~40 pS at divalent-free conditions and negative membrane voltages (Kerschbaum and Cahalan, 1999; Kerschbaum et al., 2003; Nadler et al., 2001). Activated TRPM7 channels show characteristic small inward currents at negative voltages and strong outwardly rectifying currents, at positive voltages (Runnels et al., 2001). Whereas, „at physiological, negative membrane potentials TRPM7 conducts very little inward currents which are mediated by ion flux of divalent cations such as Ca^{2+} and Mg^{2+} from the extracellular space into the cytosol down their concentration gradient" (Nadler et al., 2001).

"However, at positive membrane potentials, where divalent ions do not experience sufficient driving force to enter the cell, the outward transport rates of intracellular cations, such as K^+ or Cs^+, increase and at potentials beyond +50 mV the monovalent cation fluxes become quite prominent and shape the characteristic outwardly rectifying current voltage relationship of TRPM7. Only when completely removing extracellular divalent cations will TRPM7 transport monovalent cations inwardly and this will linearize the current-voltage relationship, revealing both TRPM7´s exquisite specificity for divalent cation transport and the lack of any significant voltage dependency" (Penner and Fleig, 2007).

1.2.3. Regulation of TRPM7

As already mentioned above, the TRPM7 cation channel is physiologically important for transportation of mainly Mg^{2+}, Ca^{2+} and Zn^{2+} (Monteilh-Zoller et al., 2003). Further, it has been implicated in the regulation of cellular and systemic

Mg^{2+} homeostasis (Jin et al., 2008; Ryazanova et al., 2010). In certain cells the regulation of Mg^{2+} can alter Ca^{2+} levels (Aarts et al., 2003; Wei et al., 2009).

At acidic pH, when the permeation of Mg^{2+} and Ca^{2+} is inhibited, monovalent ions can pass through TRPM7. At physiological pH the monovalent cations do not permeate through the pore (Jiang et al., 2005). Another study showed that monovalent cations permeability is stopped by micromolar concentrations of Mg^{2+} and Ca^{2+} at neutral (or physiological) pH (Numata and Okada, 2008).

TRPM7 currents are tightly regulated by intracellular free Mg^{2+} and Mg-nucleotide levels (Nadler et al., 2001). Thus, the current was initially named MagNuM (magnesium-nucleotide-regulated metal ion current) or MIC (magnesium-inhibited cation current). Therefore, at conditions, where free Mg^{2+} and Mg-nucleotides are intracellularly depleted, TRPM7 currents increase. Binding or interaction sites for Mg^{2+} and Mg-nucleotides at the C-terminus regulate this negative feedback loop (Schmitz et al., 2003). Other studies tried to clarify mechanisms behind a possible interplay of the channel and the kinase, located at the C-terminus. Consequently, several mutations have been created and analyzed for a regulation of channel activity via Mg^{2+} and Mg-nucleotides. Complete deletion of the kinase elicited a possible role of the kinase domain in regulating channel activity, since $TRPM7^{\Delta KD}$ showed strong current inhibition by $[Mg^{2+}]_i$ and $[Mg{\cdot}ATP]_i$ (Ryazanova et al., 2010; Schmitz et al., 2003). This effect might be explained via a higher-sensitivity of the Mg^{2+} binding site, since it is more exposed to the cytosol and loses the “protection” of the kinase, which would be typically positioned next to it. Furthermore, a single point mutation K1648R (kinase-dead mutant, K1646R for the murine mutant) elicited a reduction of current inhibition by Mg-ATP and Mg-GTP. This in turn, highlighted the importance of the mutated Lysine residue as an interaction site for nucleotides and confirms the hypothesis mentioned above (Schmitz et al. 2003, (Yamaguchi et al., 2001). Some molecules modulate TRPM7 channel activity, such as cAMP (cyclic adenosine mono-phosphate) which indirectly modulates current activity since it regulates intracellular Mg^{2+} and Mg·ATP. This was shown by deletion or site directed mutagenesis of the kinase domain (Takezawa et al., 2004). Furthermore, phosphatidylinositol 4,5-bis-phosphate (PIP_2), for instance, maintains steady state current levels or inhibits currents when it is depleted

(Runnels et al., 2002). All of these insights taken together elucidate a role for TRPM7 as sensor of different chemical or physical changes.

In summary, TRPM7 channel and kinase interact with each other and influence each other's regulation, thus determining individual biological functions, which still need further investigation, particularly since they seem dependent on cell type and context (Yee et al., 2014).

1.2.4. TRPM7 regulates various cellular processes

In one of the first studies wherein the authors correlated TRPM7 to cellular Mg^{2+} homeostasis, they also attributed a regulatory role to the kinase domain with respect to the channel activity. Both domains contain regions, facilitating the negative feedback loop exerted by Mg^{2+} (Schmitz et al., 2003). Jin et al. further identified an essential role for TRPM7 in mammalian cell survival (Jin et al. 2008), Ryazanova et al. offered further insight into the role of TRPM7 in Mg^{2+} homeostasis (Ryazanova et al. 2010). In this study, they reported inhibition of cell proliferation in TRPM7 deficient *ex vivo* derived stem cells (Ryazanova et al 2010), thus confirming data of a previously published report on TRPM7-deficient DT-40 chicken B cells (Sahni and Scharenberg 2008) and studies on cell lines from 2003 (Schmitz et al., 2003). In 2008, Sahni and Scharenberg had already reported a more complete explanation when demonstrating that TRPM7 is essential during the S-phase of the cell cycle, in particular the channel is pivotal for phosphoinositide 3-kinase dependent growth. It is likely that, TRPM7 regulates Mg^{2+} influx during the G1-phase of the cell cycle, when increasing quantities of ATP and other phospho-nucleotides need to bind additional new Mg^{2+} (Sahni and Scharenberg, 2008). The final demonstration elicited how TRPM7-deficient B cells were Mg^{2+}-deficient, but cell viability and proliferation could be rescued by supplementing the external media with Mg^{2+} (Sahni and Scharenberg 2008). Moreover, Mg^{2+} leads to phosphorylation of the translational factor eEF2 through its kinase, which in turn is known to be an mTOR (mammalian target of rapamycin, nutrition regulator) substrate (Wolf et al., 2008).

A recent review published in 2011 summarized different reports investigating TRPM7's role *in vitro* and *in vivo* as Ca^{2+} permeable cation channel in cerebral ischemia and stroke (Bae and Sun, 2011). They speculated that TRPM7 mediates Ca^{2+} influx (NMDA receptors) during the early phase of ischemic stroke, which accelerated the production of reactive oxygen/nitrogen species (Bae and Sun, 2011). Later changes in the environment, such as a decrease in pH and increase of free radicals feedback to further activate TRPM7 and facilitate additional Ca^{2+} influx and thus stroke-related reperfusion injuries. There still

remains an open discussion on a potential protective role of TRPM7 blockade. These findings may link TRPM7 to excitotoxicity, oxidative stress, inflammatory processes and cell death (Bae and Sun, 2011). Further evidence for a role of TRPM7 as a Ca^{2+} channel has been elucidated by Clapham and colleagues in $TRPM7^{-/-}$ embryonic myocardium and sinoatrial node (SAN) cells. TRPM7 ablation *in vitro* intensively reduces spontaneous Ca^{2+} "transient firing rates" and causes down-regulation of Hcn4, Cav3.1, and SERCA2a mRNA. They showed how TRPM7 disruption leads to impaired diastolic membrane depolarization and automaticity, highlighting a possible therapeutic involvement of TRPM7 in cardiac deficiencies (Sah et al., 2013). Recently, Desai et al. discussed a new role for the TRPM7 channel in the Fas-induced apoptotic process where I_{TRPM7} increases upon cleavage of the carboxy-terminus at D1510 by caspase-8. This augmented channel activity strengthens the Fas receptor signaling and Fas-receptor induces apoptosis. They outlined this chain of events after observing that $TRPM7^{-/-}$ T cells do not undergo Fas induced apoptosis. Consequently channel activity is important for Fas receptor-induced apoptotic signaling and thus, apoptosis (Desai et al., 2012).

In addition TRPM7 kinase can autophosphorylate itself at various sites. So far, 39 Ser/Thr sites have been mapped which are likely to be autophosphorylated. Moreover, it has been demonstrated that the TRPM7 kinase can phosphorylate other substrates *in vitro*, for instance, annexin1 (Dorovkov and Ryazanov, 2004), PLCγ2 (phospho-lipase-γ-2) (Deason-Towne et al., 2012), eEFk-2 (eukaryotic elongation factor kinase-2) (Perraud et al., 2011). Deason-Towne and colleagues speculated that TRPM7 plays a role in PLCγ2 activation by ensuring a certain activation level of PLCγ2 via phosphorylation of Ser/Thr sites, resulting in further channel activation (Deason-Towne et al., 2012). Annexin 1 phosphorylation is increased by TRPM7 kinase followed by Ca^{2+} augmentation. Annexin 1 is an anti-inflammatory player in the glucocorticoid cascade and is involved in many other cellular processes such as growth, proliferation and cell death (Dorovkov and Ryazanov, 2004). Recently, it has been shown that calpain and annexin 1 translocations are TRPM7 kinase-dependent, while subsequent MAP phosphorylation was kinase independent (Yogi et al., 2013). Yogi et al. finally demonstrated that aldosterone triggered Mg^{2+} influx and ROS production in a

TRPM7-sensitive, kinase-insensitive manner, whereas activation of annexin-1 was confirmed to require the TRPM7 kinase domain interaction. At the same time, the TRPM7 kinase domain was shown to be essential in the aldosterone pathway towards production of pro-inflammatory mediators. Aldosterone is a well-known renal ion regulator (mainly K^+ and Na^+ but Mg^{2+} as well), which might exert an inflammatory role while modulating TRPM7 channel activation (Yogi et al., 2013).

The eukaryotic elongation factor 2 (eEF2) mediates ribosomal translocation and thereby regulates protein translation. Its activity can be inhibited by phosphorylation at Thr56, which was thought to be mediated by the TRPM7 kinase. However, the enhanced Thr56 phosphorylation seemed to be regulated only indirectly by TRPM7. In other words, increased eEF2 phosphorylation occurred via affecting the amount of eEF2's cognate kinase eEF2-k, involving its phosphorylation at Ser77 by the TRPM7 kinase domain (Perraud et al., 2011).

Clark and colleagues showed that TRPM7 affects actomyosin contractility by phosphorylation of myosin IIA heavy chain via regulation of Ca^{2+} (Clark et al., 2008). Therefore, TRPM7 might be implicated in cell adhesion and infiltration of leucocytes through the endothelium allowing immune cells to reach the inflamed tissue. Conflicting results have been obtained on vascular endothelia: the silencing of channel activity enhanced growth, proliferation and synthesis of nitric oxide via ERK engagement in HUVECs (human umbilical vein vascular endothelial cells)(Baldoli and Maier, 2012), nonetheless, it caused a blockade of growth (G1 phase) and the migration of HMEC (human microvascular endothelial cells) (Baldoli et al., 2013; Baldoli and Maier, 2012). TRPM7 could play an essential part in the regulation of immune responses via controlling cell adhesion and trafficking through the endothelium.

TRPM7 also seems to be involved in hyperglycemic damage, where interestingly, a high glucose-induced decrease of ERK 1/2 synthesis could be prevented via silencing of TRPM7 (Sun et al., 2013). Here, TRPM7 seems to be implicated in cell death and injury as described for HUVECs (Yee et al., 2014)(table) and neurons (Bae and Sun, 2011) and many other cell types including immune cells (Desai et al., 2012).

In summary, TRPM7 has been indicated as critical for the viability of mammals, embryonic development (Ryazanova et al., 2010), cell viability and proliferation (Schmitz et al., 2003), growth (Sahni and Scharenberg, 2008) as well as apoptosis (Desai et al., 2012).

1.2.5. Ion channels, Mg^{2+} and Ca^{2+} in immune system homeostasis

Several extracellular and intracellular signaling molecules finely tune the immune system. These include ions, at the smallest molecular level. Ca^{2+} ions, for instance, are well known for their role in immune cell signaling and a defect in Ca^{2+} signaling leads to human immunodeficiencies. The most prominent regulator of intracellular Ca^{2+} signaling in immune cells is the CRAC (Ca^{2+} release activated Ca^{2}) channel, which is also the most important regulator of T cell priming (Fig. 3) (Feske et al., 2010). Other ion channels implicated in T cell activation specifically modulate membrane potential and thus sustain the driving force for Ca^{2+} influx. These channels cooperate to maintain the intensity and duration of the Ca^{2+} signal. Accordingly, ion channels, such as TRPM4 interplay with potassium channels (Kv1.3 and $K_{Ca}3.1$) and chloride channels (Cl_{swell}) to regulate the membrane potential and thus contribute to the characteristic Ca^{2+} oscillations essential for T cell activation (Cahalan and Chandy, 2009; Feske et al., 2012).

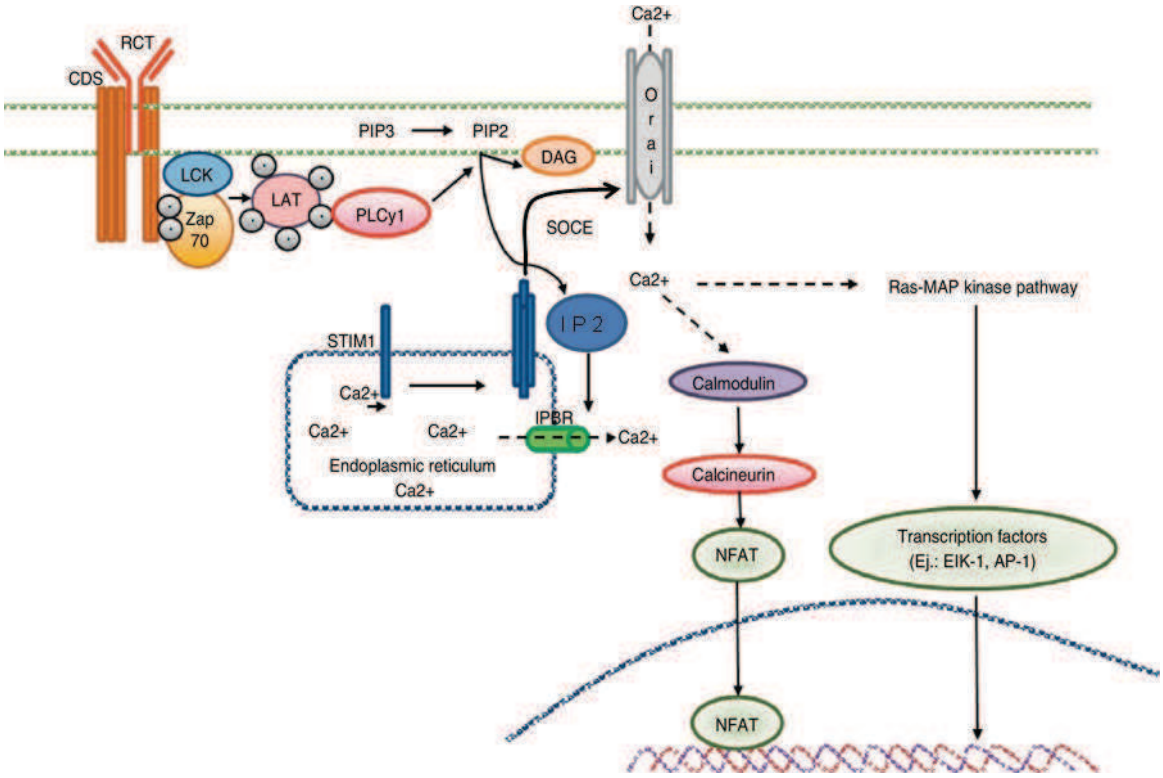

Figure 3: Calcium signaling triggered by the T cell receptor (RCT) complex (CDS are accessory molecules for instance CD3 and CD4) stimulation. When T cells recognize their antigen, the TCR signaling cascade is activated, which leads to the activation of PLCγ1 and the generation of IP_3 and DAG via PIP2 (Phosphatidylinositol 4,5-bis-phosphate) hydrolysis. IP_3 binds to the IP_3 receptor, located in the endoplasmic reticulum (ER) resulting in the efflux of calcium from the ER, the intracellular calcium store. STIM2 and STIM1 via their N-terminal region towards the lumen of the ER sense the reduction in calcium levels, aggregate in groups and permit extracellular calcium entry via the CRAC channel, Orai1. Sustained increase of the intracellular calcium concentration activates NFAT via calmodulin and calcineurin, as well as the Ras-MAP kinase pathway. PLCγ1 (phospho-lipase-C-γ1), IP_3 (inositol-trisphosphate), DAG (diacylglycerol), LAT (linker for activation of T cells), PIP2 (Phosphatidylinositol 4,5-bisphosphate), STIM (Stromal interaction molecule), CRAC (Calcium-release activated channel), NFAT (Nuclear factor of activated T-cell), MAP (Mitogen activated protein) and Zap70 (ζ-chain associated protein kinase of 70 kDa). Figure from Izquierdo et al. (2014). Published with permission of the Publisher. Original source: Izquierdo, J.H., Bonilla-Abadia, F., Canas, C.A., and Tobon, G.J. Calcium, channels, intracellular signaling and autoimmunity. Reumatol Clin. 2014;10:43-7.

Also other ion channels could potentially contribute to the fine-tuning of immune cell signaling and activation. TRPM7, for instance, like TRPM4, might coordinate immune responses by being part of an entire ion channels network.

The role of TRPM7 in immune cell signaling has not been clarified, although the ability of Mg^{2+} in modulating the activity and efficiency of immune responses is well established. Therefore, as TRPM7 is a Mg^{2+} channel highly expressed in cells of the immune system, it might facilitate some of the interactions involving Mg^{2+} (Sahni and Scharenberg, 2008).

A recent review summarized several studies indicating a role of Mg^{2+} in regulating immune responses. Mg^{2+} has been shown to be a Ca^{2+} counter-player. Systemic Mg^{2+} homeostasis is strictly controlled and maintained via intestinal absorption and urinary tract depletion. Mg^{2+} acts as a critical molecule in the brain, skeletal muscles and heart, its deregulation affects brain diseases such as migraine, depression and epilepsy. It also acts as a cooperator in synaptic excitation, modulating N-methyl-D-aspartate receptor excitability. It also influences myocardial contractility and ion channel activity in the heart. In skeletal muscle cells, Mg^{2+} competes with Ca^{2+} for the binding sites on proteins responsible for muscle contraction resulting in hyper-contractibility in case of hypomagnesemia, where it is replaced by Ca^{2+} more easily. Mg^{2+} is capable of antagonizing Ca^{2+} specifically in the pancreas, thus modulating signaling cascades and enzyme secretion. In bones it is pivotal for formation and size of crystals and in osteoblast proliferation (de Baaij et al., 2015). When considering Mg^{2+} in immunity Feng-Yen Li and colleagues elicited a role for intracellular free Mg^{2+} by analyzing a mutation within the gene of the MagT1 transporter. They demonstrated that the abrogation of the corresponding gene for the transporter nullifies Mg^{2+} influx resulting in inefficient antigen receptor engagement and subsequently impaired Ca^{2+} influx as well as improper activation of PLCy1 (Fig. 4) (Li et al., 2011). Additionally, Baaij et al. hypothesized a role for both TRPM7 and MagT1, explaining they might take over similar tasks on different cell types. However, no evidence was provided so far for separate or shared roles in Mg^{2+} regulation (de Baaij et al., 2015). Sugimoto and colleagues indicated a role for Mg^{2+} as regulator of cytokines. In detail, they proposed a correlation between Mg^{2+} up-take and a decrease in inflammatory cytokine production showing that

neonatal monocytes exposed to $MgSO_4$ decreased cytokines production. If intracellular Mg^{2+} can directly influence cytokines it can indeed affect disease pathogenesis (Sugimoto et al., 2012).

In line with these immunological reports a tissue specific deletion of TRPM7 in thymocytes resulted in altered synthesis of many growth factors and in turn caused defects in the differentiation and maintenance of thymic epithelial cells (Jin et al., 2008). Moreover, it caused a disruption of thymopoiesis with a block of thymocyte differentiation at the double negative stage and a progressive depletion of thymic medullary cells. The lymphocyte development was blocked at the $CD4^-CD8^-$ stage, which resulted in a reduced $CD4^+$ and $CD8^+$ mature naïve T cells in the thymus (Jin et al., 2008). Thus, they provide scientific evidence that TRPM7 is crucial for the complete development and activity of lymphocytes.

Accordingly, based on these reports we speculate that TRPM7 is involved in the regulation of the immune system. As TRPM7 is the only known Mg^{2+} conducting ion channel expressed in T cells, we hypothesize a crucial role in T cell physiology, maybe similar to MagT1.

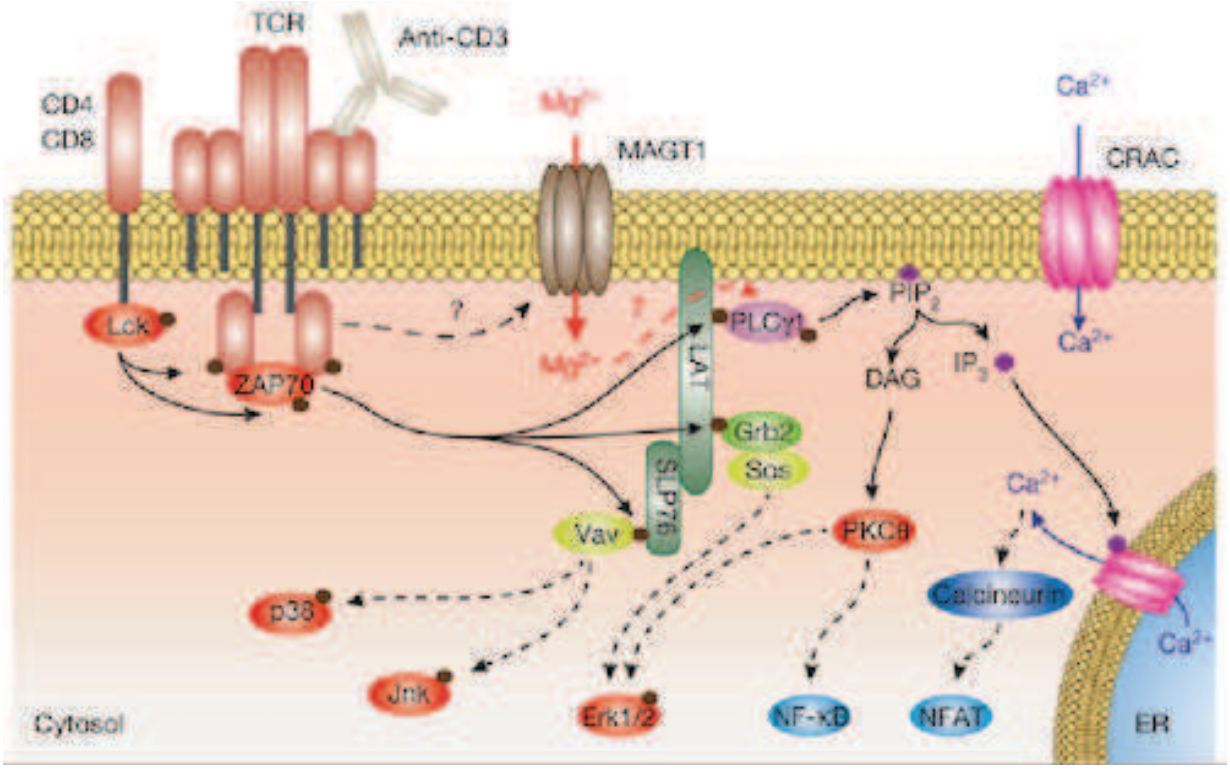

Figure 4: T cell priming due to TCR stimulation and the possible role of MagT1 in Mg^{2+} regulation. This image depicts a hypothetical regulatory mechanism for Mg^{2+} entry during T cell receptor stimulation and involvement of a recently identified Mg^{2+} transporter, MagT1. Not only

Ca^{2+}, but also Mg^{2+} is pivotal during T cell activation and thus for immune system regulation. TCR priming induces MagT1 opening, thus further causing an increase in $[Mg^{2+}]_i$, PLCγ1 activation and Ca^{2+} influx. The underlying mechanisms that connect TCR activation with MagT1 opening and PLCγ1 activation are still not completely understood, although MagT1 intracellular amino terminus is likely considered the linking element which might help TCR-dependent MagT1 activation. Dotted arrows indicate indirect effect and solid arrows report direct effects. ER (endoplasmic reticulum), Erk1/2 (extracellular signal–regulated kinases), Grb2 (growth factor receptor-bound protein 2), InsP3R (inositol-1,4,5-trisphosphate receptor), LAT (linker for activation of T cells), LcK (lymphocyte-specific protein tyrosine kinase), NFAT (nuclear factor of activated T-cells), NF-kB (nuclear factor kappa-light-chain-enhancer of activated B cells), PKC (protein kinase C), SLP76 (leukocyte protein of 76 kDa), Sos (son of Sevenless), STIM1 (stromal interaction molecule 1), Jnk (c-Jun N-terminal kinases) and ZAP70 (ζ-chain-associated protein kinase of 70 kDa. Figure from Li et al. (2011). Reprinted by permission from Macmillan Publishers Ltd: [Nature] (Li et al. , 2011), copyright (2011)

1.3. Immune system regulation

„*The immune system is a complex of processes within an organism that protects against disease. To function properly, an immune system must detect a wide variety of agents, known as pathogens, from viruses to parasitic worms, and distinguish them from the organism's own healthy tissue. The immune system can be classified into subsystems, such as the innate immune system versus the adaptive immune system, or humoral immunity versus cell-mediated immunity*.“

(Beck G, Habitat GS (November 1996). "Immunity and the Invertebrates". Scientific American 275 (5): 60–66. doi:10.1038/scientificamerican1196-60. Retrieved 1 January 2007)

The immune defense is mediated by an early reaction of the innate immunity and a later response of the adaptive immunity. The first cellular and biological reaction is in place even before an infection spreads. In order to respond rapidly and effectively the innate immunity always follows the same measures. The adaptive immunity instead, is stimulated by exposure to antigens and increases in magnitude and defensive capability with each new exposure. Its activity is very specific for each molecule and has an ability to “remember“ and respond more vigorously to contacts with the same microbes. Considering all components of the innate and adaptive immune system and their anatomic location, it is also possible to define different regional immunity subtypes, where the largest two regional immune systems are the gastrointestinal tract and the skin (Abbas et al., 2012e).

1.3.1. Immune cell signaling

As introduced above, the immune system works to protect the body from pathogens. It functions on three different levels of defenses: 1) a physical barrier (skin and epithelium), 2) a non-specific activity of the innate immunity and eventually, if necessary 3) a more specific reaction of the adaptive immunity. The

immune system can be considered in tight control and equilibrium between pro-inflammatory and anti-inflammatory events, where different cell subtypes interact accordingly to the hostile stimuli they receive (Abbas et al., 2012b). Under physiologic conditions the immune system regulates itself very precisely, by coordinating highly complex and finely developed interactions. In this picture, cytokines and their counterparts, the cytokine inhibitors, control and modulate other potential injurious elements and their effects, avoiding excessive inflammatory reactions (O'Garra and Vieira, 2004). In this sense, the cytokine milieu is an important factor implicated in the communication between T cells, macrophages and other immune cells during immune cell recruitment. In detail, during T cell-macrophage interaction the profile of cytokines secreted is relevant in T cell differentiation, towards T-helper cells 1 or 2 (Th1 or Th2). Furthermore, the different activities exerted by T cells are controlled by the cytokine profile they secrete themselves. Thus, T cell subsets were named as Th1 and Th2 and they were found to secrete IFNγ, IL-2, TNFα and IL-4, IL-10, IL-13, respectively (Fig. 5) (Belardelli, 1995). More recent studies helped to identify new additional T cell subsets such as T follicular helper cells (TFH), Th17, Th9, Th22 and regulatory T (Treg) cells. These new findings and the wider cytokine secretion profile shared between the different subsets forced the scientific community to reconsider the commonly accepted T cells subdivision. Thus, T cells are now considered as a more plastic population of cells, which are capable of repolarization and are often identified by their peculiar gene transcription program (Fig. 5) (Baumjohann and Ansel, 2013; Sakaguchi et al., 2013). Treg are one of the major critical actors, since they help maintain self-tolerance and immune system homeostasis (Sakaguchi et al., 2010). When an acute inflammation takes place IL-1(α and β), TNF-α , IL-6, IL-17 and other cytokines play an important role in modulating the pro-inflammatory response (Risbud and Shapiro, 2014; Wojdasiewicz et al., 2014), while other cytokines like IL-4, IL-10, IL-11 and IL-13 normally promote an anti-inflammatory response (Risbud and Shapiro, 2014; Wojdasiewicz et al., 2014). In this case, cell functions such as, protein expression and release, need to be very tightly regulated in order to avoid excessive responses. For instance, macrophages normally produce interferons (IFNs), TNF-α, IL-10 and IL-12 and T cells produce IFNs, IL-2, IL-4, IL-10, IL-13 and TGFβ. The latter cytokines are released during macrophage-T cell interactions, and drive the reaction in the

direction of Th1 or Th2 subtypes and respective subtype of immune responses. More specifically, Th1 cells interact with macrophages via production of IFN-γ, IL-2 and TNF-α. Th2 cells, instead abrogate macrophage activity synthetizing IL-4, IL-10 and IL-13. Especially IL-12 production from macrophages promotes Th1 differentiation. Its production can be abrogated by IL-10 and IL-4, whereas IFN-γ stimulates IL-12 production (Fig. 5) (Belardelli, 1995). The complex network and the large amount of these soluble factors regulating immune cell reactions offer only a vague idea of the entire system of necessary interactions for the maintenance of a balanced immune system.

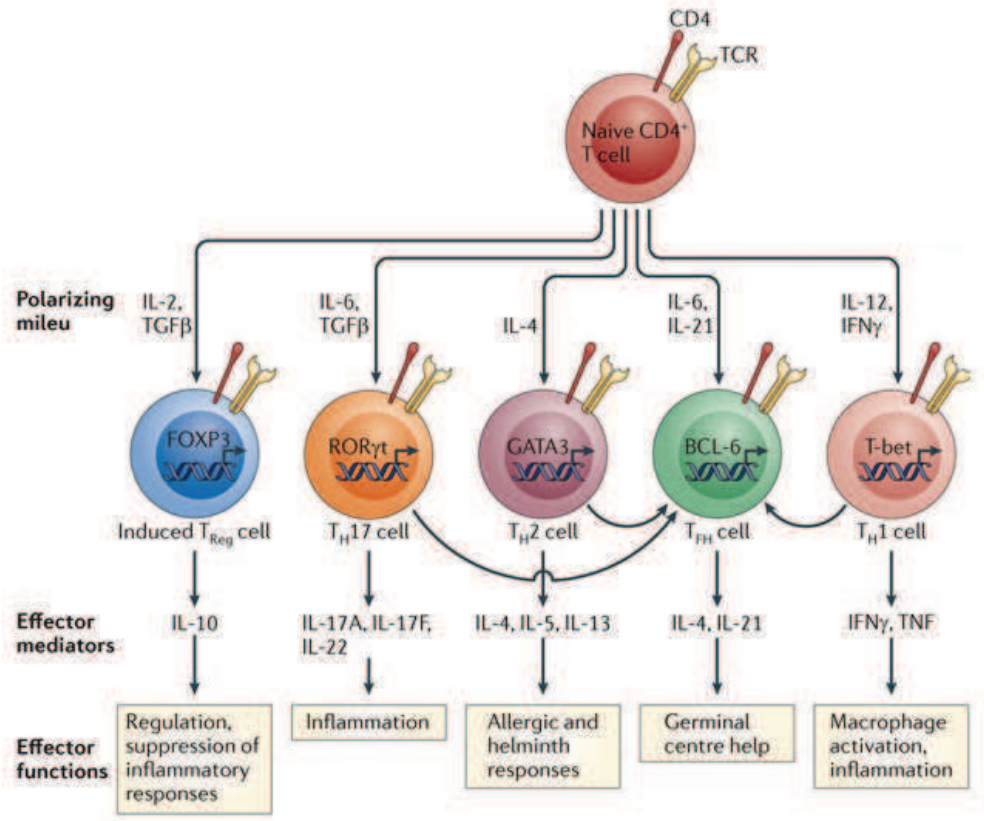

Figure 5: **Naïve CD4$^+$ T cell differentiation and replication into different T helper cell (Th) sub-families.** Right after encountering an antigen presented on an antigen-presenting cell (APC), T cells undergo different polarization mechanisms in order to exert distinct protective immune responses. The polarizing milieu is the key stimuli during T cell receptor (TCR) activation. It indicates to T cells which subset they need to differentiate into (Treg, Th1, Th2, TFH and Th17). Subsequently, activated T cells express certain transcription factors also according to their surrounding milieu. Interferon-γ, interleukin-4 (IL-4) and IL-17 are routinely referred to as signature cytokines for Th1, Th2 and Th17, respectively, but the fact that certain plasticity exists within the effector subtypes *in vivo* is more and more accepted. Moreover, certain cytokines can be released from different cell populations. Furthermore, all these primed CD4$^+$ T cells are

characterized from the capacity of memorizing their effector functions and produce respective cytokines when necessary. TFH and Treg instead, are more frequently distinguished by their functions than by their cytokine profiles. (BCL-6, B cell lymphoma 6; EOMES, eomesodermin, FASL, FAS ligand; FOXP3, forkhead box P3; GATA3, GATA-binding protein 3; RORγt, retinoic acid receptor-related orphan receptor-γt; TCR, T cell receptor; TGFβ, transforming growth factor-β; TNF, tumour necrosis factor). Figure from Swain et al. (2012). Reprinted by permission from Macmillan Publishers Ltd: [Nature Reviews Immunology], (Swain et al., 2012), copyright (2011)

1.3.2. Mast cells

Mast cells are a relevant component of the innate immunity. They were identified already more than a century ago and they are still of great interest for the scientific community. Mast cells were categorized as essential players in the allergic reaction, but recently new evidence outlines a broader function (Abraham and St John, 2010). These hematopoietic cells mature in the bone marrow and leave to circulate in the blood. They further mature passing into different tissues, where they encounter growth factors like stem cell factor (SCF) and interleukin-3 (IL-3). Adult mast cells are typically located at sites that are host-environment interfaces such as skin, mucus and mucosal tissues (Wernersson and Pejler, 2014). Thus, they actively take part in inflammatory processes by detection of pathogens and subsequent recruitment of lymphocytes and other immune cells (Abbas et al., 2012b). It is known that mast cells can prime both innate and adaptive immune responses orchestrating “complex cellular migration within tissues, from the blood and in distant lymph nodes”. They mainly store and release mediators to prime immune responses (Abraham and St John, 2010). Mast cells can exert such tasks via expression of proteases, vasodilating substances (such as histamine), various cytokines, pro-inflammatory chemokines and lipid mediators.

1.3.3. Antigen Presenting Cells

The core of inflammatory reactions (triggering the activation of adaptive immunity) is the antigen presentation and recognition where APCs (Antigen Presenting Cells) internalize (via phagocytosis) and present antigen particles to naïve T cells (Fig. 6). Antigens are potentially harmful elements for the host, and can originate from self or non-self elements. Two different types of presenting molecules, the Major Histocompatibility Complex (MHC) class I (MHCI), and class II (MHCII) exit and differ in structure and function. T cells are normally categorized into the two different families $CD4^+$ and $CD8^+$. $CD4^+$ helper T cells recognize class II MHC molecules, whereas $CD8^+$ T cells recognize class I MHC molecules with bound peptides (Abbas et al., 2012d). MHC class I molecules are expressed on every mammalian cell, not only on APCs. More specifically, naïve $CD4^+$ T cells can be activated or efficiently primed only from a specific subset of cells, which express the MHCII, as the co-receptor on CD4 which specifically recognizes MHCII molecules. This complex interaction is necessary for antigen recognition at the surface of APCs. MHC II expressing cell lineages are macrophages, dendritic cells (DCs) and B cells.

The MHC function is presenting the processed antigens (previous pathogen) in the form of a peptide at the surface of APCs such that the respective TCR (T cell Receptor) can recognize the peptide once in contact with MHC. Consequently, a naïve T cell gets primed to shape an adaptive immune response. APCs not only interact via the TCR-MHC binding, but also express co-stimulatory molecules such as CD80 or CD86 to optimize T lymphocyte activation (Fig. 6) (Abbas et al., 2012d). Most likely APCs are able to encounter antigens in the GALT (Gut Associated Lymphoid Tissue) where microbes interact with the epithelium and this in turn can actively control APCs function. APCs and luminal microbe interactions result in modification of the local milieu such as cytokines, chemokines and other factors, which affect T cell differentiation. Dendritic cells (DCs) can promote T cell differentiation into Th17, Treg, Th1 or Th2 according to the composition of the surrounding milieu (Swiatczak et al., 2011).

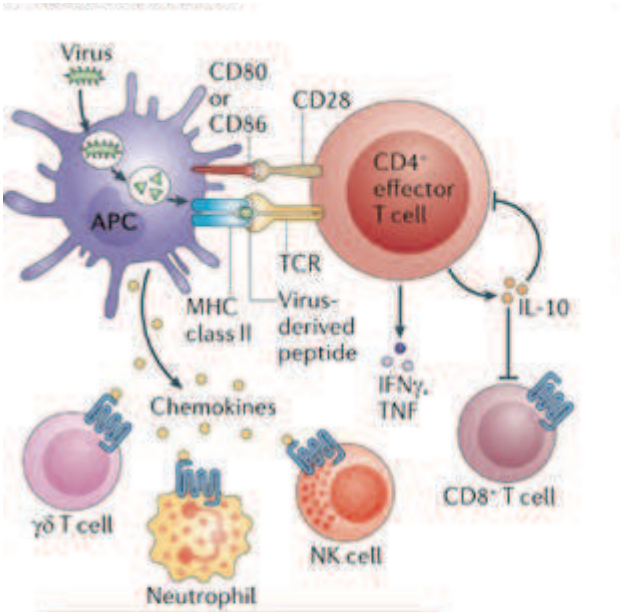

Figure 6: Antigen presentation and recognition from naïve T cells. $CD4^+$ naïve T cells are meant to recognize the antigen presented on the antigen presenting cells (APCs) as soon as they reach the site of infection. They subsequently produce a variety of cytokines that characterize the type of infection that takes place *in loco*. As mentioned above, cytokines influence and orchestrate the immune reaction and can organize a pro-inflammatory response or even suppress it. Usually the cytokine milieu also revokes other cells to participate in the immune response. Figure from Swain et al. (2012). Reprinted by permission from Macmillan Publishers Ltd: [Nature Reviews Immunology], (Swain et al., 2012), copyright (2011).

1.3.4. Function and differentiation of T cells

B and T lymphocytes develop into specific subpopulations with typical functions and phenotypes. This is the way the adaptive immunity acquires its peculiar specificity.

B and T cell precursors originate in the bone marrow where B cells also mature. B cells enter the lymphatic system and are then activated in the marginal zone of lymph follicles of a lymph node by $CD4^+$ T cells, while T cells develop into $CD4^+$ and $CD8^+$ T lymphocytes and γδ T cells in the thymus. Here, T cell precursors are double negative, which means, they do not express CD4 nor CD8 (i.e. $CD4^-$ $CD8^-$). Then they turn into double positive $CD4^+CD8^+$ T cells expressing both co-receptors. T cell development undergoes one more step when T cells become single positive, either $CD4^+$ or $CD8^+$, loosing either CD8 or CD4 expression respectively. This happens as soon as the TCR encounters MCH class I or II. Remaining double positive T cells are negatively selected, while single positive cells further differentiate into either naïve $CD4^+$ or $CD8^+$ and leave the thymus towards lymphoid tissues (Abbas et al., 2012c). $CD8^+$ T cells are also identified as cytotoxic T-lymphocytes (CTL) since they defend against viruses, bacteria and tumor cells. They bind the α3 region of the MHC I complex of virus-infected or cancerous cells. These CTLs exert their cytotoxic activity by producing cytokines, primarily TNF-α and IFN-γ, or releasing cytotoxic granules which induce apoptosis of pathogens or infected cells. A third major defense strategy is called fratricide inducing cell apoptosis via Fas/FasL induction. Fratricide is mainly useful for settling an immune response by CTLs killing each other (Online British Society for Immunology, (Wissinger, 2016)).

As previously described the activation of $CD4^+$ T cells instead, takes place after TCR-peptide recognition on MHC II of APCs. Each stimulus needs a co-stimulatory signal in order to finally activate an immune cell. In the case of naïve $CD4^+$ T cells this is mostly CD28 which binds to CD80 or CD86 expressed on mature DCs. Subsequently, a somatic rearrangement of the antigen receptor gene segments is triggered and the initial pre-antigen receptor is substituted with an *ex novo* expressed TCR. Following rearrangement of TCR, cytosolic signals

and nuclear phases are extremely specific according to the affinity of the presented antigens. All these events are fundamental for the survival, expansion and maturation of developing lymphocytes. Differentiation into one of the several subsets of T cells finally takes place in the peripheral lymphoid organs where they encounter the antigen presented from mature DCs, become antigen-specific lymphocytes, proliferate (clonal expansion) and differentiate into effector and later into memory T cells. Effector T cells are responsible for the depletion of microbes, inflammation, but also tissue damage. Memory T cells persist after T cell responses and promptly react to the same antigen ensuring a life-long immunity.

When T cells receive the stimulus from an antigen they modify the expression of surface molecules, synthetize cytokines and cytokine receptors. If a host is suffering from an infection IL-2 is the most important cytokine. It is highly expressed during T cell differentiation and stimulates proliferation as well as differentiation. However, maintenance of memory T cells is connected to IL-7 and other cytokines (Abbas et al., 2012a). A recent review focused on the notable role of the gut in imprinting and shaping proper immune system activation. Here, cytokines such as TGFβ and IL-6 produced by DCs and intestinal epithelial cells tune T cell differentiation leading to the differentiation of Th17 cells, while TGFβ and RA (Retinoic Acid) trigger polarization of Treg. A specific DCs subset responds to thymic stromal lymphopoietin (TSLP) inducing Th1 and Th2 cells or, alternatively, in co-presence with RA and TGFβ boosts tolerogenic responses (Roan et al., 2012).

1.3.5. Gastrointestinal immunity

"The gastrointestinal immune system must cope with the presence of trillions of commensal bacteria in the gut lumen by preventing their invasion and tolerating their presence in the lumen while also identifying and responding to numerically rare pathogenic organisms." Abbas et al. (2012f).

Mucus produced and secreted by goblet cells is the first protective barrier of the gut-associated lymphoid tissues (GALT) where its stickiness and viscosity can easily trap pathogens. Underneath it, mucosal epithelial cells are in tight contact with each other, thus blocking microbes from infiltrating. Located below the epithelial lining in the lamina propria there are innate immune effector cells like macrophages, dendritic cells and mast cells (Fig. 7). The intraepithelial γδ T cells also provide innate defense activity. Commensal bacteria efficiently protect from foreign pathogens as well. They are in direct competition with pathogens for nutrients and modulate the immune system activity (Kamada et al., 2013).

Further, specialized anatomic sections of the adaptive immunity are lymphoid tissues such as, Peyer´s patches in the ileum, and similar collections of cells in the colon. Here, immune cells pass through all different tissues with the intent of encountering an antigen, differentiating and spreading the stimuli for a proper immune response. Together with the gut epithelium and Peyer's patches, the mesenteric lymph nodes also belong to the GALT.

Effector B and T cells are able to enter the circulation after activation and differentiation in the GALT. T cells selectively migrate back to the intestinal lamina propria. This selective migration is due to signals that naive T cells receive from DCs, for instance, retinoic acid, TGFβ and interleukins, such as IL-2. This interplay will result in the stimuli expressing chemokine receptors and adhesion molecules on effector T cells determining their recruitment back to the gut. The $\alpha_4\beta_7$ is the most well-known gut-homing molecule. It binds to mucosal addressing cell adhesion molecule-1 (MADCAM-1) which is expressed on cells of the endothelium in the lamina propria to enable T cells to shrink in order to pass the endothelium in both directions (Fig. 7). C-C motif chemokine receptor-9 (CCR9) is another chemokine receptor responsible for gut-homing and binds to CCL25 produced by intestinal epithelial cells. Both proteins, MADCAM-1 and CCR9 are essential and very specific for gut recruitment (Gorfu et al., 2009).

Immunoglobulin A (IgA) is also an important component of the mucosal immune defense. Its secretion into the lumen helps to neutralize the activity of potential pathogens. B cells are activated by T cells and differentiate into plasma cells in mesenteric lymph nodes or Peyer's patches. They migrate to the lamina propria, where they release IgA.

The adaptive immunity is regulated via fine-tuning of the activity of different T cell subsets and cytokine secretion. For instance, changes in the bacterial composition can influence the balance between different helper T cell responses. T cells are found within the gut epithelial layer throughout the lamina propria and sub-mucosa and within Peyer´s patches and other organized follicular collections. DCs are also abundant in the gastrointestinal defense system, where they are mainly considered to be capable of inducing protective effector T cell differentiation or regulatory T cell (Treg) differentiation which suppress immune responses. Recent publications showed that they could be divided into groups depending on their functions, for instance $CD103^+$ DCs. Here, the integrin, also known as $\alpha_E(CD103)\beta_7$ is one of the central proteins for gut immune homeostasis. Specifically, $CD103^+$ DCs migrate from skin, epithelia, gut and lung tissues to the corresponding closest lymphoid compartments, where they imprint the T cells inducing their expression of $\alpha_4\beta_7$ and CCR9. In addition, it was shown that the same DC subfamily efficiently stimulates tolerance by activation and stimulation of differentiation of naive T cells into $Foxp3^+$ regulatory T cells (Treg) (del Rio et al., 2010).

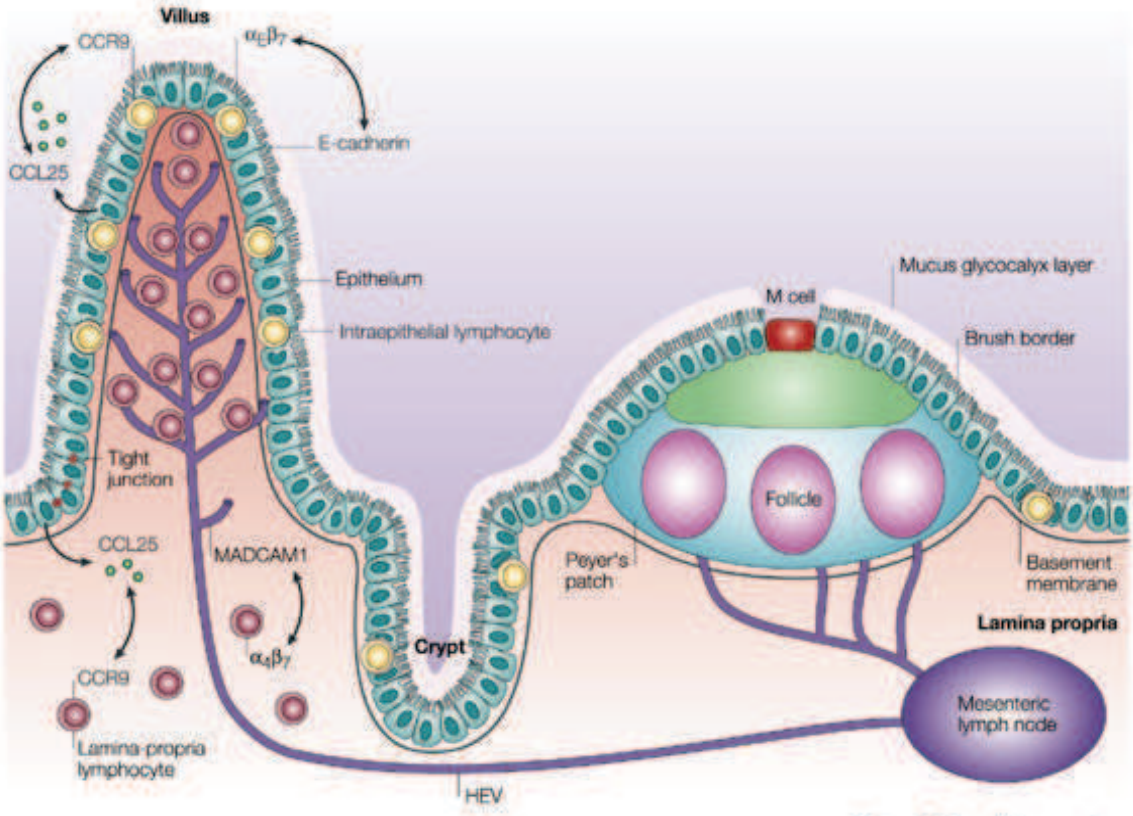

Figure 7: Gut associated lymphoid tissues (GALT) and organs, their disposition in the gastro intestinal tract and gut-homing proteins. The external layer is composed of epithelial cells which are hosting and retaining T cells (Intraepithelial Lymphocytes) and M cells known to favor transport of microbes and particles from the gut lumen to the lamina propria so interactions with immune cells can be initiated. The lamina propria (red) is the tissue located underneath the epithelium (green layer) hosting the Peyer's Patches. Here, also the mesenteric lymph nodes are shown (purple). In this image the most important gut-homing proteins expressed on T cells are indicated $\alpha_4\beta_7$ and α_E(CD103)β_7. CCR9 (C-C motif chemokine receptor-9), CCL25 (C-C motif chemokine ligand 25), MADCAM (mucosal addressing cell adhesion molecule-1), HEV (high endothelial venules). Figure taken from Cheroutre and Madakamutil (2004). Reprinted by permission from Macmillan Publishers Ltd: [Nature Reviews Immunology], (Cheroutre and Madakamutil, 2004), copyright (20)

Recently, molecular biological studies identified mechanisms of intracellular pathways that lead to the expression of these important gut-selective molecules. NFAT (nuclear factor of activated T cells) has been described as one of the potential signaling proteins involved. Hermann-Kleiter and Baier reported that NFAT functions as control master of transcription factors for cytokine expression and their correspondent receptors. In this way NFAT regulates the crosstalk between TCR and other receptors required in innate as well as adaptive immunity (Hermann-Kleiter and Baier, 2010). Similarly, Mokrani et al. showed that NFAT and SMAD (small mother against decapentaplegic) cooperate in the induction of CD103 expression in $CD8^+$ T cells in the presence of TGFβ (Mokrani et al., 2014).

One of the most important characteristics of leukocytes is that they are able to rapidly adapt their shape according to environmental conditions. This enables them to translocate very quickly to and from different tissues. They can benefit from actomyosin contraction and mediation (adhesion-dependent migration) when the formation of focal adhesion permits the cell to anchor to the extracellular matrix, notably through αV integrin (Weninger et al., 2014). Alternatively leucocytes can take advantage of a "flowing and squeezing migration" which not necessarily requires integrin intervention. Some studies better defined integrins as anchors meant to confine and retain lymphocytes. These mechanisms help leukocytes to rapidly migrate in any 2D or 3D dimensions (Lammermann et al., 2008).

All these studies underline the singularity of the immune system specifically in the gastrointestinal region. Hence, it should be taken into consideration more often that the gut homeostasis has implications for the regulation of the entire immune system (Kamada et al., 2013).

2. Aim of the thesis

So far many different research projects have focused on gaining a better understanding of the role of TRPM7 in cell physiology. The TRPM7 channel is involved in immune regulation, since it is important for cell survival and development of different types of immune cells (Jin et al., 2008; Sahni and Scharenberg, 2008; Schmitz et al., 2003). TRPM7 does not only harbor an ion channel pore, but is also a functional kinase domain, whose role is still largely unknown. The TRPM7 kinase is implicated in the phosphorylation of different substrates that are important during inflammatory processes. Two of the known *in vitro* kinase substrates are: PLCγ2 and Annexin 1 (Deason-Towne et al., 2012; Dorovkov and Ryazanov, 2004; Yogi et al., 2013).

Interestingly, the TRPM7 protein has been implicated in the regulation of the immune system (Jin et al., 2008), but the role of TRPM7 kinase in T cell survival, regulation and development is so far unexplored. Thus the **aim of my thesis was to shed light on the role of the TRPM7 kinase in the immune system**, utilizing a **novel mouse model**, where a **single point mutation abrogated the kinase activity**. We will study the effect of the lack of kinase activity on the activity and regulation of the TRPM7 channel. Further, we will investigate the effect of the kinase-deficiency on the regulation of the immune system. Using molecular biological techniques, we finally will elucidate a potential role of the TRPM7 kinase in these processes. In summary, we will show that the TRPM7 kinase is implicated in TGFβ signaling cascades via regulation of SMAD2 phosphorylation, which is important for T cell activity.

3. Material and methods

3.1. Material

Refer to Appendix 1 and 2.

3.2. Methods

TRPM7$^{KR/KR}$ mouse model

TRPM7$^{KR/KR}$ (K1646R mutant) mice were obtained from RIKEN, Japan (Kaitsuka et al., 2014). In brief, the targeting construct comprised a genomic sequence spanning exons 31-38 of the mouse Trpm7 gene. A triplet code of exon 33 encoding K1646 (AAG) of TRPM7 was changed by a point mutation in AGG coding for R1646 in the targeting vector, which introduces a mutated consensus motif for the restriction endonuclease *Mse*I. For selection of embryonic stem (ES) cell clones, a neomycin resistance cassette (Neo) was introduced in intron 32 and flanked by two LoxP sites. 129/Sv ES cells were electroporated with the targeting construct resulting in a Trpm7Neo allele after successful homologous recombination. Heterozygous recombinant Trpm7Neo ES cells were injected in C57BL/6J blastocysts and Trpm7Neo mutant offsprings were identified and produced using standard approaches. The floxed neomycin cassette was excised via *in vivo* backcrossing the Trpm7Neo mice with Cre-deleter mice expressing Cre recombinase ubiquitously.

Phenotype studies

TRPM7$^{+/+}$ and TRPM7$^{KR/KR}$ mice were weighed at an age of 4-6 weeks. Average weight values were analyzed and plotted as bar graphs.

Mendelian ratio was calculated on a total number of 100 littermates originating from TRPM7$^{+/KR}$ breeding couples. The evaluation of the Mendelian ratio was obtained utilizing a Chi-squared test.

Animal preparation

Male and female 4-8-week-old mice were euthanized using CO_2. Death of the mice was assured by cervical dislocation. The animals were subjected a surgical scrub /sanitization with alcohol after fixing the limbs on a surface using surgical pins to permit the operator to cut the first skin layer, obtaining access to the intra-peritoneal area. Blood and intestine samples as well as lymph nodes were collected or a peritoneal lavage to harvest mast cells was performed. For harvesting peritoneal mast cells HBS (see appendix) was injected into the peritoneal cavity and massaged softly to favor cell detachment. Floating mast cells were then collected together with the peritoneal solution, which was recollected with a surgical syringe. The cell suspension and all harvested organs were kept on ice until further treatment. All experiments involving animals at the LMU in Munich Germany, were performed in accordance with the EU Animal Welfare Act and were approved by the local councils on animal care (permit no. 55.2-1-54-2532-134-13 from District Government of Upper Bavaria, Germany). The use of genetically modified “knock-in” animals was approved by the District Government of Upper Bavaria, protocol no. 821–8763.14.718/1210.

T cell isolation

When peripheral or mesenteric lymph nodes, were collected they were filtered using a 40 µm sieve. This procedure allowed us to collect lymphocytes in modified RPMI (Appendix 2: Reagents, RPMI Modified). The obtained cell suspension was treated as indicated by the manufacturer’s instructions (Miltenyi Biotec Kit; either CD4$^+$ Isolation Kit (Miltenyi Biotec, no. 130-104-454). The procedure was improved by usage of sterile needles fixed at the end of each selective column and the cell

suspension was run twice in the same column, or in a new one, according to the column's cell capacity.

Cell culture

T cells

Isolated T cells were not t kept in culture for a longer period than 5-6 h, for period longer than 5-6 h were kept on ice before proceeding with the experiments.

Mast Cells

After harvesting mast cells, they were kept on ice and centrifuged at 1000rpm for 10 minutes. The supernatant was discarded and cells were resuspended in 1 ml DMEM + 10 % FBS, 1% Pen/Strep. Cells were counted and media was added to obtain a concentration of 7,5x 10^5 cells per mL of media (see Appendix 2: Reagents,) and kept in culture at 37°C, 5% CO_2 in a humidified incubator (Eppendorf) for up to three days.

Patch clamp

Before each experiment, cells were seeded to settle on a poly-D-Lysine (Sigma) coated glass coverslip, which was fixed with silicate on a 35 mm cell culture dish, filled with filtered external patch solution (see appendix). The cell culture dish was fixed in the recording chamber. We used whole-cell patch-clamp recordings which measures membrane currents of the entire cell at a defined, clamped potential, including electric ion current across the cell membrane through open ion channels. Data acquisition was performed using a fully computer controlled EPC-10 amplifier (HEKA) and the PatchMaster software (HEKA). All recordings were corrected for a liquid junction potential of 10 mV between external and internal solution since the

internal solution contained glutamate instead of chloride. A voltage-ramp ranging from -100 to +100 mV over a period of 50 ms was applied. Data were acquired at a frequency of 5 kHz and a holding potential of 0 mV. Capacitive currents and series resistance were determined and corrected before each voltage ramp using the automatic capacitance compensation of EPC-10. The patch glass pipettes (Borosilicate glass, Science products, Hofheim) were pulled to a resistance of 2-4 MΩ, depending on the cell size. As a general rule increasing cell volumes require decreasing diameters of pipette openings and increasing resistance values. After pipette pulling the pipette tip was fire-polished using a Zeitz pipette puller (Zeitz GmbH, Munich, Germany).

In brief, to obtain a successful measurement, a single, healthy looking cell, was chosen using an inverse light microscope (Axio Vert. A100, Zeiss) and camera system (AxioCam MRm, light source (Colibri, Zeiss); Zen 2 Software Zeiss) (see appendix). The Ag/AgCl reference grounding electrode was immersed into the external solution of the cell culture dish with the fixed cells. The glass pipette was filled with internal patch solution and fixed to the patch Ag/AgCl electrode. After plunging the patch electrode into the external solution in order to approach the chosen cell, program 1 is selected to set the potential to zero. The protocol applies a 10 mV voltage-step to enable the calculation of the pipette resistance, which gives an estimate of the tip opening. The patch pipette was positioned next to the cell with the help of the micromanipulator (PatchStar/PatchMan, Scientifica/Eppendorf) (see appendix) while the resistance of opening should increase. As soon as the pipette touched the cell, the operator applied gentle suction to reach a high-resistance on the interface between cell and pipette. This caused a tight sealing of the cell membrane against the pipette tip. This formation is called the cell-attached configuration and is characterized by a resistance of several GΩ and is also referred to as giga-seal. When the seal was formed, program 2 was started to compensate for pipette capacitance. In the last step of the whole-cell configuration protocol the cell membrane was broken between the pipette solution and the cytoplasm by a suction pulse while maintaining the tight seal. Immediately after the break-in, or breaking of the membrane, the program 3 and the ramp protocol were started to measure TRPM7 currents over a period of 300 s. The data were exported with the Fitmaster software (HEKA) and evaluated and analyzed with IgorPro 6.0 (Wavemetrics).

Staining of cells and Flow Cytometric Analysis

Cells of interest were resuspended in a certain amount of Macs Buffer according to the FCR gamma blocking solution protocol (Miltenyi Biotec). Thereafter, the respective amount of antibody conjugated with the fluorochrome of choice was added, as indicated in the Biolegend protocol. Samples were incubated 45- 60 min at 4° in the dark and then excess amount of fluorochrome was washed out by adding at least double the volume of cell suspension solution and subsequent centrifugation. The washing step was repeated two times and cells were resuspended in Macs Buffer and analyzed in the FACS (Guava, Merck-Millipore) via the InCyte Software (Merck-Millipore).

Proliferation assay

96 well plates with round bottom (Sigma) (see appendix) were coated with αCD3 (Bio-X-cell, Hoelzel-Biotech) as well as αCD28 (Bio-X-cell, Hoelzel-Biotech) at 5 µg/mL final concentration and incubated at 37°C in an Eppendorf incubator for 4 hours (alternatively over night at 4°C). Wells were washed three times with normal PBS and $CD4^+$ T cells were seeded at a concentration of $0.5x10^6$ cells/mL. Every day cells were resuspended in their media and 50 µL to were analyzed with the Millipore FACS using the suggested dye (Guava ViaCount, Millipore).

Ca^{2+} Imaging

Quantification of the intracellular Ca^{2+} concentration was performed on freshly isolated $CD4^+$ T cell subpopulations. Cells were resuspended at concentration of 1mio cells/mL in Macs Buffer and 4 µl Fura Red AM (Thermo Fisher Scientific) was added, previously diluted in DMSO at a stock concentration of 1 mM to obtain a final

concentration of 4 µM. Samples were kept in the dark and incubated at 37°, 5% CO_2 for 30 min. After incubation the samples were washed with external solution, prepared as mentioned before, and a small amount of cell suspension, ≅50 µL, were placed on a petri dish from Thermo Scientific Nunc Glass Base Dish, 12 mm diameter of viewing area. All values were recorded at an emission wavelength of 660 nm using dual excitation wave-length of 420 nm and 470 nm and respective ratio was calculated as R (F_{420nm}/F_{470nm}).

Ca^{2+} influx was induced by adding magnetic Dynabeads T-Activator (Invitrogen) (see appendix) coated with αCD3 and αCD28. Cells and beads were incubated for about 3 minutes before starting the recording for 20 minutes.

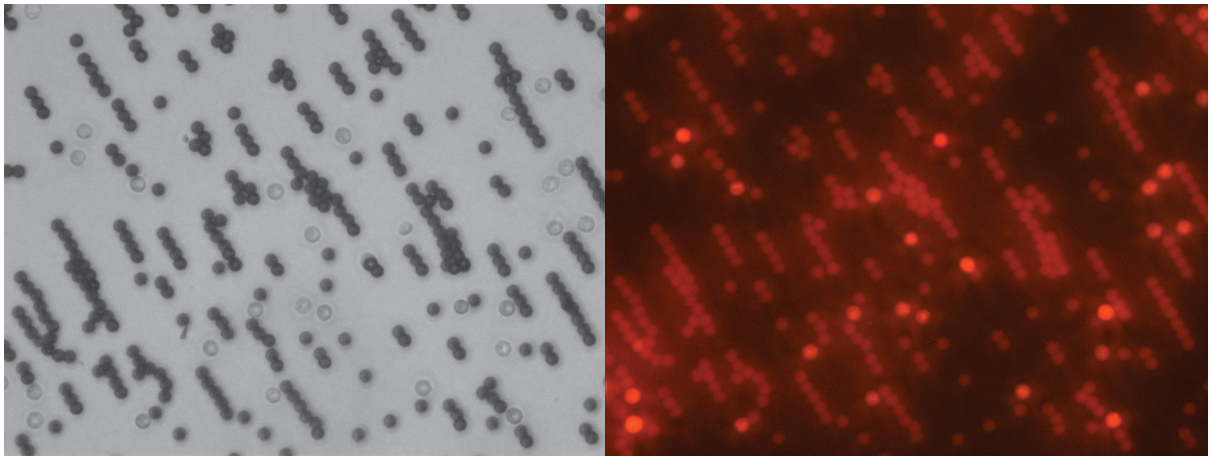

Figure 8: Ca^{2+} imaging performed with beads coated with αCD3 and αCD28. (A) Image obtained with a Zeiss microscope showing freshly isolated $CD4^+$ T cells labeled with Fura-Red and stimulated with magnetic Dynabeads (Invitrogen) (Differential interference contrast, DIC, image) **(B)** The picture shows a representative fluorescent image of Fura-Red-labeled T cells at the beginning of the measurement (excitation wavelength: F_{420nm}; emission wave length: ~660 nm).

ATP detection

For $CD4^+$ isolation we followed the Miltenyi Biotec protocol as previously described. Freshly isolated cells were lysed in 1% Triton X 100 diluted in PBS and treated as suggested in the protocol of the ATP Determination Kit (A22066). The ATP Determination Kit (A22066) contains a bioluminescence assay for quantitative determination of ATP with recombinant firefly luciferase and its substrate D-luciferin.

The assay is based on the requirement of ATP for the production of light by luciferase (emission maximum ~560 nm at pH 7.8). Quantification of ATP was possible by using a microplate luminometer detecting luminescence at ~560 nm, FLUOstar OMEGA (BMG). Data acquisition and evaluation was obtained using the included software (BMG LABTECH).

Inductively Coupled Plasma Mass Spectrometry (ICP-MS)

ALS Scandinavia executed Mass Spectrometry analysis in plasma samples, which were kindly prepared by the laboratory of AG Chubanov (Walther-Straub-Institut, Ludwig-Maximilians Universität).

Scanning Electron Microscopy (SEM)

After the intestine was harvested and washed with normal PBS, it was cut longitudinally to permit exposure of the internal surface. Portions of intestine were then fixed in 1% glutaraldehyde in 50mM cacodylate buffer (v/v) for 15 minutes at room temperature. Later they were postfixed in buffered 2% osmium tetroxide (w/v) at 4°C overnight. Scanning Electron Microcopy (SEM) was performed by the laboratory of Prof. Dr. Hubert Kerschbaum of the Department of Cell Biology at the University of Salzburg, Austria.

We performed three different assays on:

Serum

After cardiac puncture, the blood was collected in a proper collector for serum separation (Sarstedt, 20.1344) and blood cells and serum were separated by 10.000g x 5min centrifugation. Serum was stored in 1.5 mL Eppendorf at -80° and prepared for the 23-cytokine assay (Bio Rad) and the TGFβ-1, 2, 3 assay (R& D Systems). These bead-based multiplex systems enable quantification of up to 100 different analytes in a very limited sample quantity. Each of the beads is labeled with a specific dye and with an antibody, which captures the analyte of interest. Data acquisition was performed via a Bio-Plex reader and Bio-Plex Manager software. Averages of Observed Concentrations of each analyte for both genotypes were calculated.

TGFβ Assay

When lysing cells for TGFβ-1, 2, 3 assay (R& D Systems) we followed the instructions of the protocol from R&D Systems.

Phospho-Assay

For the phospho-assay (Bio Rad, LQ000000006935), isolated $CD4^+$ T cells were stimulated with TGFβ-1 5ng/mL and beads coated with αCD3 as well as αCD28 (Invitrogen). Cells were collected, pelleted and lysed immediately after activation (Lysis Buffer, Bio Rad). Protein concentrations were analyzed using a BCA protein assay (Thermo Fisher) and samples were stored as indicated in the Bio Rad protocol accompanying the phospho-assay kit. Each sample was properly thawed on ice and diluted to a concentration of 200 µg/mL following the instructions of the Bio Rad protocol.

Small Intestine Tissue

1,5 cm of small intestine tissue was isolated from mice and stored at -80°. All samples were treated with 300µl lysis buffer per sample (Bio Rad cat.n. 171304011)., vortexed, put on ice and sonicated for 30 sec. Thereafter, all samples were left on ice for 20 minutes, vortexed for 10 seconds every 2 minutes and then rapidly frozen in liquid nitrogen. Samples were thawed on ice (approximately 30 min), vortexed again, centrifuged 500g for 4 minutes at 4 °C–and the supernatants were collected. Immediately thereafter, we performed a BCA assay (Thermo Scientific cat.n. 23225), diluted the samples to a concentration of 700 µg protein per mL and froze them at -80°C. The assay was performed according to the protocol for the 23-plex cytokine assay (Bio rad, M60009RDPD)

Immunoprecipitation and Western Blot

For detection of TRPM7 spleens of both genotypes were isolated and smashed using a 100 µm strainer. In order to perform immunoprecipitation, splenocytes were washed, pelleted and lysed (Cell lysis buffer (fresh prepared) 1x Lysis-Buffer 0.5% (v/v) Igepal 0.5% (v/v) PMSF 1% (v/v) Protease and Phosphatase inhibitor 5 mM NaF). Lysates were pipetted up/down 3-4 times to completely resuspend the cells and incubated for 30 minutes at 4°C, on a rotator. Whole nuclei were pelleted by centrifugation for 5 minutes at 12000 rpm at 4°C. We added anti-TRPM7 primary antibody (ProScientifica, diluted 1:50) to bind selectively the target protein. Samples were gently rotated for 2 hours at 4°C. We added Protein-G-Sepharose (Dynabeads, Invitrogen, ~1:18) capturing beads, which were previously washed according to the manufacturer's instructions and rotated the suspension at 4°C. We pelleted the beads, discarded the supernatant and washed 3 times with 1 ml lysis buffer. 40 µl reducing SDS-PAGE sample loading buffer was added to the beads, boiled for 9 minutes at 95°C and and load carefully into wells along with a protein ladder of interest. Separate the proteins with 120 V until the blue bands migrate to the bottom of the gel. Polyacrylamide gels with separated proteins and nitrocellulose membranes are equilibrated in transfer buffer. Gel and nitrocellulose membrane are placed

between four transfer buffer-soaked filter papers and the gel membrane sandwich is smoothed with a 15 mL falcon to avoid any air bubble, between membrane and gel. Blotting is performed at 180 mA, overnight at 4°C.

The membrane is reversibly stained with Ponceau S solution to verify the protein transfer after blotting and de-stained by washing with TBS-T. Unspecific binding is blocked by incubating the membrane in TBS-T containing 5% BSA (and 1% of phosphatase inhibitor for detection of TRPM7 pSer1511) under shaking for 1h at RT or 3 h at 4°C. In the next step the membrane was incubated with the first antibody (Rabbit anti-mouse primary antibodies: αTRPM7 from ProScientifica, 1:1000; αTRPM7-S1511, kindly provided from V. Chubanov, LMU Munich, 1:60 and SMAD2/3 127475 Cell Signalling see appendix, 1:1000) overnight under shaking at 4°C to let it bind to the protein of interest. The first antibody is usually diluted in blocking solution. The second antibody directed against the Fc-part of the first antibody is coupled to horse radish peroxidase (HRP) (Goat Anti Rabbit IgG (H + L)-HRP Conjugate, Bio-Rad #1706515, 1:2000) and was diluted in TBS-T: After washing three times the membrane was incubated with the second antibody under shaking for 45-60 min at RT. After washing again three times with TBS-T for 5 min, the membrane is exposed to S1- and S2-solution (1:1) for one minute and is placed between two transparent plastic sheets proper for detection. During incubation the conjugated enzyme horseradish peroxidase (HRP) catalyzes the oxidation of luminol (S1 solution) by H_2O_2 (S2 solution) inducing photon emission, which is detected by the chemoluminescence system (ChemiSmart, PeqLab). Evaluation of Western Blots was performed using the program Image J.

Real Time PCR

$CD4^+$ T cells were isolated as previously described and stimulated with 5ng/mL of TGFβ-1 in a 24 well-plate coated with αCD3 (2µg/ml) as well as αCD28 antibodies (5µg/ml; BioXcell) for 15, 30, 45 or 60 minutes. T cells lysate was obtained following the instructions of the RNA extraction kit (Sigma). RNA was quantified in a biophotometer plus (Eppendorf). For first strand synthesis we mixed solution A: 8µL RNA and 2µL random hexamers with solution B containing 5µL first strand buffer, 2µL DTT 0,1M, 1µL dNTPs of a 10mM mix, 2µL DEPC water and 1µL SuperScript II reverse transcriptase supplied by the manufacturer (Thermo Fisher). The prepared mixes were incubated at 42°Celsius for 60 minutes and the enzyme was heat inactivated at 70° for 15 minutes. Obtained cDNAs were stored until use at -20° after DNA quantification. The Real Time Polymerase Chain Reaction was performed with a Light Cycler 480 (Roche Life Science) using a SYBR-Green PCR-Mix according to the manufacturer's protocol (Roche). ITGAE (Bio-Rad) was detected as target gene and *GADPH* gene (glyceraldehyde-3-phosphate) was used as reference gene. Samples were detected in doublets, while the complete experiment was repeated a total of four times. $2^{-\Delta\Delta CP}$ values were calculated using crossing points (Mueller and Macpherson) as suggested by the manufacturer (Roche Life Science).

Th17 differentiation and analysis

After collecting lymph nodes from mice of both genotypes, we isolated $CD4^+$ T cells and coated round bottoms 96 well plates with αCD3 as well as αCD28 antibodies (2 µg/mL) for 4 hour at 37°C. Plates were washed three times with normal PBS and kept humid until use. $CD4^+$ T cells were counted and diluted at 0,5 x 10^6 cells/mL in modified RPMI (see appendix) and a complete mix of recombinant cytokines and antibodies was added to the cell culture. TGFβ-1 was added at a concentration of 2 ng/mL, Interleukin 6 was added at a concentration of 20 ng/mL, anti-Interleukin 4 was added at a final concentration of 5 µg/mL and anti-interferon γ was diluted to a final

concentration of 10 µg/mL. Cells were cultured for 5 days in sterile incubator at 37°C, 5% CO_2 and were analyzed at day 5 by FACS (Guava EasyCyte System, Millipore). Cells were restimulated for 6 hours adding PMA 100 nM (phorbol myristate acetate X and ionomycin 1 µM at 37°C, 5% CO_2. After 3 hours, Brefeldin A was added at a concentration of 10 µg/mL (all indicated concentrations refer to ending concentrations in cell suspension). Cells were collected, washed in MACS Buffer and resuspended at a concentration of up to 1 x 10^6 cells/mL. αIL-17A and αIFN-γ antibodies coupled to fluorochromes (αIFN-γ conjugated APC and αIL-17A conjugated PE) were added in quantities suggested in the product data sheets and cells were incubated in the dark for about 20-30 minutes, depending on the protocol supplied by the manufacturer (DBioscience/ Biolegend). Stained cells were washed twice with MACS Buffer and quantified by FACS (Guava EasyCyte System, Merck-Millipore). We first performed a surface staining for $CD4^+$ and $CD8^+$ T cells to assess the purity of the cell preparation. If the cell suspension contained > 97% of $CD4^+$ T cells we proceeded with the detection of the cytokines IL-17A and IFNγ. (GuavaSoft 3.1.1 detection software, InCyte 3.1 analysis software for Mac, Millipore).

4. Results

4.1. Analysis of the gross phenotype of the TRPM7$^{KR/KR}$ mouse model

For clarification of the role of TRPM7 channel-kinases in T cell function, we utilized a mouse model carrying a point mutation at the active site of the enzyme (Fig. 9A RIKEN, Japan)(Kaitsuka et al., 2014). Mutating the lysine at position 1646 to arginine (TRPM7$^{KR/KR}$) deletes the ATP-binding site and thereby disables kinase activity (Kaitsuka et al., 2014).

Using Immunoprecipitation (IP) and Western Blot (WB) analysis, we were able to confirm that the mutation indeed disrupted native kinase activity and thus auto-phosphorylation at serine 1511 in primary splenocytes (Fig. 9B). Unlike mice lacking the entire kinase domain (Ryazanova et al., 2010), homozygous TRPM7$^{KR/KR}$ mice are viable (Kaitsuka et al., 2014; Ryazanova et al., 2014). They are normal in size, compared to TRPM7$^{+/+}$ mice (Fig. 9C, E) (Kaitsuka et al., 2014; Ryazanova et al., 2014). Figure 9C compares two representative mice TRPM7$^{KR/KR}$ and TRPM7$^{+/+}$ mice at the age of 4 weeks, demonstrating that both mice are comparable in size, development of exterior organs and fur color. When weighing mice of the same age group (4-6 weeks old), TRPM7$^{KR/KR}$ mice elicited a weight average of 19,3g (± 1.8) similar to TRPM7$^{+/+}$ mice (19,96 ± 1.2 g) (Fig. 9E).

Moreover, we were wondering whether reproduction was affected by the mutation. Therefore, we analyzed the Mendelian inheritance ratio of 100 offspring mice from heterozygous mating pairs (Fig. 9D). The expected Mendelian distribution is 25 TRPM7$^{+/+}$, 25 homozygous TRPM7$^{KR/KR}$ and 50 heterozygous TRPM7$^{+/KR}$ mice. Genotyping our animals revealed the following ratio: 24 TRPM7$^{+/+}$, 27 TRPM7$^{KR/KR}$ and 49 TRPM7$^{+/KR}$ mice. Using this ratio, we then calculated a p value, of 0.33 and concluded that the genotype distribution indeed follows the Mendelian ratio.

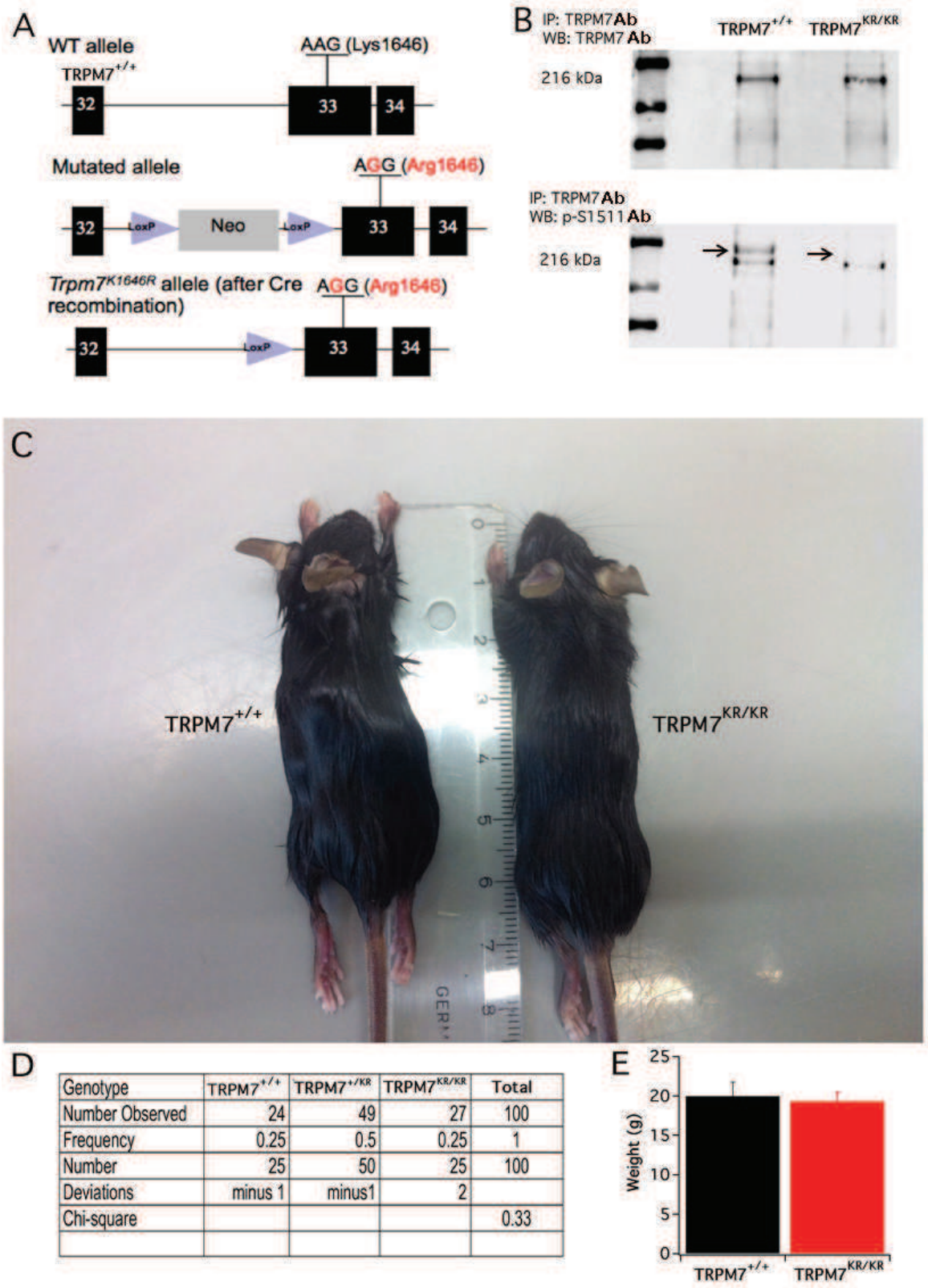

Genotype	TRPM7$^{+/+}$	TRPM7$^{+/KR}$	TRPM7$^{KR/KR}$	Total
Number Observed	24	49	27	100
Frequency	0.25	0.5	0.25	1
Number	25	50	25	100
Deviations	minus 1	minus1	2	
Chi-square				0.33

Figure 9: Phenotype of TRPM7$^{KR/KR}$ mutant mice (A) Targeting strategy for the generation of TRPM7$^{KR/KR}$ mutant mice generated by RIKEN, Japan (RBRC03318). **(B)** Immunoprecipitation (IP) and Western Blot (WB) analysis of primary splenocytes isolated from wild-type (TRPM7$^{+/+}$) or TRPM7$^{KR/KR}$ mice, respectively. **(C)** Comparison of TRPM7$^{+/+}$ and TRPM7$^{KR/KR}$ mice. **(D)** The

calculated inheritance ratio is within rage of the expected Mendelian ratio (n = 100 mice). **(E)** Comparison of the weight of $TRPM7^{+/+}$ (n = 5) and $TRPM7^{KR/KR}$ (n = 6) mice. Data represent the mean ± standard error of mean (S.E.M.).

4.2. TRPM7 kinase activity is not required for channel activity or maintenance of cation homeostasis

4.2.1. Electrophysiological characterization of TRPM7 channel activity.

Next, we were wondering, whether mutating the kinase activity affected the TRPM7 channel function in immune cells. To answer this question, we applied electrophysiological techniques.

Therefore, primary, peritoneal mast cells were harvested from $TRPM7^{+/+}$ and $TRPM7^{KR/KR}$ mice (see methods) and kept in culture overnight. Cells were patched one day after isolation via the whole-cell patch-clamp technique (see methods). We used primary, peritoneal mast cells as a model, because they are easier to maintain in culture and to analyze by patch-clamp recordings than primary T cells. Figure 10A shows characteristic TRPM7-like currents of $TRPM7^{+/+}$ and $TRPM7^{KR/KR}$ mast cells. We used Mg^{2+}-free conditions, to maximize TRPM7 currents. Currents were normalized to the initial cell size and mean current densities in picoAmpere per picoFarad (pA/pF) and plotted *versus* time in seconds (s). Figure 10A illustrates no difference in current development or amplitudes between $TRPM7^{+/+}$ and $TRPM7^{KR/KR}$ mast cells. The shape of representative I/V curves extracted at 500 s show characteristic TRPM7-like currents (Fig. 10B). Statistical analysis of the mean current densities of $TRPM7^{+/+}$ and $TRPM7^{KR/KR}$ mast cells extracted at +80 mV at 300 s and 500 s revealed no significant differences (Figure 10C).

To evaluate functional expression of TRPM7, we applied DVF (divalent free solution, containing chelators for Ca^{2+} and Mg^{2+}; see methods), after eliciting TRPM7 current activation by depletion of intracellular Mg^{2+} and Mg·ATP. In Figure 10D current densities of $TRPM7^{+/+}$ and $TRPM7^{KR/KR}$ mast cells are plotted *versus* time, similar to Figure 10A. Representative I/V curves extracted at 300 s showed similar linear shaped currents (Figure 10E). Comparison of the outward current amplitudes extracted at 200s and 300s revealed no significant differences, calculated with a student's t-test. In summary no differences in functional channel expression were detected between $TRPM7^{+/+}$ and $TRPM7^{KR/KR}$ mast cells.

To answer the question whether our point mutation affected TRPM7 channel regulation, we performed a set of experiments to elucidate the sensitivity of the channel for intracellular Mg^{2+} ($[Mg^{2+}]_i$). In Figure 10G current densities are plotted over increasing $[Mg^{2+}]_i$, obtained by varying $MgCl_2$ in the internal patch solution, calculated via WebmaxC (see methods). The dose-response curves for $[Mg^{2+}]_i$ elicited higher IC_{50} values for $TRPM7^{KR/KR}$ (IC_{50}= 257 µM) compared to $TRPM7^{+/+}$ (IC_{50}= 183 µM) mast cells, indicating that the mutant cells were slightly less sensitive to $[Mg^{2+}]_i$ dependent inhibition. However, when considering physiological ranges for $[Mg^{2+}]_i$, which vary between 700 µM and 900 µM free Mg^{2+}, current densities of both, $TRPM7^{+/+}$ and $TRPM7^{KR/KR}$ mast cells, were similar inhibited.

Finally, we wondered whether our findings could be transferred to T lymphocytes. Therefore, we isolated primary $CD4^+$ T cells from lymph nodes (see methods) and applied our standard whole-cell patch-clamp protocol (see methods) with the same conditions used for Figure 10A. Similar to mast cells, also primary T cells elicited a characteristic TRPM7-like current upon Mg^{2+} depletion. Figure 10H and I confirmed that the observed current amplitudes and I/V relationships of $TRPM7^{+/+}$ and $TRPM7^{KR/KR}$ T cells were similar. Thus, we conclude that the TRPM7 Kinase activity is not required for ion channel activity in primary, murine $CD4^+$ T cells.

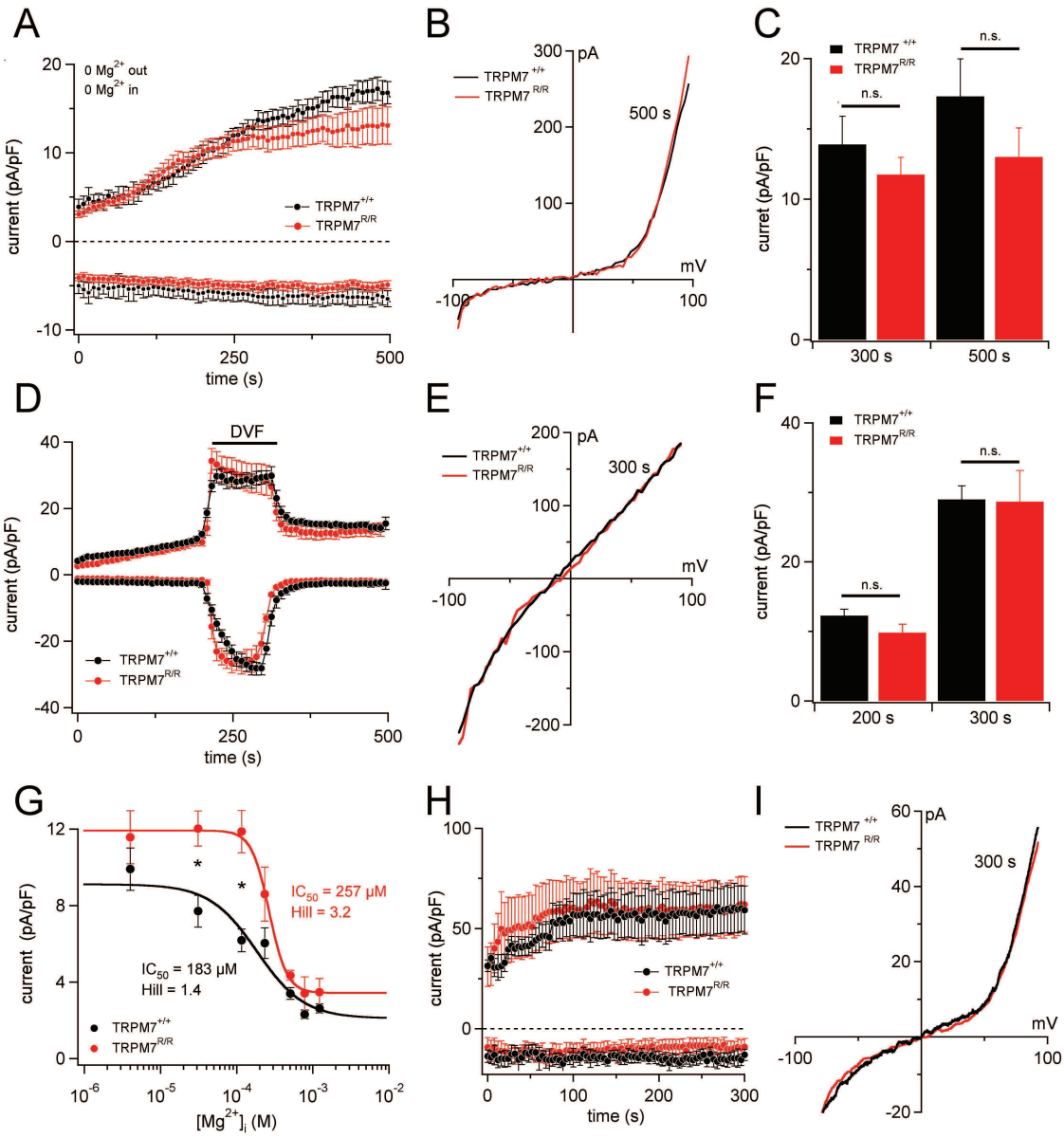

Figure 10: Electrophysiological characterization of TRPM7 in TRPM7$^{+/+}$ and TRPM7$^{KR/KR}$ derived immune cells. Whole-cell currents were recorded in freshly isolated primary peritoneal mast cells, or CD4^{+} T lymphocytes, respectively. Voltage ramps were elicited from −100 to +100 mV over 50 ms, acquired at 0.5 Hz and recorded at an interval of 2 s. TRPM7 current amplitudes were assessed at +80 mV for outward currents and at -80 mV for inward currents, averaged and normalized to cell size (pF). Error bars indicate S.E.M. (A-C) Whole-cell patch clamp analysis of TRPM7 current development in TRPM7$^{+/+}$ (black, n = 6) and TRPM7$^{KR/KR}$ (red, n = 8) mast cells. In (A) the current densities at +80 (upper curves) and -80 mV (lower curves) are plotted versus time of the experiment in seconds (s). (B) Representative current-voltage relationships extracted at 500 seconds of TRPM7$^{+/+}$ (black) and TRPM7$^{KR/KR}$ (red) cells are shown. (C) Bar graphs of current densities at +80 mV extracted at 300 and 500 seconds. These measurements have been conducted in absence of extracellular and intracellular Mg^{2+} to elicit possible differences in channel function. (D-F) In order to investigate expression levels of functional TRPM7 channels we perfused mast cells with divalent-free solution (DVF). (D) Current

densities were plotted *versus* time of the experiment of TRPM7$^{+/+}$ (black, n = 12) and TRPM7$^{KR/KR}$ (red, n = 9) mast cells. (E) Representative current-voltage relationships extracted at 300 s. (F) Bar graphs of mean current densities at +80 mV extracted at 200 s and 300 s. TRPM7$^{+/+}$ (black, n = 5-12) and TRPM7$^{KR/KR}$ (red, n = 6-12). (G) Mg^{2+}-dose-response curve of outward current densities plotted against different $[Mg^{2+}]_i$ concentrations. Note, while the IC_{50} values were only slightly shifted to the left, the current densities at low free $[Mg^{2+}]_i$ (3.1 µM, $P < 0.006$; 116 µM, $P < 0.005$) were significantly different between TRPM7$^{+/+}$ (black, n = 5-16) and TRPM7$^{KR/KR}$ (red, n = 5-18). Nonetheless, current densities at physiological free $[Mg^{2+}]_i$ values between 700 – 900 µM were not altered. (H-I) Experiments and analysis were performed as in (A & B), using, TRPM7$^{+/+}$ (black, n = 5) and TRPM7$^{KR/KR}$ (red, n = 5) primary, murine CD4$^+$ T cells. Note, also TRPM7$^{KR/KR}$ T cells show no differences in channel activation, current amplitude or I/V relationship compared to TRPM7$^{+/+}$ T cells.

Next, we asked, whether the TRPM7 kinase is involved in ion homeostasis. Therefore, we analysed systemic Mg^{2+} and Ca^{2+} conentrations in the serum of $TRPM7^{+/+}$ and $TRPM7^{KR/KR}$ mice, respectively, using inductively coupled plasma mass spectrometry (ICP-MS) (Fig. 11A, B) (ALS Scandinavia). Comparing the Mg^{2+} conentrations in serum of $TRPM7^{+/+}$ and $TRPM7^{KR/KR}$ mice, we did not observe any significant differences (Fig. 11A). Also the Ca^{2+} levels in the serum of $TRPM7^{KR/KR}$ mice were similar to $TRPM7^{+/+}$ (Fig. 11B). Together with our electrophysiological studies (Fig. 10), these data further suggest, that the TRPM7 kinase indeed does not affect TRPM7 channel function and thus maintenance of systemic ion homeostasis.

In order to detect changes in intracellular Mg^{2+} concentrations, we utilized the fact that free intracellular Mg^{2+} concentrations ($[Mg^{2+}]_i$) are very tightly linked to cellular ATP levels. In fact, the intracellular ATP concentration is often used as an estimate for $[Mg^{2+}]_i$. Therefore, we measured the cellular ATP concentration using a luciferin-luciferase assay (Molecular Probes) in 1% Triton X-100 cell lysates. In Figure 11C the luminescence was detected as OD in order to evaluate free ATP in cell lysate obtained from $CD4^+$ T cells. Therefore, our data suggest, that the two different animal models do not show differences in systemic or cytosolic Mg^{2+}.

To understand, if cellular Ca^{2+} homeostasis was altered in our $TRPM7^{KR/KR}$ mutant, we performed ratiometric Ca^{2+} imaging in freshly isolated $CD4^+$ T cells extracted from lymph nodes of our two mouse models. Therefore, T cells were loaded with 4 µM Fura-Red for 30 minutes. The concentrations were measured using an Axiovert A1 fluorescence microscope (Zeiss) equipped with a LED based excitation system (Colibri) and the ZEN software (Zeiss). We recorded the ratio of the fluorescence intensity excited at 420 nm *versus* the intensity recorded with an ecitation of 470 nm ($R(F_{420}/F_{470})$) as an estimate for basal Ca^{2+} concentrations, while keeping the cells in extracellular solution containing 1 mM Ca^{2+} and 2 mM Mg^{2+}. Figure 11D shows the mean ratio of the average of 5 time points after 30 seconds in the experiment. Analysis of the basal Ca^{2+} levels in $CD4^+$ T cells, via ratiometric Ca^{2+} imaging, revealed that the basal level of Ca^{2+} was slightly, but not significantly higher in the

TRPM7$^{KR/KR}$ cells in comparison to TRPM7$^{+/+}$. In summary, our data indicate that the mutation of the active site of the kinase domain does not affect cation homeosatsis.

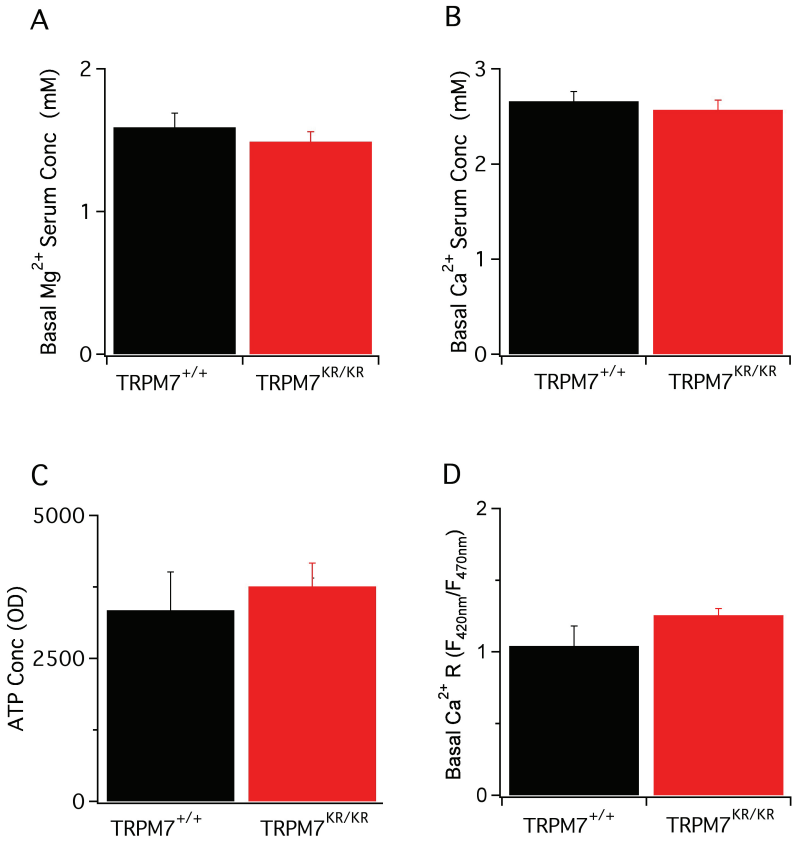

Figure 11: Mg^{2+} and Ca^{2+} homeostasis in TRPM7$^{+/+}$ and TRPM7$^{KR/KR}$ mice. (A) Mg^{2+} in the serum was measured with inductively coupled plasma mass spectrometry (ICP-MS). Data are shown as average concentration in mM of serum isolated from TRPM7$^{+/+}$ (black, n = 7) and TRPM7$^{KR/KR}$ (red, n = 8), respectively. **(B)** Similar to (A) we obtained the Ca^{2+} levels in the serum. We show averages of TRPM7$^{+/+}$(n = 13) and TRPM7$^{KR/KR}$ (n = 14), respectively. Note that TRPM7$^{KR/KR}$ mice show slightly, however significantly reduced Ca^{2+} levels in the serum ($P < 0.026$). **(C)** Bar graph showing averages of luciferase luminescence (del Rio et al.) detecting ATP levels in cell lysates of $CD4^+$ T cells. Averages of TRPM7$^{+/+}$ (black, n = 4) and TRPM7$^{KR/KR}$ (red, n = 4) are shown. **(D)** Bar graph comparing average Fura-Red ratios of TRPM7$^{+/+}$ (black, n = 28) and TRPM7$^{KR/KR}$ (red, n = 31) $CD4^+$ T cells indicating cellular, free Ca^{2+} concentrations at rest. Error bars indicate S.E.M.

4.3. TRPM7 kinase does not affect Ca^{2+} signaling and activation of T lymphocytes

4.3.1. Receptor-activated Ca^{2+} signaling is normal in $TRPM7^{KR/KR}$ T cells

After assesing that Ca^{2+} and Mg^{2+} hometasis is maintained at physiological levels, we asked wether receptor-activated Ca^{2+} signaling was altered in $TRPM7^{KR/KR}$ T lymphocytes. With this respect, we performed similar experiments as in Figure 11A. T cells were loaded with 4 µM Fura-Red for 30 minutes and transfered in our standard external solution (1 mM Ca^{2+}, 2 mM Mg^{2+}). To monitore the changes in the intracellular Ca^{2+} concentrations the ratio R(F_{420}/F_{470}) value was measured over a time frame of 6-10 minutes, while the T cell receptor (TCR) was directly stimulated using beads coated with αCD3 as well as αCD28 as co-stimulatory signal (Fig. 12A). Although the mean Ca^{2+} influx was slightly smaller in $TRPM7^{KR/KR}$ T cells, statistical analysis of the R(F_{420}/F_{470}) value at 300 s revealed no significant differences between $TRPM7^{KR/KR}$ and $TRPM7^{+/+}$ T lymphocytes (Fig. 12B, $P < 0.3$) also in experiments executed over a more prolonged time frame.

As prolonged Ca^{2+} influx is necessary for T cell activation and proliferation, we wondered whether the proliferation of $TRPM7^{KR/KR}$ T cells was normal. Therefore, freshly isolated $CD4^{+}$ T cells were cultured for 5 days in plates coated with αCD3 and αCD28 antibodies (5µg/mL αCD3 and 5µg/mL αCD28, Bio-X-cell). In Figure 12C, we show the proliferation rate in cell counts over a period of 5 days. Averages were comparable between $TRPM7^{+/+}$ cells and $TRPM7^{KR/KR}$ T cells. In the right panel average cell numbers at day 5 are shown as bar graphs. We did not see significant differences between $TRPM7^{+/+}$ and $TRPM7^{KR/KR}$ T cells (Fig. 12D, $P < 0.44$). All these data together suggested, that the Ca^{2+} signalling following TCR stimulation was normal in our $TRPM7^{KR/KR}$ T lymphocytes, using these experimental conditions.

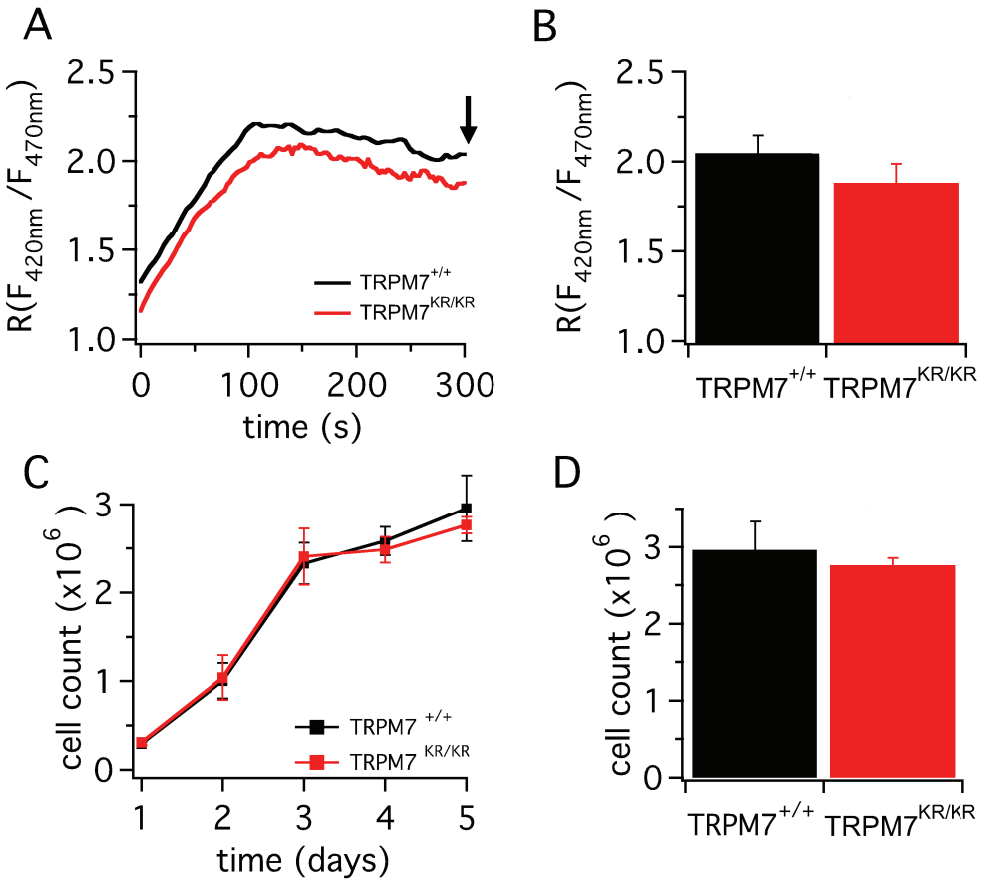

Figure 12: Ca^{2+} signaling, activation and proliferation of $CD4^+$ T cells. (A) Ratiometric Ca^{2+} measurements of $TRPM7^{+/+}$ (black, n = 28, 2 mice) and $TRPM7^{KR/KR}$ (red, n = 31, 3 mice) $CD4^+$ T cells stimulated with αCD3/αCD28 coated beads and plotted over time (s). $TRPM7^{+/+}$ and 3 $TRPM7^{KR/KR}$ mice were used. Arrow indicates time point taken for statistical analysis. **(B)** Bar graph extracted from (A) at 300 s ± S.E.M.**(C)** T cell proliferation measured as cell numbers plotted *versus* time (days). $CD4^+$ T cells isolated from $TRPM7^{+/+}$ (black, n = 3-4) and $TRPM7^{KR/KR}$ (red, n = 3-4) were cultured with CD3/CD28 antibodies in modified RPMI medium (see methods). A total number of 5 animals were used, each. **(D)** Data obtained from (C) at day 5 shown as average cell numbers ± S.E.M.

4.4. TRPM7 kinase affects basal cytokine levels in serum

As TRPM7 has been implicated in chemokine and cytokine expression profiles, we asked whether the kinase activity was essential for the secretion of different cytokines. Therefore, we performed a multiplex bead-based ELISA (Bio Rad) on serum from mice of both genotypes. This ELISA measures concentrations of 23-cytokines in the same sample. To evaluate cytokine levels we harvested serum of 7 mice per each genotype. The serum was collected through cardiac puncture after the mice were sacrificed. The serum was separated from blood cells through centrifugation and stored at -80°C until the assay was performed. The experiments were measured via a Bio-Plex-200-Reader (Bio Rad).The entire assay was repeated two times in doublets with a total number of 3-7 mice for each genotype. The data were analysed via the Bio-Plex Manager software (Bio Rad) and concentrations were calculated as pg/mL. In $TRPM7^{+/+}$ serum, IL-2 values reached 52.7 (± 6.5) pg/mL, while in $TRPM7^{KR/KR}$ serum the values were significantly reduced at 29.7 pg/mL (± 3.7) (Fig. 13C; $P < 0.12$). Also G-CSF levels were significantly lower in $TRPM7^{KR/KR}$ serum (44.1 pg/mL (± 6.4)), compared to $TRPM7^{+/+}$ (101.2 pg/mL (± 20.1)) (Fig. 13N; $P < 0.35$). The IL-17 concentration in $TRPM7^{KR/KR}$ serum was significantly decreased (82.8 (± 14) pg/mL) compared to $TRPM7^{+/+}$ (168.2 (± 8.6) pg/mL) (Fig. , 13Z; $P < 0.0008$). Taken together, our results indicate overall a tendency to reduced cytokine levels in the serum harvested from our $TRPM7^{KR/KR}$ mice.

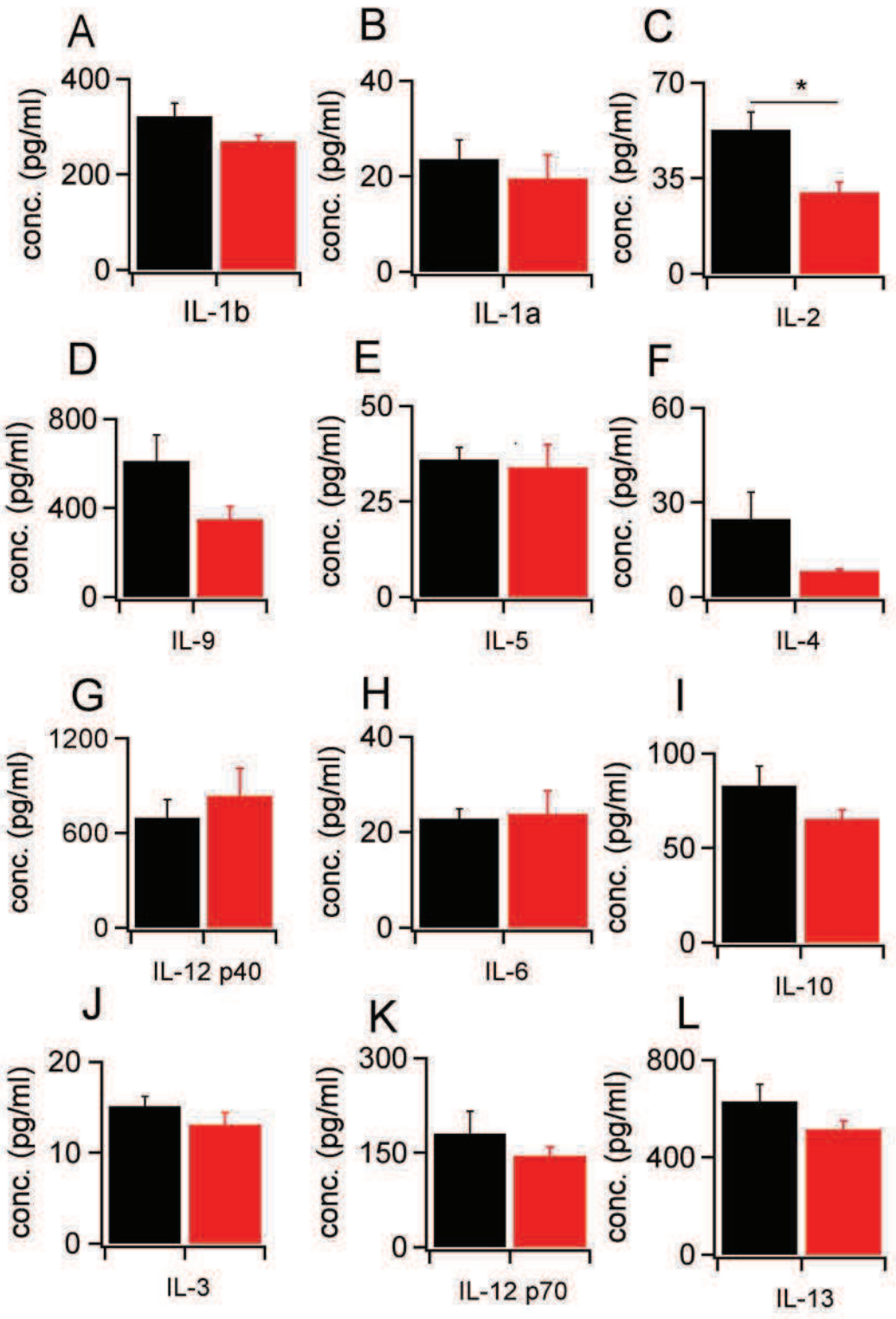
A
400
200
0
conc. (pg/ml)
IL-1b
B
40
20
0
conc. (pg/ml)
IL-1a
C
70
35
0
*
conc. (pg/ml)
IL-2
D
800
400
0
conc. (pg/ml)
IL-9
E
50
25
0
conc. (pg/ml)
IL-5
F
60
30
0
conc. (pg/ml)
IL-4
G
1200
600
0
conc. (pg/ml)
IL-12 p40
H
40
20
0
conc. (pg/ml)
IL-6
I
100
50
0
conc. (pg/ml)
IL-10
J
20
10
0
conc. (pg/ml)
IL-3
K
300
150
0
conc. (pg/ml)
IL-12 p70
L
800
400
0
conc. (pg/ml)
IL-13

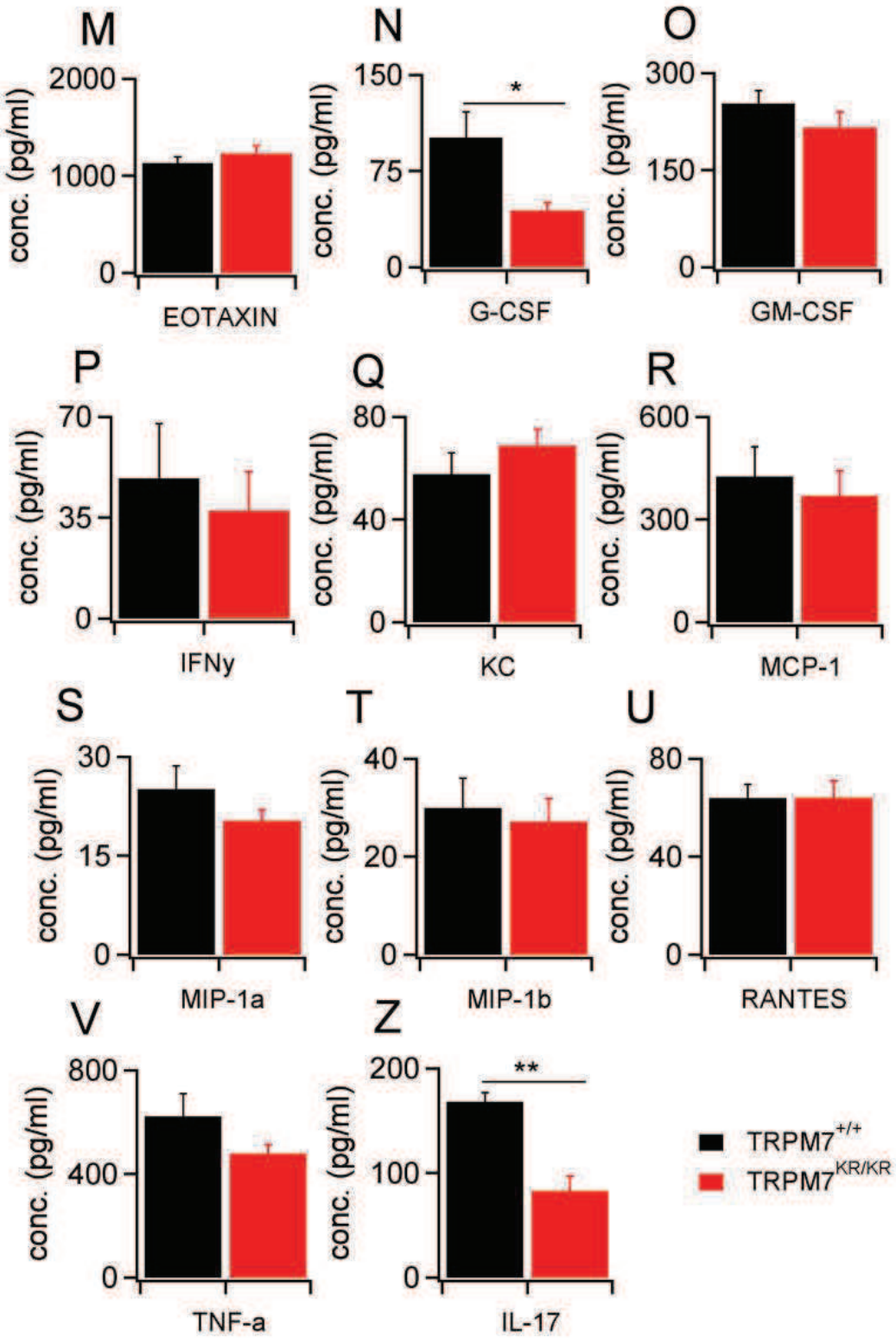

Figure 13: (A-Z) Basal cytokine levels evaluated in the serum of the TRPM7$^{+/+}$ (black, n = 3-7) and TRPM7$^{KR/KR}$ (red, n = 3-7) mice, respectively, and shown as pg/mL. Bars indicate mean ± S.E.M. A total number of 7 mice were used for each genotype. Note a significant reduction of serum levels of IL-2 ($P < 0.12$), G-CSF ($P < 0.35$), and IL-17 ($P < 0.0008$) in TRPM7$^{KR/KR}$. (IL *i.e.* interleukin; Eotaxin *i.e.* CC chemokine subfamily of eosinophil

chemotactic proteins, G-CSF *i.e.* granulocyte colony stimulating factor; GM-CSF *i.e.* granulocyte-macrophage colony-stimulating factor, IFNy *i.e.* interferon gamma, KC *i.e.* keratinocyte chemoattractant, MCP-1 *i.e.* monocyte chemoattractant protein-1, MIP *i.e.* macrophage inflammatory protein-1 alpha and beta, TNF-a *i.e.* tumor necrosis factor)

4.5. TRPM7$^{KR/KR}$ mice display normal structure of the gut tissue

After we elucidated that the TRPM7$^{KR/KR}$ mice display an impaired cytokine regulation, we addressed the question whether this was due to loss of function of the gut tissue structure and organization. As the gut is essential for immune system homeostasis an intact gut epithelial barrier is important . This barrier function of the gut depends on the outer cell layer, the *mucosal*, as well as the luminal *mucus*. Therefore, we wondered if the tissue structure and integrity of the gut to ensure functional defence was preserved in TRPM7$^{KR/KR}$ mice. Here we show images obtained by Scanning Electron Microcopy (SEM) kindly provided by Prof. Dr. Hubert Kerschbaum from the Department of Cell Biology at the University of Salzburg, Austria. We sacrificed an equal number of 3 animals per each genotype and harvested the small intestine tissue (see methods). After fixing tissues with glutaraldehyde and post-fixing with osmium tetroxide (see methods) we sent them out for further processing and image acquisition. We were able to obtain images of the intestine tissue of TRPM7$^{+/+}$ and TRPM7$^{KR/KR}$ mice, respectively (Fig. 14A and B). Both images show also intact M cells, which are important for the interaction between the external lumen and the Payer's Patches, which are located underneath the M cells. Payer's Patches are the center of the immune system in the small intestine, where lymphocytes encounter non-self particles and consequently adapt the immune response. A higher microscope magnification (Fig. 14C and D) helped us to have a closer look at the microvilli of the intestine collected from both mouse models. Our images show intact microvilli (Figure 14) in TRPM7$^{KR/KR}$ mice suggesting that deletion of TRPM7 kinase activity was not affecting tissue structure or integrity.

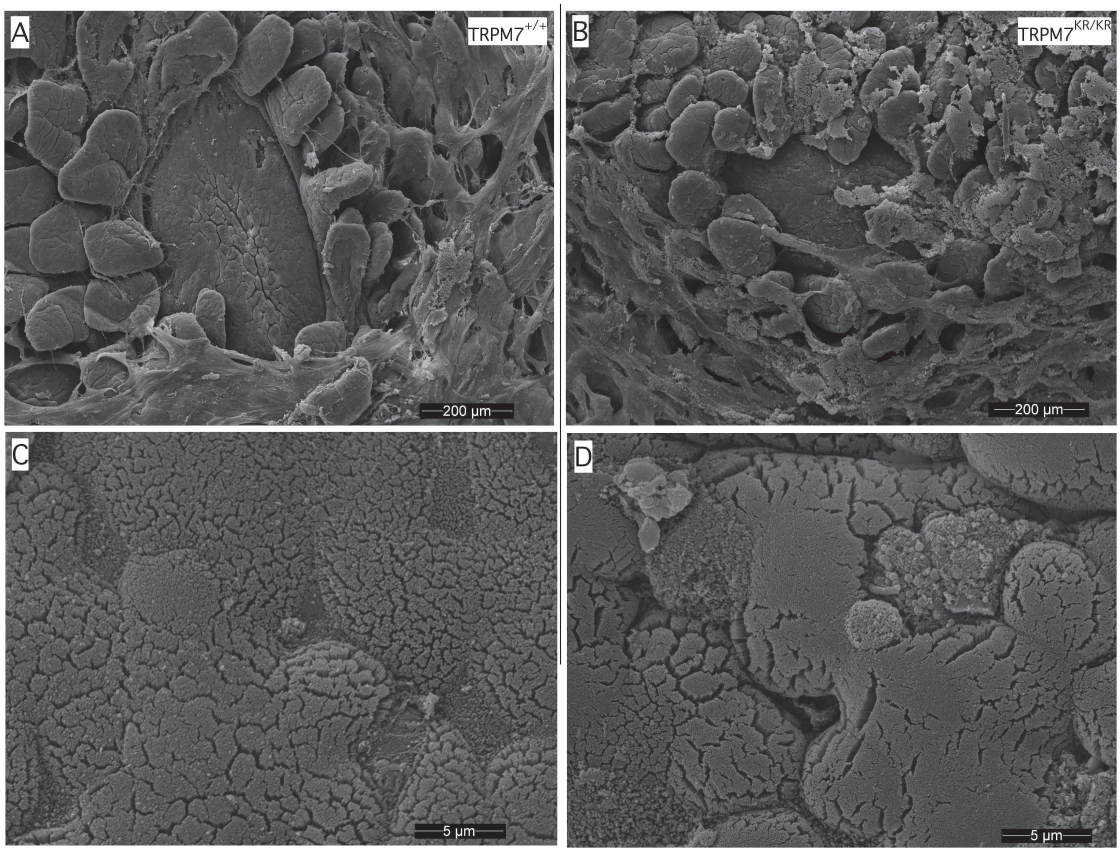

Figure 14: Scanning Electron Microscopy of gut tissue (A, B) Representative SEM images of the small intestine, showing intact microvilli as well as an M cell obtained from fixed biological tissue of $TRPM7^{+/+}$ (left panel) as well as $TRPM7^{KR/KR}$ (right panel) mice. Scale bar indicates 200 µm. A total of 3 mice for each genotype were used. **(C, D)** Representative Scanning Electron Microscopy (SEM) images of the small intestine of $TRPM7^{+/+}$ (left panel) and $TRPM7^{KR/KR}$ (right panel) mice at higher resolution, respectively. Scale bars indicate 5 µm.

4.6. TRPM7 Kinase activity is pivotal for immune system regulation

As reported above, the TRPM7$^{KR/KR}$ mouse model express functional channels and show a normal cation homeostasis, despite of the point mutation. Notably TRPM7$^{KR/KR}$ mice are also characterized by a general reduction of cytokine levels in the serum. These data promted us, to further study the immune system homeostasis at its core. In the gut and the gut associated lymphoid tissues immune cells encounter their antigens and differentiate into effector cells, affecting also systemic immune regulation.

Our collaborators Andrea Romagnani and Prof. Dr. Fabio Grassi, from the Institute for Research in Biomedicine (IRB) in Bellinzona, Switzerland, specifically examined different T cell subsets extracted from distinct gut areas using Flow Cytometric analysis. They gated several T lymphocyte subtypes on their T cell receptor (TCR), TCRγδ and TCRαβ, as well as respective co-receptors CD4 and CD8. Representative FACS (fluorsecence-activated cell sorting) images as well as quantitative analysis are shown in Figure 15A and B. T cells were isolated from the two most external gut tissue layers, the epithelium and the lamina propria. Figure 15A shows FACS analysis of lymphocytes isolated from the epithelium as intraepithelial T lymphocytes (IELs) and elicits a notable reduction of the TCRαβ subtype in the TRPM7$^{KR/KR}$ mutant. The difference in cell number was also significant for lymphocytes of the TCRγδ family. Figure 15B shows the same analysis of T cell subtypes as explained above, but obtained from the lamina propria (Lamina Propria Lymphocytes, LPLs) with a more pronounced reduction of the CD4^{+} fraction. In the bar graph of panel B a significant decrease of lymphocytes expressing TCRαβ in TRPM7$^{KR/KR}$ mice, compared to TRPM7$^{+/+}$ is demonstrated. Whithin TCRαβ, the CD4^{+} fraction was particularly reduced, while the reduction of the TCRγδ cells was less significant. All these results together confirmed our hypothesis that TRPM7$^{KR/KR}$ mice display an impaired regulation of the immune system in the gut and suggested a closer analysis of the TCRαβ CD4^{+} T cell subset.

The decreased number of T cells in the TRPM7$^{KR/KR}$ gut epithelium and lamina propria prompted us to move the focus of our studies on a family of proteins

important for the the gut-homing, specifically the integrins $\alpha_{E(CD103)}\beta_7$, $\alpha_4\beta_7$ and the chemokine receptor CCR9 (CC chemokine receptor 9). This group of proteins is responsible for the relocation of lymphocytes into the gut area and associated organs. Flow cytometric analysis of $CD4^+$ and $CD8^+$ lymphocytes, from the lamina propria and the epithelium, revealed a severe reduction of CD103 expression in $TRPM7^{KR/KR}$ mice (Fig. 15C, bars graph) which is the α-subunit of the $\alpha_{E(CD103)}\beta_7$ integrin. The expression of CD103 is known to be fundmental for lympocyte translocation into and retention in the intra-epithelium. Figure 15C displays examples of MFIs (Mean Flourescence Intensities) of T cells stained for the individual gut-homing proteins and their subunits. In the upper panel MFIs of lymphocytes isolated from the epithelial layer (IELs) and gated for TCRαβ, as well as CD4 and CD8 are shown. MFI plots obtained from T cells isolated from the lamina propria (LPLs) are demonstrated in the lower panel reports using the same gating strategy as in the upper panel. The MFI is considered a valid quantitive analysis method and helped us evaluating the expression levels of each subunit of the gut-homing proteins. Interestingly, we identified a significatly decreased CD103 subunit expression.

The results shown in Figure 15, kindly provided by Andrea Romagnani, from the IRB in Bellinzona, confirmed our previous hypothesis of an impaired immune system regulation in the gut.

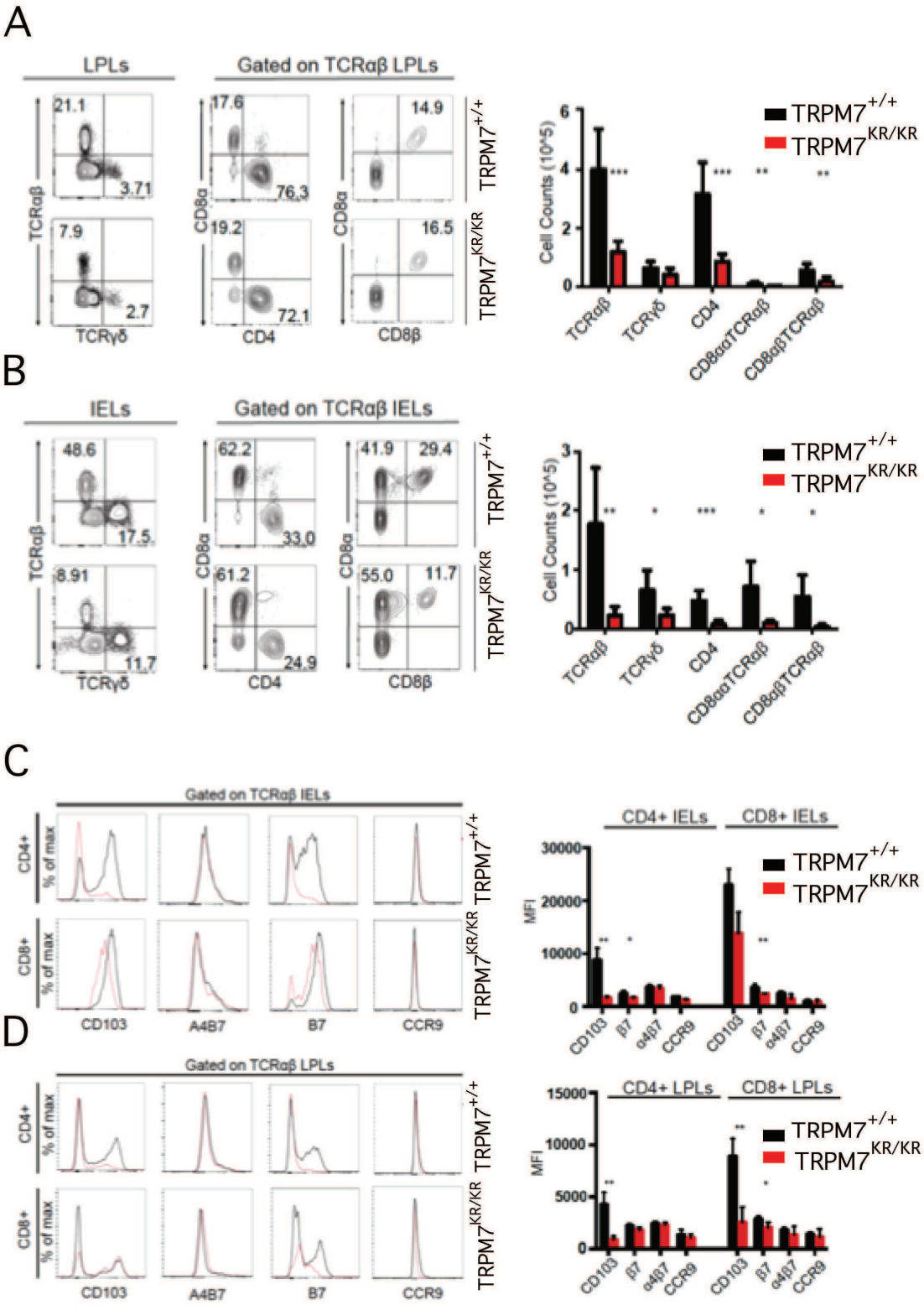

Figure 15: Flow Cytometric Analysis of T cells in the lamina propria and the gut epithelium. (A) Flow Cytometric Analysis of α and β subunits of the T cell receptor (TCR) of intra-epithelial lymphocytes (IELs) of the small intestine. Representative images for lymphocytes labeled with TCRγδ and TCRαβ markers are shown in the left panel ($TRPM7^{+/+}$, upper row and $TRPM7^{KR/KR}$, lower row). In the middle panel TCRαβ positive T cells are

further labeled with CD4 and CD8β antibodies. The bar graph summarizes the average cell count of each lymphocyte subtype ($TRPM7^{+/+}$, n = 6; $TRPM7^{KR/KR}$, n = 7). Note a significant reduction in cell numbers for TCRαβ, TCRγδ and $CD4^+$ lymphocytes in $TRPM7^{KR/KR}$ mice ($TRPM7^{+/+}$, black and $TRPM7^{KR/KR}$, red). **(B)** Flow Cytometric Analysis of α and β subunits of the TCR of lymphocytes isolated from the lamina propria (LPLs) of the small intestine. Representative images for lymphocytes labeled with TCRγδ and TCRαβ markers are shown in the left panel ($TRPM7^{+/+}$, upper row and $TRPM7^{KR/KR}$ lower row). In the middle panel TCRαβ positive T cells are also labeled with CD4 and CD8 antibodies. The bar graph summarizes the average cell count of each lymphocyte subtype ($TRPM7^{+/+}$, n = 6; $TRPM7^{KR/KR}$, n = 7). Note a significant reduction in cell number for TCRαβ, TCRγδ and $CD4^+$ lymphocytes in $TRPM7^{KR/KR}$ mice ($TRPM7^{+/+}$, black and $TRPM7^{KR/KR}$, red). **(C, D)** Representative Flow Cytometric images stained for the integrins αE (CD103), β_7, α4β7 and the chemokine receptor, CCR9. The maximal fluorescence of lymphocytes isolated from the epithelium (C) and lamina propria (D) of the small intestine tissue is shown in percent (%). The bar graphs show the statistical analysis of the FACS images as Mean Fluorescence Intensities (MFI) of intra-epithelial $CD4^+$ T cells (left) and intra-epithelial $CD8^+$ T cells (right) ($TRPM7^{+/+}$, black, n = 6 and $TRPM7^{KR/KR}$, red, n = 7). Error bars indicate S.D. Values of $P < 0.5$ were considered significant with * $P < 0.05$, ** $P < 0.01$ and *** $P < 0.001$. Image kindly provided by Dr. Fabio Grassi and Andrea Romagnani from the IRB in Bellinzona, Switzerland.

4.7. Cytokine Levels in the small intestine

As the distribution of the lymphocytes in the gut tissue was altered in the TRPM7 kinase-dead animals, we wondered whether the cytokine milieu in the gut was also affected. Therefore, we performed the same ELISA as in Figure 13 to reveal cytokine levels within the gut tissue. We sacrificed mice of both genotypes, harvested the small intestine and cut 1,5 cm of the *ileum* about 3 cm proximal the *caecum*. The harvested tissue was washed with PBS, lysed via short exposure to liquid nitrogen and further lysed with a special lysis buffer (Bio Rad, see methods). Samples were analyzed for their protein concentration using a BCA assay (Pierce^{TM}, ThermoScientific) and diluted to a final concentration of 700µg/mL. All diluted samples were stored at -80° prior to detection. Samples were detected in per mouse sample and 4-5 mice per each genotype were used. Figure 16A-Z shows average cytokine concentrations calculated as pg/ml. To perform the experiment, we sacrificed 5 TRPM7$^{KR/KR}$ mice and 4 TRPM7$^{+/+}$. The results confirmed we observed for the cytokine concentrations in the serum as most of the analyzed cytokine concentrations were reduced. Generally, our cytokine levels detected in 700 µg/ml of protein were substantially lower compared to the ones detected in the serum. When comparing TRPM7$^{KR/KR}$ with TRPM7$^{+/+}$ samples particularly striking differences were obtained for IL-13 (Fig. 16I). In TRPM7$^{+/+}$ mice 239.27 (±11.2) pg/mL IL-13 was identified, while the TRPM7$^{KR/KR}$ samples contained only showed 106.055 (±32.0) pg/mL ($P < 0.0004$). IL-9 and IL-2 levels were also significantly reduced in TRPM7$^{KR/KR}$ *ileum* ($P < 0.02$, $P < 0.013$, respectively) compared to TRPM7$^{+/+}$. Interestingly, we observed an opposite effect for IL-17, when we compared Figure 13Z with Figure 16 Z. In Figure 16Z we identified 10.055 (±4.5) pg/mL IL-17 in TRPM7$^{+/+}$ and TRPM7$^{KR/KR}$ 17.286 (±3.2) pg/mL (Fig. 16Z) ($P < 0.034$). However, the IL-17 levels detected in 700 µg/ml gut protein were almost 10-times lower compared to the one in serum. Moreover, the general tendency, we observed for the cytokines in the serum (Fig. 13), was maintained and confirmed in the gut, when comparing TRPM7$^{KR/KR}$ with TRPM7$^{+/+}$ samples.

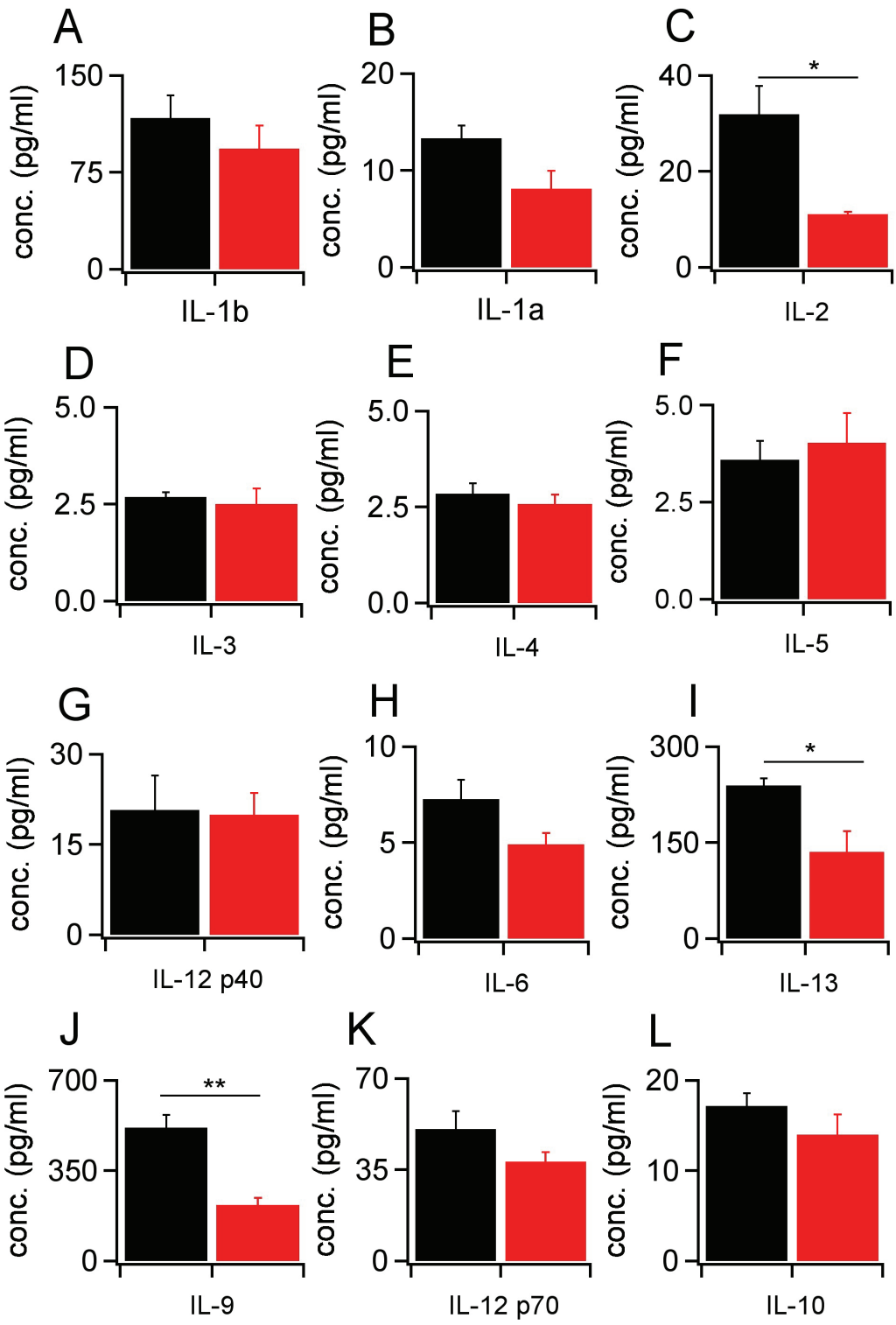
A
150
75
0
conc. (pg/ml)
IL-1b
B
20
10
0
conc. (pg/ml)
IL-1a
C
40
20
0
conc. (pg/ml)
*
IL-2
D
5.0
2.5
0.0
conc. (pg/ml)
IL-3
E
5.0
2.5
0.0
conc. (pg/ml)
IL-4
F
5.0
2.5
0.0
conc. (pg/ml)
IL-5
G
30
15
0
conc. (pg/ml)
IL-12 p40
H
10
5
0
conc. (pg/ml)
IL-6
I
300
150
0
conc. (pg/ml)
*
IL-13
J
700
350
0
conc. (pg/ml)
**
IL-9
K
70
35
0
conc. (pg/ml)
IL-12 p70
L
20
10
0
conc. (pg/ml)
IL-10

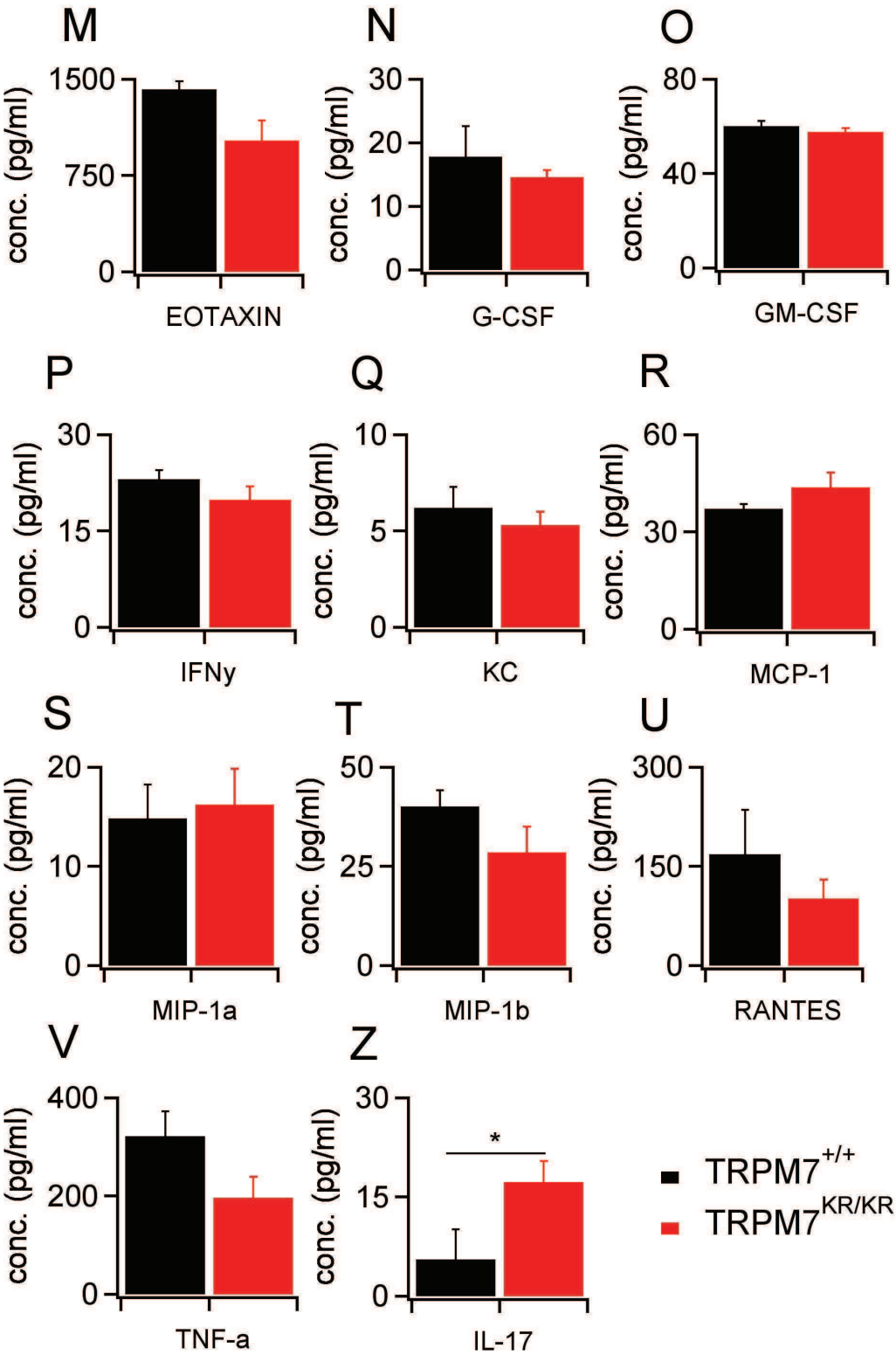

Figure 16: Cytokine levels in the small intestine. (A-Z) Basal cytokine levels evaluated in intestinal samples and shown as pg/mL. Comparison of control $TRPM7^{+/+}$ (black, n = 4) and $TRPM7^{KR/KR}$ (red, n = 5) intestine levels. Bars indicate mean ± S.E.M. Note a significant reduction of the concentrations of IL-2 ($P < 0.013$), IL-13 ($P < 0.0004$), IL-9 ($P < 0.002$) and IL-17 ($P < 0.034$) in $TRPM7^{KR/KR}$ compared to $TRPM7^{+/+}$. (IL *i.e.* interleukin; Eotaxin *i.e.* CC

chemokine subfamily of eosinophil chemotactic proteins, G-CSF *i.e.* granulocyte colony stimulating factor; GM-CSF *i.e.* granulocyte-macrophage colony-stimulating factor, IFNy *i.e.* interferon gamma, KC *i.e.* keratinocyte chemoattractant, MCP-1 *i.e.* monocyte chemoattractant protein-1, MIP *i.e.* macrophage inflammatory protein-1 alpha and beta, TNF-a *i.e.* tumor necrosis factor)

4.8. Potential targets for the TRPM7 kinase

After we characterized the effects, caused by the inactivation of the TRPM7 kinase, at organ and systemic levels, we were investigating molecular mechanisms behind the $TRPM7^{KR/KR}$ phenotype. In particular, to better understand the $\alpha_{E(CD103)}\beta_7$ down regulation that characterized the $TRPM7^{KR/KR}$ mice, we needed to identify the molecular pathway responsible for $\alpha_{E(CD103)}$ expression.

Previously, it has been reported that the Tumor Growth Factor β (TGFβ) is an essential *stimulus* to induce the expression of $\alpha_{E(CD103)}$ in lymphocytes (Schon et al., 1999). So, we first evaluated TGFβ levels in the serum, taking advantage of the ELISA technique, we used above (Fig. 16A-Z and 13A-Z). The same serum samples of both genotypes as analyzed in Figure 13 contained similar systemic TGFβ-1 concentrations. Similarly figure 17B shows the average concentrations of TGFβ-2. We did not detect significant differences in TGFβ-1 and TGFβ-2 isoforms from $TRPM7^{KR/KR}$ mice, compared to $TRPM7^{+/+}$ serum (Fig. 17A-B).

After we established that TGFβ-1 and 2 were preserved at comparable, physiologic concentrations in both genotypes, we questioned, which molecule in the TGFβ signaling cascade was affected by the loss of the TRPM7 kinase activity.

As it is known that TGFβ and SMAD2 (Mothers against decapentaplegic homolog 2) cooperate in the process that leads to CD103 up-regulation (Mokrani et al., 2014; Schon et al., 1999), we investigated SMAD2 phosphorylation using Western Blot (WB) as well as ELISA techniques. We first collected peripheral and mesenteric lymph nodes from our mice, isolated $CD4^+$ T cells and stimulated them with 5 ng/mL TGFβ-1 for a time frame of 15 minutes. We stopped the reaction and added a phosphatase inhibitor to the lysates in order to be able to detect SMAD2 phosphorylation at Serines 465 and 467. Using WB technique we were able to show a clear reduction of phosphorylation of SMAD2 (Fig. 17C) in $CD4^+$ T cells of $TRPM7^{KR/KR}$ mice compared to cells from $TRPM7^{+/+}$ mice. Similar results were detected with the bead-based ELISA technique (Fig. 17D). Freshly isolated $CD4^+$ T cells were stimulated with TGFβ-1 and beads coated with αCD3 and αCD28 antibodies. Lysates were prepared as in Figure 17C and detected with the phospho-SMAD assay (Bio Rad). In order to confirm, that up-regulation of CD103 was indeed

disturbed in our mutant mice, we performed Real-Time reverse-transcription (RT)-PCR (Polymerase Chain Reaction) experiments. Similar to above, we first collected peripheral and mesenteric lymph nodes from both mouse models, isolated $CD4^+$ T cells and stimulated them with 5ng/mL TGFβ for 15, 30, 45 and 60 minutes in a well coated with αCD3 as well as αCD28 antibodies (BioXcell) at respectively 2 µg/mL. The cells were pelleted and lysed to perform RNA extraction as indicated in the manufacturer's instructions (Sigma, see methods). We measured the RNA content in our samples and stored them at -20°. Thereafter, we transcribed the extracted RNA into cDNA (Bio Rad company for Reverse Transcriptase, see methods) and performed quantitative PCR analysis of *Itgae* mRNA expression. *Itgae* is the corresponding gene encoding for $\alpha_{E(CD103)}$. $TRPM7^{+/+}$ $CD4^+$ T cells show a time-dependent increase in *Itgae* mRNA expression, following TGFβ-1 treatment (Fig. 17E). $TRPM7^{KR/KR}$ $CD4^+$ T cells, however, fail to up-regulate *Itgae* mRNA upon TGFβ-1 stimulation. We conclude that our TRPM7 kinase-dead mutant not only showed reduction of SMAD2 phosphorylation, but also notably decreased levels of $\alpha_{E(CD103)}$ mRNA.

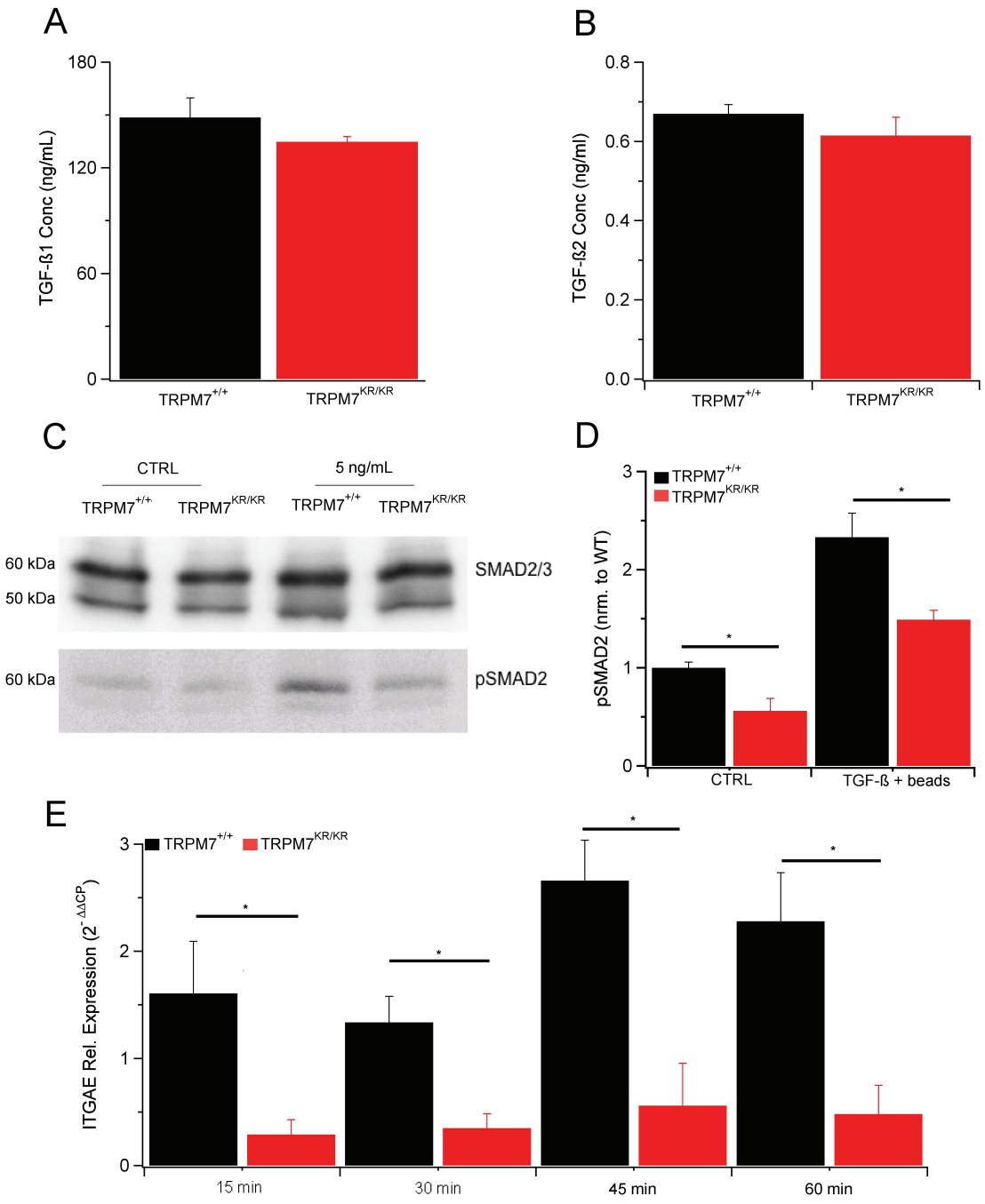

Figure 17: TRPM7 kinase regulates CD103 expression via the TGFβ/SMAD2 pathway. (Cohen and Moiseenkova-Bell) Analysis of TGFβ-1 and TGFβ-2 concentrations in serum. (A) Mouse serum was harvested after cardiac puncture and separated from cells. Bar graph reports mean of TGFβ concentrations in pg/mL ($TRPM7^{+/+}$: black bars, n = 3) ($TRPM7^{KR/KR}$: red bars, n = 3) ± S.E.M. (B) ($TRPM7^{+/+}$: black bars, n = 4) ($TRPM7^{KR/KR}$: red bars, n = 5) ± S.E.M. A total of 4 $TRPM7^{+/+}$ and 5 $TRPM7^{KR/KR}$ mice were used. **(C)** Representative Western Blot analysis of SMAD2 protein. The upper panel shows the detection of SMAD2/3 proteins at 60 and 50 kDa, respectively, using an antibody detecting SMAD2 and 3 simultaneously.

The lower panel shows the phosphorylated fraction of SMAD2 (Serine 465/467) at 60 kDa. A total number of 9 mice were analyzed for each genotype. **(D)** Evaluation of SMAD2 phosphorylation in $CD4^+$ T cells freshly isolated from $TRPM7^{+/+}$ (black bars, n = 3) and $TRPM7^{KR/KR}$ (red bars, n = 3), respectively. The values are plotted as mean fluorescence intensities (MFI) and normalized to the $TRPM7^{+/+}$ control. Error bars indicate S.E.M. A total of 3 mice were used for each genotype. Statistical significance is indicated via * ($P < 0.05$). **(E)** Real-Time PCR analysis of the *itgae* mRNA (encoding for CD103). The graph shows a time course of relative *itgae* mRNA expression (shown as $2^{-\Delta\Delta CP}$) detected at the indicated time frame in $TRPM7^{+/+}$ (black bars, n = 3) and $TRPM7^{KR/KR}$ (red bars, n = 3) $CD4^+$ T cells treated with 5ng/mL TGFβ-1, respectively. Error bars indicate S.E.M. A total of 9 mice were used for each genotype. Statistical significance is indicated via * ($P < 0.05$).

4.9. TRPM7 kinase interaction with SMAD2 is important for immune regulation

As it has been recently shown that TGFβ isoforms and SMAD2 are important for the generation and differentiation of the Th17 effector cell subpopulation (Jin and Dong, 2013; Martinez et al., 2010), we studied Th17 cell differentiation *in vitro*. Therefore, we collected lymph nodes from $TRPM7^{+/+}$ and $TRPM7^{KR/KR}$ mice, isolated $CD4^+$ lymphocytes (Miltenyi, see methods) and cultured them for 5 days with αCD3/αCD28 antibodies (2 µg/mL αCD3 and 2 µg/mL αCD28) and a specific cocktail of cytokines including TGFβ-1, IL-6 as well as αIFNγ and αIL4 neutralizing antibodies in different concentrations (see methods). The intracellular staining for IL-17 and IFNγ was performed according to manufacturer's instructions (BD bioscience, see methods). As expected, when analyzing differentiated Th17 cells *via* Flow Cytometric Analysis we noticed a slightly, but significantly reduced differentiation of $TRPM7^{KR/KR}$ T cells compared to $TRPM7^{+/+}$. In detail, after differentiation $TRPM7^{+/+}$ T cells contained 3.48 (±0.12) % IL-17A producing Th17 cells, while the $TRPM7^{KR/KR}$ Th17 cells were reduced to 2.89 (±0.07) %. We used αIL-17A antibodies conjugated with a fluorochrome to mark Th17 cells, as IL-17A is most important marker for Th17 cells.

In summary, we demonstrate that the TRPM7 kinase is involved in the phosphorylation of SMAD2 (Fig. 17) and thus is essential for the downstream signaling cascades of CD103 up-regulation as well as Th17 cell differentiation. However, the inactivation of the TRPM7 kinase has more systemic effects on the regulation of the immune system (Figure 13 and 16).

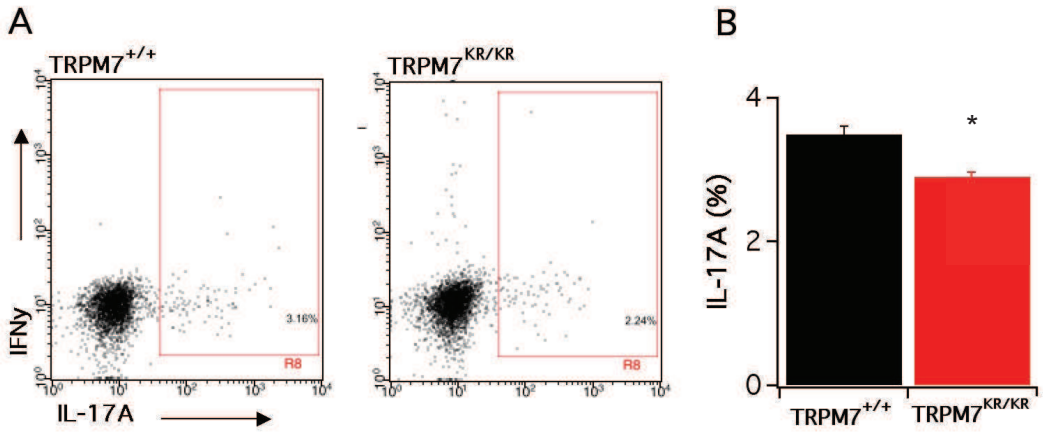

Figure 18: Differentiation of naïve CD4$^+$ T cells into Th17 cells. (A) Representative Flow Cytometric measurements of intracellular IL-17A and IFNγ in CD4$^+$ cells cultured for 5 days. The panel on the left reports staining of TRPM7$^{+/+}$ cells (n = 3) and the panel on the right reports staining of TRPM7$^{KR/KR}$ cells (n = 3). **(B)** Bar graph shows averages of Th17 cells expressing IL-17A (TRPM7$^{+/+}$ black, n = 3) (TRPM7$^{KR/KR}$ red, n = 3) in percent ± S.EM. A total of 5 mice were used for each genotype. Note that the reduction in the percentage of IL-17A expressing TRPM7$^{KR/KR}$ T cells was significantly reduced compared to TRPM7$^{+/+}$ ($P < 0.02$).

5. Discussion

In this study we report the outcome of our investigations using a mouse model with a single point mutation at the kinase domain of the TRPM7 protein, *TRPM7*$^{KR/KR}$ (TRPM7 K1646R/K1646R C57BL/6 mice, RIKEN BRC Centre, Japan) that abolishes kinase activity. Our aim was to better clarify the interactions of the channel with the kinase and to analyze the role of the kinase in cell biological functions and signaling. Our studies mainly focused on immune cells and immune system homeostasis. We hypothesized an essential role for TRPM7 in the regulation of the immune system which we based on a scientific report by Jin et al (Jin et al., 2008). Jin et al. demonstrated that TRPM7 was essential for T cell development. In mice with a T cell-specific deletion of *Trpm7*, lymphocytes underwent a developmental block at the $CD4^{-}CD8^{-}$ double negative stage. This represents one of the most profound effects of any ion channel on lymphocyte development demonstrated so far (Jin et al., 2008). Here, in my research project I proposed the role of the TRPM7 kinase in T cell function and intracellular signalling.

Characterisation of the TRPM7$^{KR/KR}$ *Mouse Model*

Originally, we confirmed the diminished activity of the kinase via immuno-precipitation of TRPM7 and Western Blot techniques of *ex vivo* isolated primary mouse splenocytes. We were able to show a diminished auto-phosphorylation at Ser1511 in Figure 4.1B. The Ser1511 is located within a Ser/Thr-rich stretch within the C-terminus near the kinase domain which is autophosphorylated (Clark et al., 2008). Similarly, Kaitsuka *et al.* reported absent kinase activity in the same mouse model using an *in vitro* kinase assay of TRPM7 protein immunoprecipitated from lysates of embryonic fibroblasts as well as peritoneal macrophages. They demonstrated a lack of ^{32}P incorporation into autologous TRPM7 and exogenous myelin basic protein (MBP) by TRPM7 immunoprecipitated from TRPM7 kinase deficient lysates (Kaitsuka et al., 2014; Ryazanova et al., 2014). TRPM7 is also capable of phosphorylating other substrates and this process is dependent on autophosphorylation. Clark et al. suggested that upon autophosphorylation an “electrostatic docking site” generates and interacts with substrates in order to enable phosphorylation. For instance, they

found actomyosin II phosphorylation was due to TRPM7 kinase activity (Clark et al., 2008; Visser et al., 2014). Lately Kim T.Y. et al. disclosed new 14 auto- and phosphorylation sites, 6 of which were already known (S1255, S1386, T1404, S1565, S1567 and S1849) while some other sites were newly discovered by authors (S1224, S1269, S1300, S1385, T1466, S1498, S1613 and S1846)(Kim et al., 2012). These new findings confirm the idea that phosphorylation sites might vary depending on cell type and conditions, although all of them were located in the same cytosolic C-terminus (Kim et al., 2012). Thus, this TRPM7 mutant mouse model ($TRPM7^{KR/KR}$) permitted investigations on the role of the kinase activity in cell signalling pathways *in vivo*, which were hardly elucidated before. Until recently, all information on kinase function or activity was obtained from mutated kinase constructs overexpressed in cell lines *in vitro* (Schmitz et al., 2003; Yogi et al., 2013). Only a mouse model with a complete deletion of the kinase domain was published recently. Homozygous mice without kinase domain were not viable longer than 7.5 days post conception (Ryazanova et al., 2010). However, it was possible to study the role of TRPM7 kinase in heterozygous mice. Unfortunately, this again brings limitations caused by a heterozygous genotype, as it is uncertain, whether some kinase activity remains.

Preliminary studies concerning the phenotype of the $TRPM7^{KR/KR}$ mouse model showed no gross significant differences compared to wild-type mice (Kaitsuka et al., 2014). In line with these observations, size, weight, and development of organs as we reported in Figure 9C and D were similar between wild-type and $TRPM7^{KR/KR}$ mice. Both male and female $TRPM7^{+/+}$ and $TRPM7^{KR/KR}$ animals were between 7-8 cm in size at the age of 4 weeks. When looking at their weight, tested in 4-6 week old mice (Fig. 9E), we again assessed no substantial differences between wild-type and $TRPM7^{KR/KR}$ mice of both genders. In our hands the average weights were around 19,96 g for wild-type and 19,3 g for $TRPM7^{KR/KR}$. Kaitsuka et al. reported similar results in their studies, when showing mouse weight over a certain time frame of 16-18 weeks (Kaitsuka et al., 2014). In addition, we analysed the offspring ratio for ($TRPM7^{+/+}$), heterozygous ($TRPM7^{+/KR}$) and homozygous ($TRPM7^{KR/KR}$) genotypes from 100 animals and compared values to a Mendelian distribution using a Chi-squared test (Figure 9D). As the calculated p-value was 0.33 our hypothesis that the analysed values are similar to the expected Mendelian ratio can be accepted. Our results together with those of other studies evaluating the same kinase mutant model,

confirmed that the *TRPM7*$^{KR/KR}$ mice do not show obvious alterations from the wild-type phenotype (Kaitsuka et al., 2014) and can be used to study the role of the TRPM7 kinase moiety in T cell function.

Electrophysiological Characterization of TRPM7 Channel Activity

Evaluation of the TRPM7 channel activity in primary murine mast cells, isolated from our mouse model showed no alterations of the current amplitude in mutant when compared to wild-type mast cells. This confirms what other studies reported previously on murine macrophages, mast cells and embryonic fibroblasts (MEFs) (Kaitsuka et al., 2014), (Ryazanova et al., 2014) (Zierler et al., 2015). In other words, despite the point mutation inactivating the kinase, TRPM7 channel activity remains unaltered and its expression is not changed but similar to wild-type control (Fig. 10A-F). Figure 10A shows the comparison between the current amplitudes of the two different genotypes while, Figure 10B shows mean wild-type and *TRPM7*$^{KR/KR}$ outward currents extracted at +80 mV at 500s and plotted as bar graphs (Fig. 10C). These data are in line with previous reports by Matsushita et al., and Schmitz et al. on HEK cells overexpressing the murine K1646R or the correspondent human K1648R mutant respectively (Matsushita et al., 2005) (Schmitz et al., 2003). Moreover, we demonstrated that TRPM7 expression levels are similar in the mutant compared to the wild-type control using a DVF (Divalent Free) solution, which induced maximized linearized monovalent currents (Fig. 10D). It was shown previously that a divalent permeation block shaped TRPM7 inward currents and when using Na^+ instead, monovalent ions are shaping a linear current-voltage relationship (Kerschbaum et al., 2003). Subsequently, we examined the sensitivity of the channels for Mg^{2+} and obtained a Mg^{2+} dose response curve (Fig. 10G) which illustrates no peculiar alterations in channel sensitivity towards Mg^{2+} in the TRPM7$^{KR/KR}$ mouse model when considering physiological cytosolic free Mg^{2+} concentrations of 700 – 900 µM. In 2003 Schmitz et al. analyzed the sensitivity for Mg^{2+} on the heterologously expressed human TRPM7 mutant and reported a similar diminished current at 3 mM Mg^{2+} (Schmitz et al., 2003), while later studies identified this effect at 2.3 mM (Matsushita et al., 2005). We now demonstrated decreasing current amplitudes already at about 100 µM intracellular free Mg^{2+} in primary murine

mast cells, which might be caused by cell type specific differences or overexpression artefacts in the previous studies.

All together we confirm a fully active ion channel characterised by a slightly reduced sensitivity for intracellular free Mg^{2+} when considering the IC_{50} values in $TRPM7^{KR/KR}$ mast cells compared to the controls (WT IC_{50} 183 µM and $TRPM7^{KR/KR}$ IC_{50} 257 µM). Sensitivity to Mg^{2+} is slightly decreased in the kinase dead mutant. This corroborates previous studies, where the authors concluded that wild-type and $TRPM7^{KR/KR}$ mutant channels in MEF cells had similar intracellular Mg^{2+} sensitivity, particularly at physiological Mg^{2+} levels (Ryazanova et al., 2014). In a more recent report, Kaitsuka and colleagues perfused macrophages with 303 µM free Mg^{2+} and observed complete abrogation of TRPM7 currents. We observed similar results, at 300 µM free Mg^{2+} (Fig. 10G) where current amplitudes are clearly nullified (Kaitsuka et al., 2014). The corresponding human mutated channel ($TRPM7^{K1648R/K1648R}$), heterologously expressed in HEK293 cells, affected Mg^{2+} sensitivity showing IC_{50} values of 3 mM $[Mg^{2+}]_i$ instead of ~720 µM of controls (Schmitz et al., 2003). Furthermore and in contrast to our kinase-dead mouse model, the overexpression of K1646R murine construct showed no altered sensitivity to Mg^{2+} (Matsushita et al., 2005). This might be the result of different internal Mg^{2+} concentrations used in the protocol as, for instance, 3 mM Mg^{2+} already blocks current activity in both mutant and wild-type channels.

To finally clarify the sensitivity of the channel to intracellular Mg^{2+}, it would be relevant to examine variables such as methodological settings, cell types and species dependent differences.

We also demonstrated a similar functional expression of TRPM7 in wild-type and $TRPM7^{KR/KR}$ naïve $CD4^+$ T cells (Fig. 10H-I) via whole-cell patch clamp. Therefore, our model can be used for further studies on the role of TRPM7 kinase activity on T cell function and signaling.

Effect of TRPM7 Kinase on Ion Homeostasis

Since the TRPM7 channel is known to conduct mainly Ca^{2+} and Mg^{2+}, we focused on the homeostasis of these two divalent cations in our TRPM7-kinase mutant.

As shown previously, TRPM7 is essential for cellular and systemic Mg^{2+} homeostasis (Ryazanova et al., 2010; Schmitz et al., 2003). Consequently, we first needed to elucidate the contribution of the kinase activity to ion homeostasis. Therefore, we studied the cytosolic free ATP concentration as a measure of intracellular Mg^{2+} concentrations. ATP is known to bind free Mg^{2+} to form intra-cellular Mg-ATP in order to be stored in this complex. Fine-tuning of the free Mg^{2+} concentration, both extra and intracellular are important to regulate cellular functions. Both Mg^{2+} and ATP are part of important cell biological processes: Mg^{2+} is important as cofactor of many enzymes (over 600), while ATP is even more relevant as it is directly linked to energy metabolism. Additionally Mg^{2+} and Mg-ATP inhibit TRPM7 currents at increasing intracellular concentration. Quantification of ATP in its free form by using a luminescence-based assay did not show any significant differences between the two animal models and as mentioned above, intracellular concentrations of Mg-ATP and free Mg^{2+} are both not altered. Feeney et al. demonstrated how the circadian circle is linked to $[Mg^{2+}]_i$ fluctuations. In order to quantify intracellular Mg^{2+}, they measured intracellular ATP instead, assuming an essential role of Mg^{2+} as an ATP cofactor (Feeney et al., 2016) Similarly, our ATP-quantification experiments indicate that Mg^{2+} homeostasis is not changed in our mutant. We also analysed Mg^{2+} in the serum of our mice and did not detect any alterations in the $TRPM7^{KR/KR}$ mice compared to wild-type mice. As the content in the serum is representative only for a very low percentage of the total Mg^{2+} in the body, it might be better to investigate Mg^{2+} also in other organs of accumulation. For instance, 99% of Mg^{2+} is stored in bones, muscle and soft tissues (de Baaij et al., 2015). In these terms, although Mg^{2+} might remain within physiological ranges in the blood, there could still be a severe overall depletion of Mg^{2+} detectable in other organs, but not in the serum (de Baaij et al., 2015). Consequently production of inflammatory cytokines might worsen due to hypomagnesaemia (Sugimoto et al., 2012). Kaitsuka and colleagues also showed an analysis of the Mg^{2+} content in the serum of the $TRPM7^{KR/KR}$ mouse model and showed equal Mg^{2+} levels compared to wild-type mice as in our Fig. 11A (Kaitsuka et al., 2014). Interestingly Ryazanova et al. studied Mg^{2+} variability in more detail showing that the Mg^{2+} concentration varies in the bone marrow. The Mg^{2+} reservoir in the bone marrow was even significantly reduced in the $TRPM7^{KR/KR}$ when mice underwent “normal” Mg^{2+} diet (0.2 %) (Ryazanova et al., 2014). Nonetheless, preliminary unpublished data of colleagues showed no differences in bone morrow

Mg^{2+} content in our mouse models (personal communication). In the end, we conclude a generally maintained Mg^{2+} homeostasis, so we consider the immune system not to be affected by Mg^{2+} variations.

Furthermore, we evaluated potential differences in the intracellular free Ca^{2+} concentration in freshly isolated $CD4^+$ T lymphocytes from $TRPM7^{KR/KR}$ and wild-type mice (Fig. 11D). We used the ratiometric Ca^{2+} indicator Fura-Red and analysed basal Ca^{2+} concentrations measured at physiological conditions when $CD4^+$ T cells were in a resting state. Our results revealed that the basal Ca^{2+} homeostasis was not altered in $TRPM7^{KR/KR}$ T cells. Similarly our studies on metal ion traces in the serum showed no significant alteration of basal Ca^{2+} in the blood when analysing and comparing serum content in the two different mouse models. In detail $TRPM7^{KR/KR}$ elicited an almost equal amount of Ca^{2+} (Fig 12A). A similar result was obtained and shown by Kaitsuka et al. in their very recent report on the same mouse model. They showed that there were no significant differences in the Ca^{2+} concentrations in the serum compared to wild-type mice (Kaitsuka et al., 2014). To better understand whether cellular Ca^{2+} signaling was affected by the TRPM7 kinase, we performed additional investigations with the ratiometric Ca^{2+} indicator Fura-Red (Figure 12) specifically in T cells.

The importance of intracellular Ca^{2+} signalling is highlighted by the fact that mutations in proteins involved in store-operated-Ca^{2+} entry cause immunodeficiencies and autoimmunities (Feske et al., 2010). To study a potential role of the TRPM7 kinase in receptor-mediated Ca^{2+} entry, we conceived a protocol analysing Ca^{2+} influx during $CD4^+$ T cell activation. Lymphocytes were loaded with Fura-Red and treated with αCD3/αCD28-coated beads (Fig. 12). As shown in Fig. 12A-B, no significant differences in Ca^{2+} signaling in $TRPM7^{KR/KR}$ compared to wild-type T cells were detected during TCR stimulation over a time frame of 5 minutes. Lymphocytes show prolonged Ca^{2+} influx, following T cell receptor stimulation (APCs-CD3/CD28 binding) and essential players contributing to these characteristic intracellular Ca^{2+} increase are ORAI1/CRACM (calcium release-activated calcium modulator) channel and STIM (Stromal Interaction Molecule)(Feske et al., 2010). In a more indirect approach, we investigated Ca^{2+} signaling via evaluation of $CD4^+$ T cell proliferation. T cell proliferation is based on TCR stimulation and subsequent Ca^{2+} fluxes elaborated by ORAI1 and STIM (Lioudyno et al., 2008), (Qu et al., 2011). In other words, in these

experiments we considered a proper T cell proliferation as direct indication of a functioning Ca^{2+} signaling. Our results suggest that Ca^{2+} homeostasis and signaling are normal in our kinase-deficient mutant compared to $TRPM7^{+/+}$, at least under the conditions we used for our experiments.

The *TRPM7 Kinase Mutation Causes Alterations in the Homeostasis of the Immune System*

Besides its importance for ion homeostasis, the entire TRPM7 channel-kinase has been previously shown to be important for chemokine and cytokine expression profiles and thus for immune system homeostasis. For instance, Jin et al. studied a mouse model with a tissue-specific deletion of the *trpm7* gene in thymocytes and revealed that TGF-β2 mRNA expression was altered (Jin et al., 2008). Thus, they demonstrated the role of TRPM7 in cytokines production and in the control of the immune system response. Another recent report elucidated lower cytokine secretion (histamine, IL-6, IL-13 and TNF-α) in bone-marrow derived mast cells when TRPM7 channel activity was inhibited (Huang et al., 2014). Basing on these results, we utilized the TRPM7 kinase-deficient mouse model to study the role of the kinase in cytokine production. Therefore, we performed a bead-based ELISA on serum harvested from both mouse models. Our data revealed a general reduction of cytokines in serum from $TRPM7^{KR/KR}$ mice compared to wild-type mice. These data gave us a first confirmation of a potential role of the TRPM7 kinase in the regulation of cytokine release and/or expression and we conclude that the kinase at least in part, is responsible for the reduced cytokine production. Furthermore the TRPM7 kinase (M7CKs) is said to relocate into the nucleus once it has been cleaved off and to interact with transcription factors, thus affecting cell differentiation (Krapivinsky et al., 2014). Therefore, it is possible that M7CKs might interact with other transcription factors such as, NFAT (nuclear factor of activated T cells). NFAT is also known as key transcription factor, shaping T cells differentiation and cytokine production (Hermann-Kleiter and Baier, 2010), (Naito et al., 2011). Consequently, it is tempting to speculate a possible interaction of TRPM7 kinase with NFAT, which might explain the dysfunctional cytokine secretion in kinase deficient animals. When we analysed the cytokine levels in serum we found significant differences in the concentrations of IL-2, IL-17 and G-CSF. IL-2 is known as the first cytokine, which is secreted at the

frontier of a pro-inflammatory response. It was formerly known as T cell growth factor (TCGF) indicating that it is the quickest and most important signal that T cells receive in order to proliferate and increase lymphokine secretion (Olejniczak and Kasprzak, 2008). This might already be part of an explanation why we observed a generalized down regulation of different cytokines. In other words, low IL-2 concentrations might cause ineffective immune responses as the stimulation, production and secretion of further cytokines is not triggered. IL-17, is part of a pro-inflammatory cytokine profile with peculiar functionalities depending on its different isoforms (Jin and Dong, 2013). Unfortunately, one limitation of our applied ELISA technique was that it was not possible to identify specific IL-17 isoforms. It might still be interesting to further clarify, which isoforms is reduced, either IL-17A or IL-17F (Jin and Dong, 2013). Furthermore, IL-17 is closely related to G-CSF since different publications refer to the so-called IL-17/G-CSF axis. IL-17 and G-CSF concentrations are correlated to each other since IL-17 is responsible for inducing innate immune cells, stromal cells and epithelial cells to secrete G-CSF and other chemokines (Maynard et al., 2012). In line with these data, we also found a significant reduction in G-CSF in the serum of our mutants.

Although we show an intriguing picture, revealing an altered homeostasis of the immune system in our TRPM7 kinase-deficient animal model, we still do not know the molecular basis underlying our phenotype.

Gut-associated Lymphoid Tissues are Particularly Dependent on TRPM7 Kinase Activity

Since we observed a generalized reduction of cytokine concentrations in the serum of TRPM7$^{KR/KR}$ mutant compared to wild-type mice, we further speculated that the immune system homeostasis was altered in our mutant mice. To address this hypothesis, we studied the activity of the immune system in the gut. The importance of the gut and its interplay with the immune system to promote development, maintenance and renewal of the immune system itself, has been accepted by the scientific community (Maynard et al., 2012). The gut is the broadest body surface after the skin, which is exposed to the external milieu, its pathogens, commensal bacteria, non-self elements and food antigens. Therefore, in such a “dangerous”

environment the immune system needs to be tightly regulated and “updated”. For this purpose more than 50-70% of the total lymphocytes (mainly T cells) in the body, populate the mucosal immune compartment where they are the first to encounter novel pathogens (Mueller and Macpherson, 2006), (Qiu et al., 2015). Scanning electron microscopy (SEM) captured images of the gut tissue surface of our mouse models and they were used in order to identify possible alterations in the structure that could have caused infiltration of pathogens or commensal bacteria and subsequently compromise or stress immune responses. Images of luminal tissues (Fig. 14A-B) and microvilli (Fig. 14C-D) harvested from both animal models indicate that the cellular organization and structure are preserved and comparable to wild-type controls (Fig. 14A-D). Our images also show an unaltered shape of M cells (Microfold cells) (Fig. 14A-B), which are known to be the direct gate between the lumen and the Peyer’s patches where the dendritic cells encounter the antigen (Mueller and Macpherson, 2006). These images confirm that the first physical protective barrier, the epithelial layer, is properly structured and could represent a functional barrier.

Since we demonstrated that altered tissue structure and ion homeostasis were not the cause for an improper immune system regulation resulting in altered basal concentration of cytokines in the blood, we closely investigated the organization of the different T cells populations in the gut and analysed the intestinal tissue and its T cells compartments.

Therefore, our collaborators, Andrea Romagnani and Fabio Grassi from the T cell development laboratory at the Institute for Research in Biomedicine (IRB) in Bellinzona, Switzerland, analysed the distribution of lymphocytes at different layers of the intestinal tissue. As reported in Figure 15 the amount of T cells was remarkably diminished in the TRPM7$^{KR/KR}$ model. Most strikingly, TCRαβ and TCRγδ T lymphocytes were noticeably reduced in number within the external layer, the epithelium (IEL). Here the great majority of intraepithelial lymphocytes (IEL) are T cells and exert several different regulatory, as well as effector immune activities, (Mowat and Agace, 2014). We concluded that their effector and regulatory activities were compromised due to a reduced cell number. Similarly, the amounts of both TCRαβ and TCRγδ T cells were significantly reduced in the TRPM7 kinase mutant model in the lamina propria, the layer underneath the epithelium. The lamina propria

hosts T cells, B cells and innate immune cells (Agace, 2006). Some of them re-locate towards the epithelium once they up-regulate certain proteins, defined as gut homing proteins. They are specific for each tissue; for instance $\alpha_4ß_7$ is required for T cells to cross the endothelium via binding to mucosal addressin cell adhesion molecule (MAdCAM) on endothelial cells. These proteins are topics of great interest when researching new therapeutic targets and some are part of established therapies against inflammatory bowel diseases (IBDs) (Gerner et al., 2013), (Habtezion et al., 2016). Considering these results, it is tempting to speculate that our mutant T cells might have a defect in the expression of a gut homing protein.

We investigated different gut-homing proteins to explain the less defensive immune system and the lower lymphocyte number in the kinase deficient mice. These proteins are up regulated when lymphocytes are induced to reach a certain organ of the body, i.e. the skin or intestine and help them to pass through the membranes of lymph vessels. M. P. Schoen et al. reported that mice lacking one of these gut homing proteins, CD103 (α_E), had selectively reduced numbers of T lymphocytes (Schon et al., 1999), (Gorfu et al., 2009).

Therefore, we investigated the expression of CD103, also known as $\alpha_{E(CD103)}ß_7$ and found a significant reduction of lymphocytes of the intraepithelial layer of $TRPM7^{KR/KR}$ mice compared to wild-type controls. CD103 was evidently down regulated in our mutants compared to $TRPM7^{+/+}$ mice, (data kindly provided by our Swiss collaborators Andrea Romagnani and Fabio Grassi at the IRB; Fig. 15A-D). In the epithelial layer CD103 binds its ligand E-cadherin expressed on epithelial cells thus, favouring retention of T lymphocytes *in loco* where they exert their activity as sentries of the immune system (Suffia et al., 2005).

TRPM7 Kinase affects Gut Immune Homeostasis

These interesting results encouraged us to evaluate the cytokine concentrations also in the small intestine. Similar to the serum (Fig. 13A-Z), we noticed a strong reduction in the concentration of most cytokines in the $TRPM7^{KR/KR}$ mice compared to $TRPM7^{+/+}$ (Fig. 16A-Z). Surprisingly the IL-17 concentration (Fig. 16Z) was enhanced in $TRPM7^{KR/KR}$ mice compared to $TRPM7^{+/+}$ controls. The reason for this result might be a strong compensation exerted by the innate lymphocyte population which is

known to secrete IL-17A as well as IL-17F in the lamina propria (Maynard et al., 2012). TCRγδ T cells most likely do not facilitate this “compensatory role”, as this subset was also reduced in the intra epithelial layer of TRPM7$^{KR/KR}$ animals (Fig. 15, kindly provided by Andrea Romagnani and Fabio Grassi, IRB). However, albeit reduced in number, they might still in part compensate for the reduced IL-17 levels. Since we examined cytokines in the lysate obtained from the entire intestinal tissue, including its different cell layers (epithelial as well as lamina propria and muscular layers) we need to also consider other innate and adaptive cell subsets, which might cooperate in order to compensate for a compromised immunity. The increase in IL-17 levels shown in Figure 16Z might be the result of secretion from other cell subtypes located deeper in the intestinal tissue (such as innate lymphocytes). We should also mention recent studies in which a protective role for IL-17 was elicited. It was shown that abrogation of IL-17A leads to exacerbation of IBD (Inflammatory Bowel Disease) because the epithelial layer became more permeable to pathogens. It was speculated that IL-17 is meant to regulate and maintain integrity of tight junctions and thus protect epithelial tissue from incoming insults (Lee et al., 2015). IL-17 might properly help to maintain the structure of the epithelial barrier but the lack of intraepithelial lymphocytes causes a failure to react against pathogens from the lumen. Similarly to the results we obtained in Figure 13, we were also able to report a significantly reduced IL-2 concentration in the gut. Furthermore, concentrations of IL-13 and the Th2 related cytokine IL-9 (Wynn, 2015) were significantly diminished in the kinase-dead mouse model when compared to TRPM7$^{+/+}$. IL-13 together with IL-4 are part of the type 2 immune response (Van Dyken and Locksley, 2013). Interestingly, IL-4 concentrations were below the detection value also indicating an impaired Th2 activity in theTRPM7$^{KR/KR}$ mutant. In this respect we should mention that IL-9 was shown to be synergistically activated by IL-2 exposure and SMADs both recruiting IRF4 (interferon regulatory factor 4), thus explaining the strong IL-9 reduction reported in Figure 16J (Kaplan et al., 2015). The expression of IL-13 (Mannon and Reinisch, 2012) as well as IL-9 (Kaplan et al., 2015) is regulated by STAT6. The scientific community often refers to IL-13 as the cytokine responsible for apoptosis of epithelial cells and increased pore formation leading to ulcerative colitis (Van Dyken and Locksley, 2013). Thus, in turn, our mutant model should be protected from intestinal insults.

The role of TRPM7 for CD103 expression however is still elusive. Scientific reports indicated TGFβ as the major signal for $\alpha_{E(CD103)}ß_7$ expression (Hahm et al., 2001), (Boutet et al., 2016). Moreover, another scientific report indicated that CD103 expression required the cooperation of NFAT and phosphorylated SMAD2/3, which is a downstream transcription factor in the TGFβ-1 signalling cascade (Mokrani et al., 2014). Interestingly TRPM7 seemed to be implicated in R-SMAD (SMAD2, SMAD3 complex) phosphorylation (Fang et al., 2014). Taken together these findings suggest a contribution of TRPM7 in R-SMAD phosphorylation. R-SMAD activation is essential for CD103 gene expression and is downstream of TGF-β–signalling. To test this hypothesis, we evaluated the concentration of TGFβ-1 and 2 via the bead-based ELISA technique in the serum and in $CD4^+$ T cells. As shown in Figure 17A for the serum and 8B for the lymphocyte lysates, no significant differences were found between the two different genotypes. Therefore, TGFβ-1 and 2 are synthetized (Fig. 17B) and secreted (Fig. 17A) in equal amounts in both mouse models, suggesting that TGFβ-1 itself is not the cause of the reduced CD103 expression. The defect must be located downstream of TGFβ receptor activation. As already mentioned, SMAD2/3 may play a key role in the downstream signalling of TGFβ (Bruce and Sapkota, 2012). Thus, we extended our studies to investigate SMAD2 phosphorylation. Interestingly, we found that SMAD2 was indeed less phosphorylated at its Ser465 residue upon TGFβ-1 stimulation than in wild-type controls as shown by Western Blotting in Figure 17C, as well as via multiplex ELISA (Bio Rad) in Figure 17D. Intriguingly, it has been also shown that SMAD2 regulates Th17 cell differentiation. (Jin and Dong, 2013) (Martinez et al. 2010). SMAD2 positively regulates cell differentiation and thus indirectly supports IL-17A secretion (Jin and Dong, 2013; Martinez et al., 2010). All these findings provide a possible explanation for the reduced IL-17A concentrations in the serum of the mutant mice, which might be due to improper Th17 differentiation as a consequence of reduced SMAD2 activity. This hypothesis might also explain enhanced IL-17 levels in the gut due to other cell types, which are compensating for the lack of IL-17 in the serum. Therefore, we finally investigated, whether naïve $CD4^+$ T cells from our $TRPM7^{KR/KR}$ mice had a defect in Th17 polarization. Figure 18 shows that Th17 cell differentiation is significantly compromised in $TRPM7^{KR/KR}$ T cells, most likely due to improper SMAD2 phosphorylation (Fig. 17C-D).

In summary, we suggest that the TRPM7 kinase is involved in TGFβ-1 downstream signaling, where it affects SMAD2 phosphorylation at Ser465. However it remains questionable, whether this phosphorylation is direct or indirect and this mechanism needs to be answered through an *in vitro* kinase assay.

This initial study of TRPM7$^{KR/KR}$ provides first evidence for an interesting role of the TRPM7 kinase function in immune regulation in the gut. Moreover, we can position the TRPM7 kinase in the signal transduction cascade downstream of the TGF-β activation cascade as essential for the phosphorylation of SMAD2. In the future the TRPM7 kinase domain may be a new pharmacological target in the development of therapeutic options for gut-associated diseases such as IBD (inflammatory bowel disease) and UC (ulcerative colitis).

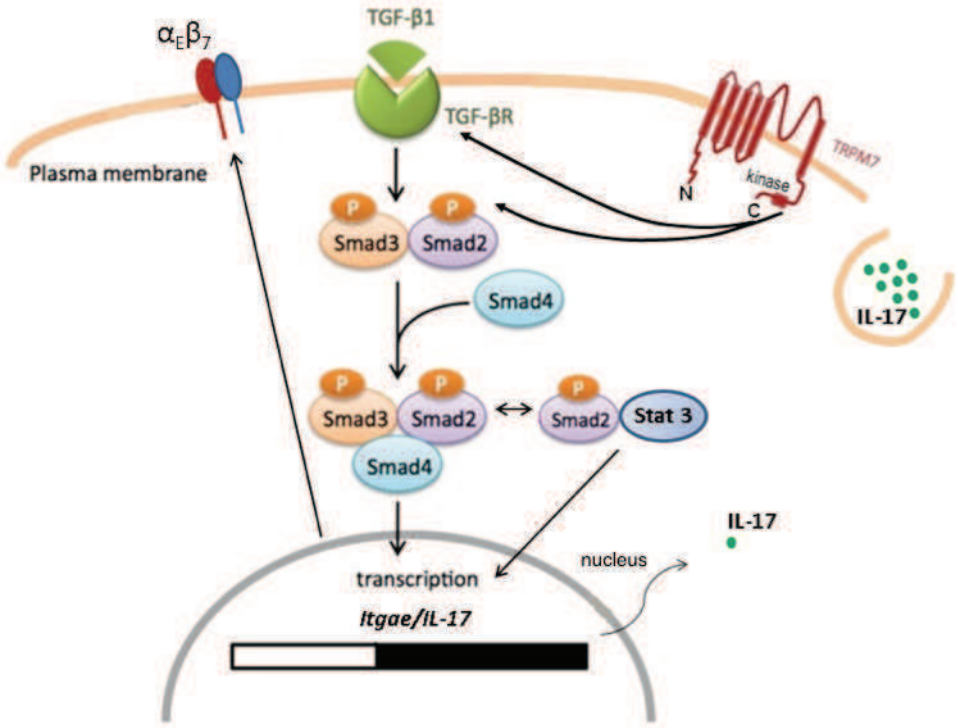

Figure 19: TRPM7 kinase interaction with SMAD2 is important for immune regulation.

Itgae mRNA expression pattern, where *Itgae* is the corresponding gene encoding for α_E (CD103) (Blue and red protein on plasma membrane). TRPM7$^{KR/KR}$ CD4$^+$ T cells showed an impaired expression of *Itgae* mRNA, following TGFβ-1 treatment (green complex TGFβ-1 and TGFβ receptor). TRPM7 kinase-dead mutant elicited a decrease of SMAD2 (violet) phosphorylation and levels of α_E (CD103) mRNA. Further investigations are needed to determine whether TRPM7 kinase affects SMAD2 phosphorylation (question mark) directly or indirectly. Similarly, SMAD2 phosphorylation is essential for Th17 cell differentiation and IL-17 production (green dots). TRPM7$^{KR/KR}$ mice show decreased IL-17 levels in serum and TRPM7$^{KR/KR}$ CD4$^+$ T cells produce less IL-17 following Th17 cell polarization for 5

days. Figure modified from Fang et al. (2014). Reprinted by permission from Macmillan Publishers Ltd: [Toxicology and Applied Pharmacology], (Fang et al., 2014), copyright (2014)

6. Appendix 1

Laboratory Equipment

Name of item	Company, Location
AxioCam MRm camera	Zeiss, Jena
Cell culture dishes (35 mm, 60 mm, 90 mm)	Sarstedt, Nümbrecht
Cell culture flask (75 cm2)	Sarstedt, Nümbrecht
Cell culture plates (6- and 24-well)	Sarstedt, Nümbrecht
Cell incubator New Brunswick Galaxy 170 S	Eppendorf, Hamburg
Cell strainer (45 µm)	Sarstedt, Nümbrecht
Centrifuge 5424 R	Eppendorf, Hamburg
Centrifuge 5804 R	Eppendorf, Hamburg
Centrifuge HERAEUS Biofuge Stratos	Thermo Scientific, Waltham (USA)
Centrifuge HERAEUS Pico 17	Thermo Scientific, Waltham (USA)
Centrifuge bottles (250 mL)	Sarstedt, Nümbrecht
Centrifuge tubes (15 mL, 50 mL)	Sarstedt, Nümbrecht
Coverslips (12 mm)	Sarstedt, Nümbrecht
Cryo tubes (1.5 mL)	Sarstedt, Nümbrecht
Cytostatic safety cabinet FlowSafe® C-[MaxPro]3-190	Berner, Elmshorn
Electrophoresis chamber Mini-PTOTEAN Tetra	Bio-Rad, Hercules (USA)

cell	
Erlenmeyer flask (1 L, 250 mL, 50 mL)	Duran Group, Mainz
Faraday cage	HEKA, Lambrecht
Filter papers	Munktell, Bärenstein
Fluostar, Omega	BMG Labtech
Freezer, -20°C	Bosch, München
Freezer, -80°C	Eppendorf, Hamburg
Fridge, 4°C	Siemens, München
Glass bottles (1 L, 500 mL, 250 mL, 50 mL)	Duran Group, Mainz
Glass capillary GB150TF-8P	Science products, Hofheim
Heat block	PeqLab, Erlangen
Hemacytometer	Brand, Wertheim
Incubated orbital shaker MaxQ™ 6000	Thermo Scientific, Waltham (USA)
Inverted microscope Axio Vert.A1	Zeiss, Jena
LED light source for fluorescence Colibri 2	Zeiss, Jena
Light Cycler 480	Roche Life Science
Light microscope Axiovert 35 M	Zeiss, Jena
Magnetic stirrer C-MAG HS7	IKA, Staufen
Micromanipulator PatchStar	ΨScientifica, Uckfield (UK)
Micromanipulator PatchMan NP2	Eppendorf, Hamburg
Microscope slides	Roth, Karlsruhe

Osmometer VAPRO 5600	Wescor, Logan (USA)
Pasteur pipettes	Roth, Karlsruhe
Parafilm	Pechiney Plastic, Chicago (USA
Patch clamp Amplifier EPC-10	HEKA, Lambrecht
pH meter FiveEasy Plus	Mettler Toledo, Albstadt
Pipetboy	Eppendorf, Hamburg
Pipette tips (1000 µl, 200 µl, 20 µl)	Sarstedt, Nümbrecht
Pipettes (1000 µl, 200 µl, 100 µl, 10 µl, 2.5 µl)	Eppendorf, Hamburg; Brand, Wertheim
Platform shaker Duomax 1030	Heidolph, Kehlheim
Polyethylene tube film, 200 x 0.2 mm	Rische + Herfurth, Hamburg
Power supply PowerPac basic	Bio-Rad, Hercules (USA)
Puller DMZ-Universal Puller	Zeitz, Martinsried
Reaction tubes (200 µl, 500 µl, 1.5 ml, 2 ml)	Sarstedt, Nümbrecht
Safety vacuum system EcoVac	Schuett-biotech, Göttingen
Serological pipettes (2 ml, 5 ml, 10 ml, 25 ml)	Sarstedt, Nümbrecht
Spectrophotometer BioPhotometer plus UV-Visible	Eppendorf, Hamburg
Syringe (15 mL, 2 mL)	Sarstedt, Nümbrecht
Thermomixer compact	Eppendorf, Hamburg
Transfer pipettes	Sarstedt, Nümbrecht
Tube rotator	Heidolph, Kehlheim

Vibration isolation table	TMC, Peabody (USA)
Vortex mixer MS 3 basic	IKA, Staufen
Water bath	Memmert, Schwabach
Wet/Tank Blotting system	Bio-Rad, Hercules (USA)
Whatman PVDF membrane	GE Healthcare, München

Name of chemicals and ready-to-use solutions	Company, Location
Acetic acid	Sigma-Aldrich, Deisenhofen
Agar-agar	Roth, Karlsruhe
Albumin Fraction V (BSA)	Roth, Karlsruhe
Ampicillin	Sigma-Aldrich, Deisenhofen
Ammonium persulfate (APS)	Roth, Karlsruhe
β-Mercaptoethanol	Sigma-Aldrich, Deisenhofen
Bio-plex Cell Lysis Kit 171304011	Bio Rad
Bradykinin	Sigma-Aldrich, Deisenhofen
Brilliant Blue R-250	Sigma-Aldrich, Deisenhofen
Broad range protein ladder, #26634	Thermo Scientific, Waltham (USA)
Bromphenolblue	Sigma-Aldrich, Deisenhofen
CaCl2	Sigma-Aldrich, Deisenhofen
Cs-glutamate	Roth, Karlsruhe
CsOH	Roth, Karlsruhe
p-Coumaric acid	Sigma-Aldrich, Deisenhofen
EDTA	Sigma-Aldrich, Deisenhofen
EGTA	Roth, Karlsruhe
Ethanol	Roth, Karlsruhe

DH5 cells	Life technologies, Carlsbad
DMSO	Roth, Karlsruhe
Dulbecco's Modified Eagle's Medium	Sigma-Aldrich, Deisenhofen
Dulbecco's phosphate buffered saline	Sigma-Aldrich, Deisenhofen
Dynabeads Protein G	Life technologies, Carlsbad (USA)
FastAP Thermosensitive alkaline phophatase	Thermo Scientific, Waltham (USA)
Fetal Bovine Serum (FBS)	Life technologies, Carlsbad (USA)
Glycerol	Sigma-Aldrich, Deisenhofen
Glycine	Sigma-Aldrich, Deisenhofen
D-(+)-glucose	Sigma-Aldrich, Deisenhofen
H2O2	Roth, Karlsruhe

HCl	Roth, Karlsruhe
HEPES	Sigma-Aldrich, Deisenhofen
High range protein ladder, #26625 (USA)	Thermo Scientific, Waltham
Igepal Ca-630	Sigma-Aldrich, Deisenhofen
Isopropanol	Roth, Karlsruhe
Kanamycin	Sigma-Aldrich, Deisenhofen
KCl	Sigma-Aldrich, Deisenhofen
KH2PO4	Sigma-Aldrich, Deisenhofen
KOH	Roth, Karlsruhe
Lipofectamin Reagent	Life technologies, Carlsbad (USA)
Luminol	Sigma-Aldrich, Deisenhofen
Minimum essential medium eagle (MEME)	Sigma-Aldrich, Deisenhofen
Methanol	Roth, Karlsruhe
MgCl2	Sigma-Aldrich, Deisenhofen
NaCl	Roth, Karlsruhe
NaF	Sigma-Aldrich, Deisenhofen
Na2HPO4*7H2O	Sigma-Aldrich, Deisenhofen

Naltriben	Tocris Bioscience, Bristol (UK)
NaN3	Roth, Karlsruhe
NaOH	Roth, Karlsruhe
Penecillin/Streptomycin	Sigma-Aldrich, Deisenhofen
Phosphatase-Inhibitor	Sigma-Aldrich, Deisenhofen
Phosphatase	Thermo Scientific, Waltham (USA)
10xPhosphatase Buffer	Thermo Scientific, Waltham (USA)
PMA	Sigma-Aldrich, Deisenhofen
Poly-L-Lysin	Sigma-Aldrich, Deisenhofen
Ponceau S	Sigma-Aldrich, Deisenhofen
Protease-Inhibitor tablets	Thermo Scientific, Waltham (USA)
Protease & Phosphatase-Inhibitor Mini tablets	Sigma-Aldrich, Deisenhofen
Phosphatase-Inhibitor Cocktail	Thermo Scientific, Waltham (USA)
Phenylmethylsulfonyl fluoride (PMSF)	Sigma-Aldrich, Deisenhofen
Rotiphorese Gel 30	Roth, Karlsruhe
Sodium dodecylsulfate (SDS)	Roth, Karlsruhe
S.O.C. Medium (USA)	Life technologies, Carlsbad
Sucrose	Sigma-Aldrich, Deisenhofen

Temed	Roth, Karlsruhe
Tris	Roth, Karlsruhe
Triton X-100	Sigma-Aldrich, Deisenhofen
Trichlorol	Lysoform, Berlin
Tryptone (peptone ex casein)	Roth, Karlsruhe
0.05% Trypsin-EDTA solution (1x)	Sigma-Aldrich, Deisenhofen
Tween-20	Sigma-Aldrich, Deisenhofen
Yeast extract	Roth, Karlsruhe

7.Appendix 2

Mouse surgery

PBS	Sigma Aldrich
RPMI modified (500mL)	Sigma Aldrich, Invitrogen

5 mL Glutamin 200mM, 5 mL PenStrep 100X, 5 mL Sodium Pyruvate 100mM, Non Essential Amminoacids 100mM, 50µM β-Mercaptoethanol, 50 mL FCS (10%), up to final volume with RPMI were mixed, filtered and stored at 4°.

Isolation

PBS	Sigma Aldrich
RPMI	Sigma Aldrich
CD4+ isolation Kit	Miltenyi Biotec
γδ T cell Isolation Kit	Miltenyi Biotec
FcR Blocking Reagent	Miltenyi Biotec

Macs-Buffer*

500 mL PBS, 2,5g BSA, 2,0 mL EDTA 100mM were mixed, filtered and stored at 4°.

Flow Cytometry Analysis

Anti-mouse CD4 antibody	Biolegend
Anti-mouse CD154 antibody	Biolegend
Anti-mouse CCR9 antibody	Biolegend

Anti-mouse CD103 antibody	Biolegend
Anti-mouse CD3 antibody	Biolegend
Anti-mouse LPAM antibody	Biolegend
Anti-mouse CD40 antibody	Biolegend
Anti-Biotin	Biolegend
FcR Blocking Reagent	Miltenyi Biotec
Macs Buffer* (as previously)	

ATP assay

ATP determination Kit	Invitrogen cat.A22066
Triton X-100	Sigma Aldrich

Cell Lysis Buffer

1% triton mixed with PBS and stored at 4°.

Electrophysiology

CesiumOH L-Glutamic Acid	Sigma Aldrich
EDTA	Sigma Aldrich
EGTA	Sigma Aldrich
Glucose	Sigma Aldrich
CaCl	Sigma Aldrich
$MgCl_2$	Sigma Aldrich

NaCl	Sigma Aldrich
Hepes	Sigma Aldrich
CsOH	Sigma Aldrich

Mg^{2+}-free Cs-Glutamate Ringer (1L), stock solution 120mM Cs-Glut.

Cs-Glutamate 120mM (120mL 0f 0.2M stock), NaCl 8mM (0.32mL of 5M stock) and Hepes-CsOH 10mM (0.2mL of 1M stock).

PH and osmolarity were adjusted at 7.2 and ≅250 mOsm, respectively with CsOH.

Mg^{2+}-free Cs-Glutamate Ringer (1L), stock solution 140mM Cs-Glut.

Cs-Glutamate 140mM (140mL 0f 0.2M stock), NaCl 8mM (0.32mL of 5M stock) and Hepes-CsOH 10mM (0.2mL of 1M stock).

PH and osmolarity were adjusted at 7.2 and ≅300 mOsm, with CsOH.

Mg^{2+} and Mg-ATP free, internal solution.

5mM EDTA end concentration, 10mM EGTA end concentration, in proper amount of Mg^{2+}-free Cs-Glutamate Ringer (120mM or 140mM)

Ca^{2+}-free Sodium Ringer (1L), stock solution.

140mM NaCl, 2,8mM KCl, 2mM $MgCl_2$, 10mM Hepes-NaOH all components are indicated in end concentration values.

2mM Mg^{2+}, external solution.

50mg Glucose, 25µL $CaCl_2$ (1M) mixed to 25mL of Ca^{2+}-free Sodium Ringer.

PH and osmolarity were adjusted at 7.2 and ≅300 mOsm, respectively with NaOH or KCl and respectively glucose.

Mg^{2+}- and Ca^{2+}-free Sodium Ringer, stock solution.

140mM NaCl, 2,8mM KCl, 10mM Hepes-NaOH all components are indicated in end concentration values.

PH and osmolarity were adjusted at 7.2 and ≅300 mOsm with NaOH.

Mg^{2+}-free, external solution.

50mg Glucose, 75µL $CaCl_2$ (1M) mixed to 25mL of Mg^{2+} and Ca^{2+} free Sodium Ringer.

Divalent-free solution.

Mg^{2+}- and Ca^{2+}-free external solution, 100mM EDTA end concentration.

All the mentioned solutions were stored at 4°.

Cytokine Assay

Bio-plex, Cell Lysis Kit 171304011	Bio Rad
23 Cytokines Assay M60009RDPD	Bio Rad

TGFβ Assay

TGFβ Assay Kit	R&D system

Phospho-Assay

Bio-plex Phosphoprotein Detection Kit LQ000000006935	Bio Rad

Immunoprecipitation and Western Blot

Rabbit anti-mouse αTRPM7	ProScientifica
Rabbit anti-mouse αTRPM7-S1511	V. Chubanov, LMU
SMAD2/3 Antibody Kit	Cell Signaling cat.127475
Rabbit anti-mouse αWASP	Cell Signaling cat. 2860
Anti-Rabbit	

Bradford Assay:

stock solution.

250 mg Coomassie blue G250 (0,1% w/v) was mixed together with 250 mL EtOH (100%), they were filtered and stored in the dark at 4°C.

Bradford Reagent for 5 ml stock Solution (5% v/v)

10 ml Phosphoric acid (85%; 8,5% v/v) were mixed and filled up with distilled H_2O up to 100 mL.

Protein determination:

For each sample: 2 µL probe/standards added to 98 µL of distilled H20.

For each standard probe: 2 µL of buffer that was used for probes, were added to 96 µL of distilled H20.

1,5 mL Bradford Reagent were added to each sample and standard probe.

Before detection all were mixed with vortex, incubated for 5‘ at least, at RT and were measured within an hour. For detection were used an excitation at 595 nm.

Buffers:

PBS – Stock (10x):

Substance	MW (g/mol)	Needed conc. (10x)
KCl	74,55	26, 8 mM
KH_2PO_4	136,09	14, 7 mM
NaCl	58,44	1,37 M
$Na_2HPO4 \times 7\ H_20$	268,07	80,58 mM

We stored 1-5 L (w/ $_{dd}H_20$), adjust to pH 7,4; dilute 1:10 in H_2O for use

Transfer buffer (Blotting Buffer) w/ Methanol (MeOH):

Substance	MW (g/mol)	Needed conc.
Tris HCl	121,14	59,8 mM
Glycine	75,07	48,6 mM
SDS	288,4	1,63 M
MeOH	100%	20%

Transfer buffer (Blotting Buffer) w/out Alcohol – Stock (10x):

Substance	MW (g/mol)	Needed conc. (for 10x)
Tris HCl	121,14	250 mM
Glycine	75,07	1,92 M

We prepared 1-5 L (w/ $_{dd}H_20$); dilute 1:10 in H_2O for use

TBS-Stock (10x):

Substance	MW (g/mol)	Needed conc. (for 10x)
Tris HCl	121,14	500 mM
NaCl	58,44	1,5 M

We prepared at least 1 L (w/ $_{dd}H_20$); dilute 1:10 in H_2O for use

TBS-T (0,1 %):

Substance	Needed conc. (for 10x)	Volume
TBS-Stock (10x)	1 x	100 ml
Tween 20	0,001%	1 ml
add $_{dd}H_20$ up to		1000 ml

4x SDS-sample buffer:

Substance	Stock conc.	Volume
Tris HCl (pH 8,8)	1 M	8 ml
SDS	20%	16 ml
Glycerol	100%	16 ml
EDTA	0,5 M	320 µl
Bromphenol blue		Little bit => achieve deep blue

color

SDS-PAGE buffer was prepared adding 40 µl β-ME (Mercaptoethanol) to 960 µl SDS-Sample buffer before use.

For Western Blot detection:

Luminol-Stock.

444 mg L-3-Aminophtalhydrazid (Fluka 09253) in 10 mL DMSO. 1 ml aliquots were store at -20°C.

Stabilizer.

0,15g of p-coumaicacid (Sigma C 9008) in 10 mL DMSO, 0,44 ml aliquots were stored at -20°C.

S1-Solution

Substance	Volume
1M Tris HCl, pH 8,5	10 ml
Luminol-Stock	1 ml
Stabilizer	0,44 ml
Dissolve in 80 ml H_2O first, then fill up to	100 ml total

S2-Solution

Substance	Volume

1M Tris HCl, pH 8,5	10 ml
30% H_2O_2	60 µl
Dissolve in 80 ml H_2O first, then fill up to	100 ml total

S1 and S2 were stored at -20°C in 10 ml aliquots and were freshly mixed (1:1) immediately before applying on to the membrane.

Ca^{2+} imaging

Fura Red	Invitrogen

Solution of 25mL was freshly mixed every time, mixing 50mg Glucose, 25µL MgCl2 (1M stock solution) and 50µL CaCl (1M stock solution).

Real Time PCR

Super Script II Reverse Transcriptase	Invitrogen by Thermo Fisher Scientific art# 18064014
PrimePCR SYBR Green Assay	Itgae, Mouse, Bio-Rad, art# 10025636
PrimePCR Template for SYBR Green Assay	Itgae, Mouse, Bio-Rad, article# 10029101
LightCycler 480 SYBR Green I Master	Roche, article # 04707516001
LightCycler 480 Multiwell Plate 96, white	Roche, article# 04 729 69200
Oligo dT 18 Bases	Metabion

Primer pair HPRT forward CTC ATG GAC TGA TTA TGG ACA GG and the reverse was TTA ATG TAA TCC AGC AGG TCA GC

RNA Miniprep Kit	Sigma-Aldrich, Article# RTN70

Aarts, M., Iihara, K., Wei, W.L., Xiong, Z.G., Arundine, M., Cerwinski, W., MacDonald, J.F., and Tymianski, M. (2003). A key role for TRPM7 channels in anoxic neuronal death. Cell *115*, 863-877.

Abbas, A.K., Lichtman, A.H., and Pillai, S. (2012a). Activation of T Lymphocytes. In Cellular and Molecular Immunology (Philadelphia : Elsevier/Saunders).

Abbas, A.K., Lichtman, A.H., and Pillai, S. (2012b). Cells and Tissues of the Immune System. In Cellular and Molecular Immunology (Philadelphia: Elsevier/Saunders).

Abbas, A.K., Lichtman, A.H., and Pillai, S. (2012c). Lymphocyte Development and Antigen Receptor Gene Rearrangement. In Cellular and Molecular Immunology (Philadelphia: Elsevier/Saunders).

Abbas, A.K., Lichtman, A.H., and Pillai, S. (2012d). Major Histocompatibiloity Complex Molecules and Antigen Presentation to T Lymphocytes. In Cellular and Molecular Immunology (Philadelphia : Elsevier/Saunders).

Abbas, A.K., Lichtman, A.H., and Pillai, S. (2012e). Properties and Overview of Immune Responses. In Cellular and Molecular Immunology (Philadelphia, PA : Elsevier/Saunders).

Abbas, A.K., Lichtman, A.H., and Pillai, S. (2012f). Regional Immunity: Specialized Immune Responses in Epithelial and Immune Privileged Tissues. In Cellular and Molecular Immunology (Philadelphia: Elsevier/Saunders).

Abraham, S.N., and St John, A.L. (2010). Mast cell-orchestrated immunity to pathogens. Nat Rev Immunol *10*, 440-452.

Agace, W.W. (2006). Tissue-tropic effector T cells: generation and targeting opportunities. Nat Rev Immunol *6*, 682-692.

Bae, C.Y., and Sun, H.S. (2011). TRPM7 in cerebral ischemia and potential target for drug development in stroke. Acta Pharmacol Sin *32*, 725-733.

Baldoli, E., Castiglioni, S., and Maier, J.A. (2013). Regulation and function of TRPM7 in human endothelial cells: TRPM7 as a potential novel regulator of endothelial function. PLoS One *8*, e59891.

Baldoli, E., and Maier, J.A. (2012). Silencing TRPM7 mimics the effects of magnesium deficiency in human microvascular endothelial cells. Angiogenesis *15*, 47-57.

Baumjohann, D., and Ansel, K.M. (2013). MicroRNA-mediated regulation of T helper cell differentiation and plasticity. Nat Rev Immunol *13*, 666-678.

Belardelli, F. (1995). Role of interferons and other cytokines in the regulation of the immune response. APMIS *103*, 161-179.

Belmonte, C., and Viana, F. (2008). Molecular and cellular limits to somatosensory specificity. Mol Pain *4*, 14.

Boutet, M., Gauthier, L., Leclerc, M., Gros, G., de Montpreville, V., Theret, N., Donnadieu, E., and Mami-Chouaib, F. (2016). TGFbeta Signaling Intersects with CD103 Integrin Signaling to Promote T-Lymphocyte Accumulation and Antitumor Activity in the Lung Tumor Microenvironment. Cancer Res.

Bruce, D.L., and Sapkota, G.P. (2012). Phosphatases in SMAD regulation. FEBS Lett *586*, 1897-1905.

Cahalan, M.D., and Chandy, K.G. (2009). The functional network of ion channels in T lymphocytes. Immunol Rev *231*, 59-87.

Cheroutre, H., and Madakamutil, L. (2004). Acquired and natural memory T cells join forces at the mucosal front line. Nat Rev Immunol *4*, 290-300.

Clark, K., Middelbeek, J., Lasonder, E., Dulyaninova, N.G., Morrice, N.A., Ryazanov, A.G., Bresnick, A.R., Figdor, C.G., and van Leeuwen, F.N. (2008). TRPM7 regulates myosin IIA filament stability and protein localization by heavy chain phosphorylation. J Mol Biol *378*, 790-803.

Cohen, M.R., and Moiseenkova-Bell, V.Y. (2014). Structure of thermally activated TRP channels. Curr Top Membr *74*, 181-211.

Cosens, D.J., and Manning, A. (1969). Abnormal electroretinogram from a Drosophila mutant. Nature *224*, 285-287.

Crawley, S.W., and Cote, G.P. (2009). Identification of dimer interactions required for the catalytic activity of the TRPM7 alpha-kinase domain. Biochem J *420*, 115-122.

de Baaij, J.H., Hoenderop, J.G., and Bindels, R.J. (2015). Magnesium in man: implications for health and disease. Physiol Rev *95*, 1-46.

Deason-Towne, F., Perraud, A.L., and Schmitz, C. (2012). Identification of Ser/Thr phosphorylation sites in the C2-domain of phospholipase C gamma2 (PLCgamma2) using TRPM7-kinase. Cell Signal *24*, 2070-2075.

del Rio, M.L., Bernhardt, G., Rodriguez-Barbosa, J.I., and Forster, R. (2010). Development and functional specialization of CD103+ dendritic cells. Immunol Rev *234*, 268-281.

Desai, B.N., Krapivinsky, G., Navarro, B., Krapivinsky, L., Carter, B.C., Febvay, S., Delling, M., Penumaka, A., Ramsey, I.S., Manasian, Y., and Clapham, D.E. (2012). Cleavage of TRPM7 releases the kinase domain from the ion channel and regulates its participation in Fas-induced apoptosis. Dev Cell *22*, 1149-1162.

Dorovkov, M.V., and Ryazanov, A.G. (2004). Phosphorylation of annexin I by TRPM7 channel-kinase. J Biol Chem *279*, 50643-50646.

Fang, L., Huang, C., Meng, X., Wu, B., Ma, T., Liu, X., Zhu, Q., Zhan, S., and Li, J. (2014). TGF-beta1-elevated TRPM7 channel regulates collagen expression in hepatic stellate cells via TGF-beta1/Smad pathway. Toxicol Appl Pharmacol *280*, 335-344.

Feeney, K.A., Hansen, L.L., Putker, M., Olivares-Yanez, C., Day, J., Eades, L.J., Larrondo, L.F., Hoyle, N.P., O'Neill, J.S., and van Ooijen, G. (2016). Daily magnesium fluxes regulate cellular timekeeping and energy balance. Nature *532*, 375-379.

Feske, S., Picard, C., and Fischer, A. (2010). Immunodeficiency due to mutations in ORAI1 and STIM1. Clin Immunol *135*, 169-182.

Feske, S., Skolnik, E.Y., and Prakriya, M. (2012). Ion channels and transporters in lymphocyte function and immunity. Nat Rev Immunol *12*, 532-547.

Gerner, R.R., Moschen, A.R., and Tilg, H. (2013). Targeting T and B lymphocytes in inflammatory bowel diseases: lessons from clinical trials. Dig Dis *31*, 328-335.

Gorfu, G., Rivera-Nieves, J., and Ley, K. (2009). Role of beta7 integrins in intestinal lymphocyte homing and retention. Curr Mol Med *9*, 836-850.

Habtezion, A., Nguyen, L.P., Hadeiba, H., and Butcher, E.C. (2016). Leukocyte Trafficking to the Small Intestine and Colon. Gastroenterology *150*, 340-354.

Hahm, K.B., Im, Y.H., Parks, T.W., Park, S.H., Markowitz, S., Jung, H.Y., Green, J., and Kim, S.J. (2001). Loss of transforming growth factor beta signalling in the intestine contributes to tissue injury in inflammatory bowel disease. Gut *49*, 190-198.

Harteneck, C., Plant, T.D., and Schultz, G. (2000). From worm to man: three subfamilies of TRP channels. Trends Neurosci *23*, 159-166.

Hermann-Kleiter, N., and Baier, G. (2010). NFAT pulls the strings during CD4+ T helper cell effector functions. Blood *115*, 2989-2997.

Huang, L., Ng, N.M., Chen, M., Lin, X., Tang, T., Cheng, H., Yang, C., and Jiang, S. (2014). Inhibition of TRPM7 channels reduces degranulation and release of cytokines in rat bone marrow-derived mast cells. Int J Mol Sci *15*, 11817-11831.

Izquierdo, J.H., Bonilla-Abadia, F., Canas, C.A., and Tobon, G.J. (2014). Calcium, channels, intracellular signaling and autoimmunity. Reumatol Clin *10*, 43-47.

Jiang, J., Li, M., and Yue, L. (2005). Potentiation of TRPM7 inward currents by protons. J Gen Physiol *126*, 137-150.

Jin, J., Desai, B.N., Navarro, B., Donovan, A., Andrews, N.C., and Clapham, D.E. (2008). Deletion of Trpm7 disrupts embryonic development and thymopoiesis without altering Mg2+ homeostasis. Science, pp. 756-760.

Jin, W., and Dong, C. (2013). IL-17 cytokines in immunity and inflammation. Emerg Microbes Infect *2*, e60.

Kaitsuka, T., Katagiri, C., Beesetty, P., Nakamura, K., Hourani, S., Tomizawa, K., Kozak, J.A., and Matsushita, M. (2014). Inactivation of TRPM7 kinase activity does not impair its channel function in mice. Sci Rep, p. 5718.

Kamada, N., Seo, S.U., Chen, G.Y., and Nunez, G. (2013). Role of the gut microbiota in immunity and inflammatory disease. Nat Rev Immunol *13*, 321-335.

Kaplan, M.H., Hufford, M.M., and Olson, M.R. (2015). The development and in vivo function of T helper 9 cells. Nat Rev Immunol *15*, 295-307.

Kerschbaum, H.H., and Cahalan, M.D. (1999). Single-channel recording of a store-operated Ca2+ channel in Jurkat T lymphocytes. Science *283*, 836-839.

Kerschbaum, H.H., Kozak, J.A., and Cahalan, M.D. (2003). Polyvalent cations as permeant probes of MIC and TRPM7 pores. Biophys J *84*, 2293-2305.

Kim, T.Y., Shin, S.K., Song, M.Y., Lee, J.E., and Park, K.S. (2012). Identification of the phosphorylation sites on intact TRPM7 channels from mammalian cells. Biochem Biophys Res Commun *417*, 1030-1034.

Krapivinsky, G., Krapivinsky, L., Manasian, Y., and Clapham, D.E. (2014). The TRPM7 chanzyme is cleaved to release a chromatin-modifying kinase. Cell *157*, 1061-1072.

Lammermann, T., Bader, B.L., Monkley, S.J., Worbs, T., Wedlich-Soldner, R., Hirsch, K., Keller, M., Forster, R., Critchley, D.R., Fassler, R., and Sixt, M. (2008). Rapid leukocyte migration by integrin-independent flowing and squeezing. Nature *453*, 51-55.

Lazzeri, M., Costantini, E., and Porena, M. (2009). TRP family proteins in the lower urinary tract: translating basic science into new clinical prospective. Ther Adv Urol *1*, 33-42.

Lee, J.S., Tato, C.M., Joyce-Shaikh, B., Gulen, M.F., Cayatte, C., Chen, Y., Blumenschein, W.M., Judo, M., Ayanoglu, G., McClanahan, T.K.*, et al.* (2015). Interleukin-23-Independent IL-17 Production Regulates Intestinal Epithelial Permeability. Immunity *43*, 727-738.

Li, F.Y., Chaigne-Delalande, B., Kanellopoulou, C., Davis, J.C., Matthews, H.F., Douek, D.C., Cohen, J.I., Uzel, G., Su, H.C., and Lenardo, M.J. (2011). Second messenger role for Mg2+ revealed by human T-cell immunodeficiency. Nature *475*, 471-476.

Lioudyno, M.I., Kozak, J.A., Penna, A., Safrina, O., Zhang, S.L., Sen, D., Roos, J., Stauderman, K.A., and Cahalan, M.D. (2008). Orai1 and STIM1 move to the immunological synapse and are up-regulated during T cell activation. Proc Natl Acad Sci U S A *105*, 2011-2016.

Mannon, P., and Reinisch, W. (2012). Interleukin 13 and its role in gut defence and inflammation. Gut *61*, 1765-1773.

Martinez, G.J., Zhang, Z., Reynolds, J.M., Tanaka, S., Chung, Y., Liu, T., Robertson, E., Lin, X., Feng, X.H., and Dong, C. (2010). Smad2 positively regulates the generation of Th17 cells. J Biol Chem *285*, 29039-29043.

Matsushita, M., Kozak, J.A., Shimizu, Y., McLachlin, D.T., Yamaguchi, H., Wei, F.Y., Tomizawa, K., Matsui, H., Chait, B.T., Cahalan, M.D., and Nairn, A.C. (2005). Channel function is dissociated from the intrinsic kinase activity and autophosphorylation of TRPM7/ChaK1. J Biol Chem *280*, 20793-20803.

Maynard, C.L., Elson, C.O., Hatton, R.D., and Weaver, C.T. (2012). Reciprocal interactions of the intestinal microbiota and immune system. Nature *489*, 231-241.

Mokrani, M., Klibi, J., Bluteau, D., Bismuth, G., and Mami-Chouaib, F. (2014). Smad and NFAT pathways cooperate to induce CD103 expression in human CD8 T lymphocytes. J Immunol *192*, 2471-2479.

Monteilh-Zoller, M.K., Hermosura, M.C., Nadler, M.J., Scharenberg, A.M., Penner, R., and Fleig, A. (2003). TRPM7 provides an ion channel mechanism for cellular entry of trace metal ions. J Gen Physiol *121*, 49-60.

Montell, C. (2003). Mg2+ homeostasis: the Mg2+nificent TRPM chanzymes. Curr Biol *13*, R799-801.

Montell, C., Birnbaumer, L., Flockerzi, V., Bindels, R.J., Bruford, E.A., Caterina, M.J., Clapham, D.E., Harteneck, C., Heller, S., Julius, D*., et al.* (2002). A unified nomenclature for the superfamily of TRP cation channels. Mol Cell *9*, 229-231.

Montell, C., and Rubin, G.M. (1989). Molecular characterization of the Drosophila trp locus: a putative integral membrane protein required for phototransduction. Neuron *2*, 1313-1323.

Mowat, A.M., and Agace, W.W. (2014). Regional specialization within the intestinal immune system. Nat Rev Immunol *14*, 667-685.

Mueller, C., and Macpherson, A.J. (2006). Layers of mutualism with commensal bacteria protect us from intestinal inflammation. Gut *55*, 276-284.

Nadler, M.J., Hermosura, M.C., Inabe, K., Perraud, A.L., Zhu, Q., Stokes, A.J., Kurosaki, T., Kinet, J.P., Penner, R., Scharenberg, A.M., and Fleig, A. (2001). LTRPC7 is a Mg.ATP-regulated divalent cation channel required for cell viability. Nature *411*, 590-595.

Naito, T., Tanaka, H., Naoe, Y., and Taniuchi, I. (2011). Transcriptional control of T-cell development. Int Immunol *23*, 661-668.

Nilius, B., and Owsianik, G. (2011). The transient receptor potential family of ion channels. Genome Biol *12*, 218.

Numata, T., and Okada, Y. (2008). Proton conductivity through the human TRPM7 channel and its molecular determinants. J Biol Chem *283*, 15097-15103.

O'Garra, A., and Vieira, P. (2004). Regulatory T cells and mechanisms of immune system control. Nat Med *10*, 801-805.

Olejniczak, K., and Kasprzak, A. (2008). Biological properties of interleukin 2 and its role in pathogenesis of selected diseases--a review. Med Sci Monit *14*, RA179-189.

Park, H.S., Hong, C., Kim, B.J., and So, I. (2014). The Pathophysiologic Roles of TRPM7 Channel. Korean J Physiol Pharmacol *18*, 15-23.

Penner, R., and Fleig, A. (2007). The Mg2+ and Mg(2+)-nucleotide-regulated channel-kinase TRPM7. Handb Exp Pharmacol, 313-328.

Perraud, A.L., Zhao, X., Ryazanov, A.G., and Schmitz, C. (2011). The channel-kinase TRPM7 regulates phosphorylation of the translational factor eEF2 via eEF2-k. Cell Signal *23*, 586-593.

Qiu, Y., Wang, W., Xiao, W., and Yang, H. (2015). Role of the intestinal cytokine microenvironment in shaping the intraepithelial lymphocyte repertoire. J Leukoc Biol.

Qu, B., Al-Ansary, D., Kummerow, C., Hoth, M., and Schwarz, E.C. (2011). ORAI-mediated calcium influx in T cell proliferation, apoptosis and tolerance. Cell Calcium *50*, 261-269.

Risbud, M.V., and Shapiro, I.M. (2014). Role of cytokines in intervertebral disc degeneration: pain and disc content. Nat Rev Rheumatol *10*, 44-56.

Roan, F., Bell, B.D., Stoklasek, T.A., Kitajima, M., Han, H., and Ziegler, S.F. (2012). The multiple facets of thymic stromal lymphopoietin (TSLP) during allergic inflammation and beyond. J Leukoc Biol *91*, 877-886.

Runnels, L.W., Yue, L., and Clapham, D.E. (2001). TRP-PLIK, a bifunctional protein with kinase and ion channel activities. Science *291*, 1043-1047.

Runnels, L.W., Yue, L., and Clapham, D.E. (2002). The TRPM7 channel is inactivated by PIP(2) hydrolysis. Nat Cell Biol *4*, 329-336.

Ryazanova, L.V., Hu, Z., Suzuki, S., Chubanov, V., Fleig, A., and Ryazanov, A.G. (2014). Elucidating the role of the TRPM7 alpha-kinase: TRPM7 kinase inactivation leads to magnesium deprivation resistance phenotype in mice. Sci Rep *4*, 7599.

Ryazanova, L.V., Rondon, L.J., Zierler, S., Hu, Z., Galli, J., Yamaguchi, T.P., Mazur, A., Fleig, A., and Ryazanov, A.G. (2010). TRPM7 is essential for Mg(2+) homeostasis in mammals. Nat Commun *1*, 109.

Sah, R., Mesirca, P., Van den Boogert, M., Rosen, J., Mably, J., Mangoni, M.E., and Clapham, D.E. (2013). Ion channel-kinase TRPM7 is required for maintaining cardiac automaticity. Proc Natl Acad Sci U S A *110*, E3037-3046.

Sahni, J., and Scharenberg, A.M. (2008). TRPM7 ion channels are required for sustained phosphoinositide 3-kinase signaling in lymphocytes. Cell Metab *8*, 84-93.

Sakaguchi, S., Miyara, M., Costantino, C.M., and Hafler, D.A. (2010). FOXP3+ regulatory T cells in the human immune system. Nat Rev Immunol *10*, 490-500.

Sakaguchi, S., Vignali, D.A., Rudensky, A.Y., Niec, R.E., and Waldmann, H. (2013). The plasticity and stability of regulatory T cells. Nat Rev Immunol *13*, 461-467.

Schlingmann, K.P., and Gudermann, T. (2005). A critical role of TRPM channel-kinase for human magnesium transport. J Physiol *566*, 301-308.

Schmitz, C., Perraud, A.L., Johnson, C.O., Inabe, K., Smith, M.K., Penner, R., Kurosaki, T., Fleig, A., and Scharenberg, A.M. (2003). Regulation of vertebrate cellular Mg2+ homeostasis by TRPM7. Cell *114*, 191-200.

Schon, M.P., Arya, A., Murphy, E.A., Adams, C.M., Strauch, U.G., Agace, W.W., Marsal, J., Donohue, J.P., Her, H., Beier, D.R., *et al.* (1999). Mucosal T lymphocyte numbers are selectively reduced in integrin alpha E (CD103)-deficient mice. J Immunol *162*, 6641-6649.

Suffia, I., Reckling, S.K., Salay, G., and Belkaid, Y. (2005). A role for CD103 in the retention of CD4+CD25+ Treg and control of Leishmania major infection. J Immunol *174*, 5444-5455.

Sugimoto, J., Romani, A.M., Valentin-Torres, A.M., Luciano, A.A., Ramirez Kitchen, C.M., Funderburg, N., Mesiano, S., and Bernstein, H.B. (2012). Magnesium decreases inflammatory cytokine production: a novel innate immunomodulatory mechanism. J Immunol *188*, 6338-6346.

Sun, H., Leng, T., Zeng, Z., Gao, X., Inoue, K., and Xiong, Z.G. (2013). Role of TRPM7 channels in hyperglycemia-mediated injury of vascular endothelial cells. PLoS One *8*, e79540.

Swain, S.L., McKinstry, K.K., and Strutt, T.M. (2012). Expanding roles for CD4(+) T cells in immunity to viruses. Nat Rev Immunol *12*, 136-148.

Swiatczak, B., Rescigno, M., and Cohen, I.R. (2011). Systemic features of immune recognition in the gut. Microbes Infect *13*, 983-991.

Takezawa, R., Schmitz, C., Demeuse, P., Scharenberg, A.M., Penner, R., and Fleig, A. (2004). Receptor-mediated regulation of the TRPM7 channel through its endogenous protein kinase domain. Proc Natl Acad Sci U S A *101*, 6009-6014.

Van Dyken, S.J., and Locksley, R.M. (2013). Interleukin-4- and interleukin-13-mediated alternatively activated macrophages: roles in homeostasis and disease. Annu Rev Immunol *31*, 317-343.

Venkatachalam, K., and Montell, C. (2007). TRP channels. Annu Rev Biochem *76*, 387-417.

Visser, D., Middelbeek, J., van Leeuwen, F.N., and Jalink, K. (2014). Function and regulation of the channel-kinase TRPM7 in health and disease. Eur J Cell Biol *93*, 455-465.

Wei, C., Wang, X., Chen, M., Ouyang, K., Song, L.S., and Cheng, H. (2009). Calcium flickers steer cell migration. Nature *457*, 901-905.

Weninger, W., Biro, M., and Jain, R. (2014). Leukocyte migration in the interstitial space of non-lymphoid organs. Nat Rev Immunol *14*, 232-246.

Wernersson, S., and Pejler, G. (2014). Mast cell secretory granules: armed for battle. Nat Rev Immunol *14*, 478-494.

Wissinger, E. (2016). CD 8^+ Cells. B.S. Immunology, ed. (Imperia College London, UK. online source http://bitesized.immunology.org/cells/cd8-t-cells/, British Society for Immunology).

Wojdasiewicz, P., Poniatowski, L.A., and Szukiewicz, D. (2014). The role of inflammatory and anti-inflammatory cytokines in the pathogenesis of osteoarthritis. Mediators Inflamm *2014*, 561459.

Wolf, F.I., Trapani, V., and Cittadini, A. (2008). Magnesium and the control of cell proliferation: looking for a needle in a haystack. Magnes Res *21*, 83-91.

Wynn, T.A. (2015). Type 2 cytokines: mechanisms and therapeutic strategies. Nat Rev Immunol *15*, 271-282.

Yamaguchi, H., Matsushita, M., Nairn, A.C., and Kuriyan, J. (2001). Crystal structure of the atypical protein kinase domain of a TRP channel with phosphotransferase activity. Mol Cell *7*, 1047-1057.

Yee, N.S., Kazi, A.A., and Yee, R.K. (2014). Cellular and Developmental Biology of TRPM7 Channel-Kinase: Implicated Roles in Cancer. Cells *3*, 751-777.

Yogi, A., Callera, G.E., O'Connor, S., Antunes, T.T., Valinsky, W., Miquel, P., Montezano, A.C., Perraud, A.L., Schmitz, C., Shrier, A., and Touyz, R.M. (2013). Aldosterone signaling through transient receptor potential melastatin 7 cation channel (TRPM7) and its alpha-kinase domain. Cell Signal *25*, 2163-2175.

Zierler, S., Sumoza-Toledo, A., Suzuki, S., F, O.D., Ryazanova, L.V., Penner, R., Ryazanov, A.G., and Fleig, A. (2015). TRPM7 kinase activity regulates murine mast cell degranulation. J Physiol.

Acknowledgements

Completion of this doctoral dissertation and research project was possible with the support of several scientists and colleagues. I would like to express my special appreciation and thanks to my supervisors Professor Dr. Alexandra Dietrich and Dr. Susanna Zierler and our head of institute Professor Dr. Thomas Gudermann. You all have been tremendous mentors when I have needed help and encouragement. I would like to thank you for supporting my research and for allowing me to grow as a research scientist and person. Your advice and suggestions on both research as well as my career have forged who I have become today. I would also like to thank my committee members, for serving as my committee members even at hardship. I would especially like to thank all the scientists at the AG Zierler and at the Walter-Straub-Institute for their enormous help when approaching new research techniques. A very special thanks to the collaborators on this project: Professor Dr. Fabio Grassi and Dr. Andrea Romagnani. Words can not express how grateful I am to you for your knowledge, love and deep interest in Immunology that consequently filled my heart and thoughts. My final and most important dedication is to my family. There is no amount of love and affection which will ever sufficiently express my devotion to you all, your words of wisdom still guide me through my everyday. Thank you for supporting me in my endeavour, and especially I can't thank you enough for encouraging me throughout this experience. To my beloved brother, I would like to express my thanks for being such a beautiful human being and personal fan.

God grant me the serenity

to accept the things I cannot change;

courage to change the things I can;

and wisdom to know the difference.

Errata Corrige

"TRPM7 in T-cell signaling"
Kinase-coupled Ion Channel in
Immune System Homeostasis.

Page 27, Figure 5. Image from https://media.nature.com/lw685/nature-assets/nri/journal/v12/n2/images/nri3152-i1.jpg. Image modified for the mere understanding of the thesis.

Page 30, Figure 6. Image from https://media.springernature.com/m685/nature-assets/nri/journal/v12/n2/images/nri3152-f3.jpg.

Page 35, Figure 7. Image from https://media.springernature.com/m685/nature-assets/nri/journal/v4/n4/images/nri1333-f1.jpg

Page 93, Figure 19. This image was modified (from Fang *et al.* 2014) for the mere understanding of thesis. Original image at https://ars.els-cdn.com/content/image/1-s2.0-S0041008X14002981-gr6.jpg.

LMU LUDWIG-MAXIMILIANS-UNIVERSITÄT MÜNCHEN

Dean's Office
Faculty of Medicine

MMRS

Affidavit

Vettore Valentina
Surname, first name

Street

Zip code, town

Country

I hereby declare, that the submitted thesis entitled

TRPM7 in T-cell signaling

is my own work. I have only used the sources indicated and have not made unauthorised use of services of a third party. Where the work of others has been quoted or reproduced, the source is always given.

I further declare that the submitted thesis or parts thereof have not been presented as part of an examination degree to any other university.

1st January 2018, Sydney
Place, date

Valentina Vettore
Signature doctoral candidate